이학박사 학위논문

PV-dependent adenylate cyclase 5 signaling mediates regulation of excitatory synapses of parvalbumin interneuron for auditory sensorimotor gating

청 감각제어를 위한 parvalbumin 인터뉴론의 흥분성 시냅스 조절기전을 매개하는 PV 의존적 adenylate cyclase 5 신호전달

2021년 8월

서울대학교 대학원

뇌인지과학과 뇌인지과학 전공

신 재 진

Ph.D Dissertation of Brain and Cognitive Science

청 감각제어를 위한 parvalbumin 인터뉴론의 흥분성 시냅스 조절기전을 매개하는 PV 의존적 adenylate cyclase 5 신호전달

PV-dependent adenylate cyclase 5 signaling mediates regulation of excitatory synapses of parvalbumin interneuron for auditory sensorimotor gating

August 2021

The Department of Brain and Cognitive Science,
Seoul National University
College of Natural Science

Jae Jin Shin

청 감각제어를 위한 parvalbumin 인터뉴론의 홍분성 시냅스 조절기전을 매개하는 PV 의존적 adenylate cyclase 5 신호전달

지도 교수 김 상 정

이 논문을 이학박사 학위논문으로 제출함

2021년 08월

서울대학교 대학원
뇌인지과학과 뇌인지과학 전공

신 재 진

의
이학박사 학위논문을 인준함

2021년 07월

위원장	이 석 호
부위원장	김 상 정
위원	박 주 민
위원	이 용 석
위원	오 석 배

PV-dependent adenylate cyclase 5 signaling mediates regulation of excitatory synapses of parvalbumin interneuron for auditory sensorimotor gating

A Dissertation Submitted to the Faculty of the Department of Brain and Cognitive Science
at
Seoul National University
by
Jae Jin Shin

in Partial Fulfillment of the Requirements for the Degree of Doctor of Philosophy

Advisor: Sang Jeong Kim
August 2021

Approved by Thesis Committee:
July 2021

Chair	Suk Ho Lee
Vice Chair	Sang Jeong Kim
Examiner	Joo Min Park
Examiner	Yong Seok Lee
Examiner	Seog Bae Oh

Preface

This Ph.D dissertation written by Jae Jin Shin contains two chapters with all unpublished data. The chapter I addresses that parvalbumin (PV) deficiency induced by NMDAR hypofunction in Pv interneurons causes AMPAR downregulation associated with sensorimotor gating deficits. The chapter II suggests that distinctive AMPAR regulation by PV-mediated AC 5 signaligng in Pv interneurons is required for sensorimotor gating.

Abstract

PV-dependent adenylate cyclase 5 signaling mediates regulation of excitatory synapses of parvalbumin interneuron for auditory sensorimotor gating

Jae Jin Shin
Department of Brain and Cognitive Science
The Graduate School
Seoul National University

Parvalbumin-expressing (Pv) interneuron dysfunction has been increasingly implicated in cognitive deficits and disruption of auditory sensorimotor gating, but how the cellular substrates for Pv interneuron abnormality have remained elusive.

Here, I report that modulation of PPI measured as a psychophysiological index of pre-pulse inhibition (PPI) in mPFC depends on parvalbumin (PV)-mediated adenylate cyclase isoform 5 (AC 5) regulation to coordinate synaptic changes of AMPA receptor (AMPAR), which is adaptive to NMDA receptor (NMDAR) function at glutamatergic synapses onto Pv interneurons.

Studies in mPFC of NMDAR antagonism and PV shRNA-silencing models demonstrated downregulation of AMPAR in Pv interneurons and PPI deficits associated with aberrant network activity. Furthermore, deletion of AC 5 impaired PPI without affecting other behavioral effects. Overexpression of PV and reactivation of AC 5 signaling promoted to improve Pv interneuronal synaptic activity in line with PPI effects, which is comparable to PPI rescue by optogenetic stimulation of Pv interneurons.

These results suggest that PV-AC 5 signaling is the novel Pv interneuronal mechanisms for mediating synaptic changes of AMPAR and thus NMDAR hypofunction-induced disruption of this signaling impairs synaptic regulation of AMPAR, leading to PPI deficits with abnormal network activity.

Keyword: Parvalbumin, Parvalbumin interneuron, NMDA receptor hypofunction, Sensorimotor gating, Pre-pulse inhibition, Adenylate cyclase, Protein kinase A, AMPA receptor

Abbreviation: Pv, parvalbumin expressing; PV, parvalbumin; PN, pyramidal neuron; ASR, acoustic startle response; PPI, pre-pulse inhibition; dB, decibel; AC, adenylate cyclase; PKA, protein kinase A; AMPAR, α-amino-3-hydroxy-5-methyl-4-isoxazolepropionic acid receptor; NMDAR, N-methyl-D-aspartate receptor; EPSC, excitatory postsynaptic current; sEPSC, spontaneous EPSC; eEPSC, evoked EPSC; E/I, excitation to inhibition; IPSC, inhibitory postsynaptic current; sIPSC, eIPSC, evoked IPSC; oIPSC, optogenetically evoked IPSC; spontaneous IPSC; mIPSC, miniature IPSC; PPR, paired pulse ratio; PL, prelimbic; mPFC, medial prefrontal cortex; shRNA, small hairpin RNA; OX, overexpression vector for PV; EM, empty vector for PV; KD, knockdown for PV; SCR, scrambled vector for PV; Ca^{2+}, calcium; SA, saline injected; MK, mk-801 injected; cAMP, cyclic Adenosine Monophosphate; EEG, electroencephalogram; ASSR, auditory steady-state response; FK, forskolin; DM or DMAGO, [D-Ala2, N-MePhe4, Gly-ol]-enkephalin; LCM, laser capture microdissection; WT, wild-type; HT, hetero-type; KO, knockout; PGC-1α, Peroxisome proliferator activated receptor gamma coactivator-1 alpha; VVA, Vicia Villosa Lectin; ON, laser on; OFF, laser off; PreMK, before mk-801 injection; GluR, glutamate receptor; CaMKII , Ca^{2+}/calmodulin-dependent protein kinase II; GABAR, Gamma-aminobutyric acid receptor; IP, immunoprecipitation; RNA, ribonucleic acid; cDNA, complementary DNA; qPCR, quantitative polymerase chain reaction; LFP, local field potential; Hz, Hertz or frequency; mV, millivolt; μV, microvolt; FFT, fast Fourier transform;

Student Number: 2011-24033

국문요약

청 감각 제어를 위한 parvalbumin 인터뉴론의 흥분성 시냅스 조절기전을 매개하는 PV 의존적 adenylate cyclase 5 신호전달

신 재 진

서울대학교 대학원

자연과학대학 뇌인지과학과 (뇌인지과학 전공)

Parvalbumin 인터뉴론의 기능 장애는 인지 기능 및 청각 감각 운동 동기의 악화에 연루되어 있음이 많은 이전 연구들에서 진행되었다. 하지만, parvalbumin 인터뉴론에 대한 구체적인 분자적 및 세포학적 수준에서의 기질연구는 여전히 많은 부분이 탐구되지 않았다.

본 연구에서 나는 mPFC에서 청각 감각 운동 동기의 정신생리학적 측정 지표인 Prepulse 억제 (PPI)의 조절이 AMPA 수용체 (AMPAR)의 시냅스 변화에 의해서 기저하며, 이러한 AMPA 수용체는 Parvalbumin 단백질 (PV) 매개된 adenylate cyclase 이소형 5 (AC 5) 조절에 의존된다고 보고한다. 이러한 parvalbumin 중간게재 세포 특이적인 신호전달 경로는 NMDA 수용체 (NMDAR)의 기능에 따라 적응적으로 조절됨을 시사한다. NMDAR 길항작용 및 PV shRNA 억제 (silencing) 모델의 mPFC에 대한 연구는 비정상적인 네트워크 활동과 관련된 parvalbumin 인터뉴론에서의 하향 조절된 AMPA 수용체의 기능 및 PPI 결핍이 나타남을 입증했다. 또한, AC 5의 유전자 제거 모델에서는 다른 행동 효과에는 영향을 미치지 않으면서 특이적으로 PPI의 결핍만이 나타남을 발견하였다. Parvalbumin

단백질의 과발현과 AC 5 신호전달의 재활성화는 PPI에 대한 효과와 일치하여 parvalbumin 인터뉴론의 시냅스 활성을 개선하도록 촉진시키는데 기여하였으며, 이는 parvalbumin 인터뉴론을 직접적으로 광유전학적 자극을 함으로서 회복되어지는 PPI 정도와 유사한 수준의 개선임을 밝혔다.

이러한 결과는 parvalbumin 단백질 (PV)에서 AC 5로 연결되어지는 신호가 AMPA 수용체의 시냅스 변화를 매개하기 위한 새로운 parvalbumin 인터뉴론안의 특이적인 신경 메커니즘이며 따라서 NMDA 수용체 기능저하로 야기되어지는 이 신호의 방해가 AMPA 수용체의 조절을 손상시켜 비정상적인 네트워크 활동과 함께 PPI 결손을 초래함을 시사한다.

주요어 : Parvalbumin 인터뉴론, 청감각 운동동기, Prepulse 억제, NMDA 수용체 기능저하, adenylate cyclase 5, AMPA 수용체

학 번 : 2011-24033

Graphical Abstract

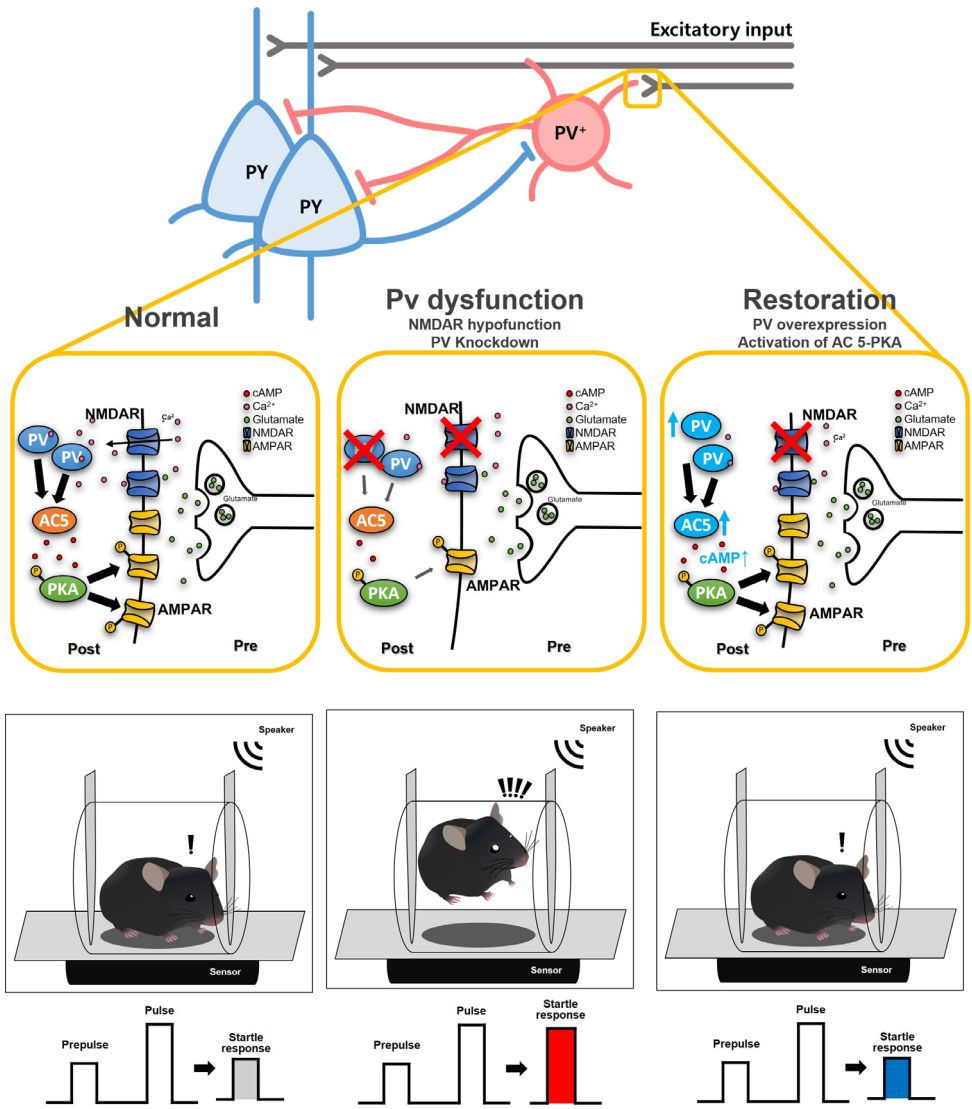

Pv interneuron-specific signal transduction for coupling NMDAR activity to PKA signaling is through PV-mediated AC 5, which is implicated in synaptic regulation of AMPAR to coordinate mPFC network activity and its-related PPI effects.

Table of Contents

List of Figures and Tables

Chapter I

Chapter II

Chapter I. PV deficiency induced by NMDAR hypofunction in Pv interneurons causes AMPAR downregulation associated with sensorimotor gating deficits

Introduction

Sensorimotor gating is a neurological process important for information filtering of distracting stimuli to attend and process relevant stimuli.[1] This is assessed by pre-pulse inhibition (PPI) of acoustic startle response (ASR). Impairment of PPI of the ASR has been believed to be linked to a core feature of sensorimotor gating dysfunction in several psychiatric diseases including schizophrenia (SZ).[1,2] Medial prefrontal cortex (mPFC) is crucial region involved in regulation of sensorimotor gating, which is characterized by functional connectivity to PPI-mediated networks including auditory cortex and pedunculopontine nucleus[3–7] and mPFC neuronal responses to auditory pulse stimuli.[8,9] Multiple lines of evidence demonstrate that the disruption of neural circuitry in mPFC impair PPI, which indicates sensorimotor gating deficits observed in neurological and psychiatric disorders.[10–13] However, from the perspective of local neural circuit in mPFC, the distinct cellular mechanisms and neural substrates underlying PPI modulation are poorly understood.

Related to pathophysiology of psychiatric diseases in patients, parvalbumin-expressing (Pv) interneuron dysfunctions appear to be present in various mouse models including genetic or pharmacological manipulation, which pronounced PPI deficits associated with abnormal neural network activities such as excitation/inhibition (E/I) imbalance and aberrant gamma oscillations.[14,15] For instances, Gad1-knockout ($Gad1^{-/-}$) mice (deficiency in GAD 67), which had GABAergic expression disturbances in Pv interneurons[16], revealed impairments in PPI[17] and also reduced gamma oscillatory activity.[18] Furthermore, direct Pv

interneuron inhibition by pharmacogenetic neuromodulator hM4D impaired PPI and network oscillatory activity of gamma frequency.[19]

Besides abovementioned Pv interneuron abnormality models, NMDA receptor (NMDAR) hypofunction mouse models, which has been suggested to underlie core feature of psychiatric disease models such as SZ showed contradictory results in PPI impairment. Significantly, pharmacologically-induced NMDAR antagonism, which is prominent in fast-spiking Pv interneurons disproportionately more sensitive to NMDA antagonists such as ketamine and MK-801[20–24], expressed PPI deficits as well as alteration in network activity[10,25–33], although genetical NR1 ablation in Pv interneurons indicated changes in network activity (E/I imbalance) notably without corresponding effects on PPI.[34–37] Considering that NMDAR impacts on functional state or trafficking of AMPAR, NMDAR dysfunction is significantly associated with abnormal AMPAR activity.[38] Therefore, not only reduced NMDAR currents and but also NMDAR-dependent synaptic changes of AMPAR in Pv interneurons would be conjointly implicated in severe SZ-phenotypes such as sensorimotor gating deficits. Accumulating evidence have suggested that AMPARs are modulated primarily through NMDAR-dependent mechanisms in which several molecular players are mediated by calcium influx through NMDAR to elicit synaptic modification.[39] However, whether and how Pv interneuronal specific mechanisms contribute to NMDAR hypofunction-induced synaptic changes and thereby underlie sensorimotor gating deficits remains unclear. Although seemingly sharing NMDAR hypofunction hypothesis as a key pathogenesis of schizophrenia, there is a huge dissociation between pharmacologically induced NMDAR hypofunction and NMDAR knockout

in Pv interneurons. Pharmacological blockades of NMDAR such as ketamine and mk-801 induces positive, as well as cognitive and negative symptoms of schizophrenia while NMDAR knockout in Pv interneurons mimics limited deficits in self caring and sociality as negative symptoms [35,37] and complex cognitive dysfunction such as spatial reference memory without affecting working memory [34]. The counter-intuitive finding that Pv interneuron-specific NMDAR ablation mouse models do not induce positive symptom validity including pre-pulse inhibition (PPI) has driven me to hypothesis that progression of NMDAR hypofunction-mediated synaptic changes is implicated in PPI deficits. Previous evidence has suggested that NMDAR dependent synaptic plasticity involves rapid changes in the trafficking of highly mobile AMPAR.[40] However, Pv interneuronal mechanisms underlying regulation of AMPAR and how they translate into delicate synaptic modification in response to NMDAR activity are still poorly understood.

Multiple lines of evidence have reported that parvalbumin (PV) deficiency, reduced PV protein expression, is prevalent in animal models and even [41–45] tissue from patients with psychiatric diseases, which is identified as biomarkers.[45–48] Sub-chronic administration of NMDA receptor antagonists decreased the expression of parvalbumin (PV), the calcium (Ca^{2+})-binding protein expressed in Pv interneurons.[41,49] Considering that NMDAR is the main source of Ca^{2+} influx in Pv interneurons, NMDAR hypofunction would disrupt Ca^{2+}-dependent transcription and translation of PV proteins, resulting in loss of PV (PV dysfunction).[50–53] Of note, knock out of PV mouse model ($PV^{-/-}$) disrupted synaptic regulation in Pv interneurons[54–56] accompanied by SZ-related phenotypes including defects of acoustic startle response and even PPI.[54,57] However, it remains elusive whether and

how function of PV proteins involves in synaptic regulation associated with sensorimotor gating deficits.

These intersecting lines of evidence strongly suggest that NMDAR hypofunction itself on Pv interneurons would not be sufficient to propagate Pv dysfunction implicated in PPI deficits with abnormal network activities in mPFC. Therefore, I hypothesized that reduced NMDAR activity on Pv interneurons causes distinct mechanisms in mediating disruptive changes of synaptic and neuronal property in Pv interneurons through PV deficiency, leading to sensorimotor gating deficits in line with abnormal network activity.

In the chapter I, I investigated whether PPI of ASR is modulated specifically by Pv interneuronal function in mPFC of my NMDAR hypofunction model. I further observed NMDAR hypofunction at excitatory synapses onto Pv inter neuron resulted in reduction of AMPAR activity and downregulation of parvalbumin (PV) which required PGC1-alpha (PGC-1α), leading to PPI deficit. PV overexpression enhanced AMPAR synaptic strength and rescued impairment of PPI in NMDAR hypofunction mice. Consistent with defects in NMDAR hypofunction model, my PV knockdown model also revealed abnormal AMPAR synaptic activity, leading to PPI deficits, importantly, without affecting NMDAR function. These results suggest that the level of PV expression is required to modulate AMPAR-mediated synaptic strength in response to NMDAR activity as Pv interneuronal distinct mechanisms. This indicates that it is the function of NMDAR that is critical for proper coregulation of PV levels together with AMPAR changes in Pv interneurons to maintain PPI modulation in mPFC.

Material and Methods

Animals

All inbred mouse strains, Pv-Cre, Pv-Cre;Ai14. SOM-Cre, and SOM-Cre;Ai14 were obtained from the Jackson laboratories and GAD65-GFP was obtained from a colony of Korean Institute for Science and Technology (KIST). All strains were maintained in a C57B/6J or 129S2/SV background (> N10 backcross). All experimental procedures were performed on male mice with P55-70. All the mice were maintained under standard temperature controls with housing up to five animals per cage under 12/12h light/dark cycle. Animals received water and food ad libitum. All experiments including behavioral tests, electrophysiological experiments, and biochemistry were done in littermate males at 8-10 weeks of age. For mk-801 & saline mouse model, mice were treated with mk-801 (1.0 mg/kg, intraperitoneally [i.p.], daily) or 0.9% saline as vehicle control for 7 consecutive days from P55 to P60. I modified mk-801 model dosage based on previous publication (Xi, D., Zhang and Gao, W.-J. et.al 2009). Animal procedures were approved by the Institutional Animal Care and Use committee of Seoul National University (SNU) and Institute for Basic Science (IBS).

In vivo surgery

P50-55 mice were anesthetized with 8 mg/ml ketamine (16% by volume) and xylazine (2.8% by volume) in saline solution by intraperitoneal injection and were mounted stereotactic frame (David Kopf Inc., USA) with a heating pad for maintenance of core body temperature at 36℃. For electrophysiology or behavioral experiments, a volume of about 0.5 μl virus solution was bilaterally injected into the

dorsal region of medial prefrontal cortex (AP 1.94mm; ML 0.8mm; DV 1.75mm; 15-degree angle relative to Bregma) by 20 psi pressure with 5 msec duration (Picospritzer III, Parker Hannifin Corp.). The injection glass pipette was then removed after 10-15min for diffusion. The optic fiber (Doric Lenses Inc., 100μm core, 0.22 NA, ZF 1.25, DFL) was targeted to the same position as virus injection coordination. Cell-type-specific expression of virus was obtained using the following Cre-dependent AAV: AAV5-EF1a-DIO-eNpHR3.0-mcherry-WPRE (UNC vector core), AAV9-Ef1a-DIO-ChETA(E123T/H134R)-eYFP-WPRE-hGH (Penn vector core).

Preparation of mice brain lysate, solubilization

The brain tissues were added to homogenization buffer (0.32-M sucrose in phosphate-buffered saline solution) and homogenized using a homogenizer. The lysate was centrifuged for 10 min at 1400 × *g* at 4 °C. The pellet was saved as P1. The supernatant (S1) was collected and spun again at 13,800 × *g* for 10 min at 4 °C. The second supernatant (S2) and pellet (P2) were saved. Solubilization buffer was made with PBS by freshly adding p0.5% Triton X-100, 0.5 mM EDTA, 0.5 mM EGTA, protease inhibitor mixture, and additional detergents as indicated for each experiment. The P2 was resuspended in solubilization buffer, mixed gently for 60 min at 4 °C on a rotator, and spun down at 14,000 × *g* for 15 min to collect the supernatant including solubilized proteins.

Western Blot Analysis

50 micrograms of protein were used for the western blot. The blots were then blocked in PBS including 1% bovine serum albumin and 0.1% Tween-20 for 1h at

room temperature and incubated with the antibodies at 4 °C overnight. All primary antibodies used in my study, except the GluA1 antibody, were purchased and used in the dilution of GluA1 (1:1000), GluA4 (1:1000), NR2A (1:500), NR2B (1:500), PKA (1:500), AC5(1:500), PGC1α (1:500) and GAPDH (1:1000). The following day, the blots were washed and incubated with specify secondary antibodies using a goat anti-mouse IgG (1:10000, abcam) and goat anti-rabbit IgG (1:10000, abcam) at room temperature for 1h. The blots were developed with enhanced chemiluminescence (SuperSignal, Thermo Sciences) and imaged with an image capturing system (ChemiDoc XRS, Bio-Rad). For quantification of the western blots, the protein signals were measured and analyzed using ImageJ software.

Immunohistochemistry

The animals were then transcardially perfused with phosphate buffered saline (PBS, pH 7.4) followed by 4% paraformaldehyde (PFA) in PBS. After this, brains were extracted, postfixed in 4% PFA at 4°C overnight. They were immersed in a solution of 30% sucrose in PBS at 4°C until they sank. Brains were sectioned in the coronal plane at 20 μm. The slices were immune-labeled at 4°C overnight using antibodies against pv (1:1000, swant). After this, the slices were washed with 1X PBST (0.3% Triton X-100 in 1X PBS) and incubated at room temperature for 2 hours in secondary antibody (1:800, Cy™5-conjugated Affinity Pure Goat Anti-Mouse IgG (H+L), Jackson Immuno Research, 115-175-146). The slices were then washed with 1X PBST and mounted on slide glass.

Brain slice preparation

P63-80 mice were anesthetized with isoflurane and decapitated. After brain

dissection, coronal slices of medial prefrontal cortex (300µm) were cut in ice-cold oxygenated sucrose-based cutting solution containing (in mM): 75 Sucrose, 76 NaCl, 2.5 KCl, 25 $NaHCO_3$, 25 Glucose, 1.25 NaH_2PO_4, 7 $MgSO_4$, 0.5 $CaCl_2$ with pH 7.3, and 310 mOsm by using vibratome 7000smz-2 (Campden instruments, England), and then recovered in the same solution for 30min at 33-34 °C. Slices were then transferred to a incubation chamber filled with oxygenated artificial cerebral spinal fluid (ACSF) containing (in mM): 124 NaCl, 2.5 KCl, 1.3 $MgCl_2$, 2.5 $CaCl_2$, 1.0 NaH_2PO_4, 26.2 $NaHCO_3$, 20 Glucose with pH 7.4 and 310 mOsm at room temperature and slices were kept in less than 7hrs before recordings.

Electrophysiology

Cells in prelimbic region were visualized with 80x and 20x magnification objective (Olympus) on the stage of upright microscope (BX61W1, Olympus) equipped with infrared-differential interference contrast optics in combination with digital camera (AquaCAM Pro/S3) and equipped with sCMOS camera for fluorescence imaging (Zyla, ANDOR). Patch microelectrodes were pulled from borosilicate glass (O.D.:1.5mm, I.D.: 1.10mm, WPI) on a Flaming-Brown micropipette puller model P-1000 (Sutter Instruments, USA). Patch microelectrodes had a resistance of 4-8MΩ. Signals were recorded using a patch-clamp amplifier (Multiclamp 700B, Axon Instruments, USA) and digitized with Digidata 1550A (Axon Instruments, USA) using Clampex software. Signals were amplified, sampled at 10 kHz, and filtered to 2 or 5 kHz. Pyramidal neurons were identified by large apical dendrites, and SOM & Pv interneurons were identified by tdTomato, YFP, or mcherry fluorescence expression. During current-clamp recordings for intrinsic

excitability and EPSP summation, membrane potential was held at -70mV with intracellular solution (in mM): 135 K-gluconate, 7 NaCl, 10 HEPES, 0.5 EGTA, 2 Mg-ATP, 0.3 Na_2-GTP, 10 Na-phosphocreatine with pH 7.3 and 295 mOsm. Current-clamp experiments were recorded 5min after obtaining whole-cell configuration. Action potentials (APs) were generated by injecting 500 ms current steps increasing by 50 pA. During voltage-clamp recordings for eEPSC eIPSC, sEPSC, and mEPSC, Cell membrane potential was kept at -70mV for AMPAR mediated EPSC, +40mV for NMDAR mediated EPSC, and 0mV for eIPSC with the following intracellular solution (in mM): 135 CsMS, 10 CsCl, 10 HEPES, 0.2 EGTA, 4 Mg-ATP, 0.4 Na_2-GTP with pH 7.3 and 295 mOsm. sIPSC and mIPSC were recorded at -60mV membrane holding potential with normal chloride intracellular solution (in mM): 110 CsMS, 40 CsCl, 2 $MgCl_26H_2O$, 0.1 $CaCl_22H_2O$, 10 HEPES, 1 EGTA, 2 Na-ATP, 0.4 Na-GTP and with high chloride intracellular solution (in mM): 150 CsCl, 2 $MgCl_26H_2O$, 0.1 $CaCl_22H_2O$ 10 HEPES, 1 EGTA, 2 Na-ATP, 0.4 Na-GTP respectively. Cells were voltage or current-clamped at each holding potential with liquid-junction potential correction of estimated 10.5 mV. During EPSC recording, to block inhibitory synaptic responses, 20 μM SR95531 (GABAzine, Tocris) was bath applied but for IPSC recording, 10 μM NBQX and 50 μM AP-5 (Tocris) were bath applied to block excitatory synaptic responses. For mEPSC and mIPSC, 1 μM tetrodotoxin (TTX, Abcam) was added to bath. To isolate NMDAR mediated EPSC, 10 μM NBQX (Tocris) was added to bath to block AMPAR mediated synaptic responses.

Optogenetics

In vitro slice stimulation: When virus for eNpHR3.0 was specifically expressed in Pv interneurons 4weeks after virus injection as described in viral targeting method, acute coronal slices of prelimbic in mPFC were prepared. Pv interneurons were identified by fluorescence labeling for optogenetic cellular manipulations. Di-synaptic inhibitory postsynaptic currents (IPSC) in pyramidal neurons were isolated by holding cells at 0mV and abolished by not only GABAA receptor antagonist GABAzine but also combination of AMPAR receptor antagonist NBQX and NMDA receptor antagonist AP-5. While electrically evoked di-synaptic IPSC were obtained, Pv interneuron mediated IPSC was isolated by calculating differentiation between total IPSC with and without 561 nm light-evoked suppression of Pv interneurons. In addition to this, while EPSP temporal summation in pyramidal neurons was recorded by 20 or 50Hz repetitive electrical stimulation, 561 nm light was delivered to suppress Pv interneurons to figure out its effect on excitation and inhibition temporal summation of excitatory neurons. 561 nm light pulse was delivered for 300-500ms with 1.5mW intensity.

Data analysis

All waveforms were analyzed in pClamp, Igor Pro, or LabVIEW with custom written scripts. In IgorPro, a Neuromatic package was used. All graphs were made with Prism 9. Synaptic currents were analyzed by pClamp. The sEPSC events were detected with Minhee Analysis Package (https://github.com/parkgilbong/Minhee_Analysis_Pack) using a detection threshold of 10 pA.

RESULTS

NMDAR hypofunction impairs PPI-related Pv interneuronal function, leading to sensorimotor gating deficits.

To better understand whether NMDAR dysfunction impairs modulation of PPI, I examined pharmacologically-induced NMDAR hypofunction mouse model which indicates defects in glutamatergic signals preferentially in Pv interneurons than other neurons.[20–24] I induced NMDAR hypofunction through the pharmacological approach by repetitive injection of 0.9 % saline (SA) as control group or mk-801 (MK) once-daily for 7 days systemically (Figure 1.1a). Acoustic startle response (ASR) trials which consist of 40 ms auditory startle pulses of variant decibels from 75- to 120- dB displayed no significant difference between SA and MK groups, which reveals that my NMDAR hypofunction mice are not affected in a hearing ability and motor reaction to sudden acoustic signals (Figure 1.2b). In PPI trials, consistent with previous studies, my MK group showed a significant reduction in PPI percentage of both 75- and 80-dB pre-pulse compared to SA group (Figure 1.2c). I also performed other behavioral tests in NMDAR hypofunction models, revealing hyper-locomotion in spontaneous activity and working memory impairment in an alteration test. However, elevated plus maze test showed no significant difference between SA and MK groups, indicating that PPI deficits and the other behavioral abnormalities are irrelevant to anxiety levels in my NMDAR hypofunction model (Figure 1.1b-d).

Next, to explore how Pv interneuronal function is implicated in PPI in mPFC, I investigated Pv interneuronal activity during ASR and PPI paradigms. I first

measured ASR or PPI-evoked c-fos expression of Pv interneurons in prelimbic region (PL). Mice were exposed to abovementioned ASR or PPI trials and then sacrificed 2 hours later. Imaging analysis for parvalbumin (PV) and c-fos expression showed significantly increased number (~ 10-fold) of c-fos positive Pv interneurons in PPI session compared to ASR session, which suggests that Pv interneurons in PL are strongly activated during PPI session (Figure 1.3). To further identify whether Pv interneuronal dysfunction induced by NMDAR hypofunction affects PPI between SA and MK groups, I investigated Pv interneuronal activation in PL after PPI trials. Mice were sacrificed 2 hours after PPI trials. In ANOVA analysis, while the number of c-fos positive cells was significantly reduced in MK compared to SA group, there was a huge decrease in the number of PV positive neurons in MK compared with SA group (~ 2-fold), leading to a reduced number of PV positive neurons that were merged with c-fos (Figure 1.4). Moreover, the proportion of merged neuron (PV and c-fos) in PV pool was significantly reduced in MK compared with SA group although there was no change in ratio of merged neuron in c-fos pool between SA and MK groups. These results suggest that NMDAR hypofunction considerably impairs PPI-related (not ASR) regulatory Pv interneuronal function without significant changes of c-fos activity in other neural circuitry associated with PPI modulation in PL mPFC.

To test if Pv interneuronal function is required to modulate PPI in mPFC, I attempted direct and specific regulation of Pv interneuron activity. Therefore, I utilized wireless optogenetic tools which are implantable and ultraminiaturized because the plexiglass cylinder enclosing a mouse in a startle chamber is too tight to access optic fibers. For Pv interneuronal modulation, Pv-Cre mice were injected in the mPFC with AAV-

Ef1α-DIO-eNpHR3.0 for optogenetic suppression or AAV-Ef1α-DIO-ChETA for optogenetic excitation. During PPI sessions, in Pv-Cre mice infected in the mPFC with AAV-Ef1α-DIO-eNpHR3.0 for 3 weeks, continuous optogenetic suppression of Pv interneurons in PL at each full-time 200ms PPI trial with yellow light induced a significant decrease in PPI percentage of 75 dB pre-pulse compared to PPI trials without yellow light (Figure 1.5b). These data consistently indicate that Pv interneuronal function is critical component that mediates PPI in mPFC.

Furthermore, to reverse PPI deficits in my NMDAR hypofunction model, Pv-Cre mice were infected in the mPFC for 3 weeks and then injected with 0.9 % saline (SA) or mk-801 (1.0 mg/kg) (MK) once a day for 1 week. I attempted excitation of Pv interneurons activity with wireless optogenetic blue light in PL. Continuous optogenetic stimulation of Pv interneurons with blue light for 200 ms full in each PPI trial in PL recovered PPI levels in MK to normal states (Pre MK) compared to PPI trials without blue light in MK (Figure 1.5c). Intriguingly, Pv interneuronal stimulation during pre-pulse or followed pulse respectively had no effect on rescue of PPI deficits in MK, and rather aggravated PPI levels (Figure 1.6). After PPI assay, to validate optical stimulation of Pv interneurons in PL, I confirmed an increase in c-fos expression of Pv interneurons (Figure 1.7). These results collectively suggest that reduced Pv interneuronal activity induced by NMDAR hypofunction is implicated in PPI defects which are rescued by excitation of PPI-related Pv interneuronal circuitry that specifically mediates sensorimotor gating in mPFC.

NMDAR hypofunction in Pv interneurons induced aberrant regulation of AMPAR, leading to hyperexcitation in mPFC network activity.

To better understand neural impairments in NMDAR hypofunction, I measured synaptic and neuronal properties of excitatory neurons and inhibitory interneurons by whole-cell recordings in PL mPFC in acute brain slices. To identify Pv interneurons, I examined Pv-Cre mice which are crossed with Cre-dependent $^{R26LSL\text{-}tdTomato}$ (Ai14) reporter line or injected by pAAV-Ef1α-DIO-anti {mCherry (stop)} to label Pv interneurons with a red fluorescent protein.[58] Pyramidal neurons (PNs) were morphologically identified by large apical dendrites. After I estimated PPI assay in SA and MK groups, I performed *ex vivo* recording of PNs and Pv interneurons. I first tested if NMDAR hypofunction is manifested in Pv interneurons. As NMDAR to AMPAR ratio was calculated by current ratio of NMDAR- and AMPAR-mediated evoked EPSCs at +40 and -70 mV holding respectively, this ratio analysis revealed a significant decrease in Pv interneurons in MK compared to SA group (Figure 2.1a), although there is no difference in NMDAR to AMPA ratio in PNs between SA and MK groups (Figure 2.1b). These results indicate that NMDAR hypofunction is selectively affected in Pv interneurons in my mouse models.

To further determine AMPAR-mediated synaptic strength onto Pv interneurons and PNs, I performed recording of spontaneous excitatory postsynaptic currents EPSC (sEPSCs). In sEPSCs, Pv interneurons in MK group revealed a significant decrease both in the amplitude and frequency of AMPAR-mediated synaptic currents compared to SA group (Figure 2.2a). Moreover, the amplitude I/O curve of AMPAR-mediated eEPSCs elicited lower slope of Pv interneurons in MK compared with SA

group (Figure 2.3a) but paired-pulse ratio of AMPAR-mediated eEPSC in Pv interneurons showed no significant difference between SA and MK group (Figure 2.3b). In contrast to these, AMPAR synaptic amplitude and frequency in PNs were not affected in my NMDAR hypofunction mode (Figure 2.2b). These results suggest that NMDAR hypofunction in Pv interneurons also causes downregulation of AMPAR in post-synapses (not pre-synapses) of Pv interneuron, leading to considerably attenuated glutamatergic input onto Pv interneurons in my mouse model. For information processing, Pv interneurons have a fundamental role of equalizing excitation and inhibition (E/I) ratio in mPFC microcircuits with proportional inhibition on neighboring excitatory neurons.[59–64]. I thus test if reduced synaptic strength in Pv interneurons affect E/I balance in mPFC network. The amount of evoked EPSCs and inhibitory postsynaptic currents (IPSCs) of layer 5 (L5) PNs was measured in response to electrical stimulation of layer 2 (L2) afferents with holding potential respectively at -70mV (EPSCs) or 0mV (IPSCs), and then was calculated as ratio of excitation to inhibition. MK showed increased E/I ratio compared to SA group, indicating hyperexcitability in PL network (Figure 2.4a).

I next examined if increased E/I ratio in MK group is caused by Pv interneuronal disinhibition onto PNs without changes in excitatory input onto PNs as shown above. Accordingly, spontaneous inhibitory postsynaptic currents (sIPSC) with network activity was measured in L5 PNs, resulting in a decrease in frequency but not amplitude of sIPSC in MK group compared to SA group (Figure 2.4b). In contrast, measurements of miniature inhibitory postsynaptic current (mIPSC) without network activity (with TTX application) revealed that there are no significant

differences in amplitude and frequency of mIPSC between SA and MK groups (Figure 2.5). This evidence suggests that hyperexcitability of PL in MK group is characterized by elevated E/I ratio due to reduction in activity-dependent release of GABAergic signaling but not alterations in excitation currents onto PNs. However, this attenuated release of GABAergic signaling would derive from various inhibitory interneurons surrounding L5 PNs in PL. In accordance with the weakened excitatory drive onto Pv interneurons, I assumed that inhibitory outputs from Pv interneurons would be a key component to be altered, consequently leading to disinhibition onto L5 PNs. To dissect Pv interneuron-mediated inhibitory synaptic outputs in PL microcircuits, I examined optogenetic silencing of Pv interneurons located in nearby L5 PNs with L2/3 afferent electrical stimulation while a L5 PN was clamped at membrane potentials of 0 mV to record evoked IPSC. Optogenetic suppression of Pv interneurons was determined by whole-cell recordings in HR3.0-expressing Pv interneurons (Figure 2.6a). Evoked IPSCs from L5 PNs were diminished by AMPA and NMDA receptor antagonists (NBQX and AP-5, respectively), underpinning di-synaptic evoked IPSCs (Figure 2.6b). eIPSC amplitude from L5 PNs was attenuated by silencing of Pv interneurons. This reduced amplitude was calculated as differentiation % between with and without silencing Pv interneuron. Interestingly, MK group revealed less differentiation % in eIPSC amplitude than SA group, thereby ensuring that diminished excitatory inputs onto Pv interneurons lead to attenuated Pv interneuronal inhibitory outputs onto PNs in MK group (Figure 2.7a). Alteration of Inhibitory output could be caused by modification of GABAergic release probability in axon terminal. To trigger GABAergic releases of Pv interneurons onto L5 PNs, ontogenetically evoked inhibitory postsynaptic currents

(oIPSCs) were measured in L5 PNs while illuminating blue light (470 nm) in an adjacent single Pv interneuron soma only. To record paired-pulse ratio (PPR) of oIPSC, I delivered two consecutive pulses with different inter-pulse intervals (50, 100, 150, 200 ms) respectively on Pv interneurons. PPR of oIPSC from L5 PN was calculated as the ratio of the peak amplitude of the second oIPSC to that of the first. There is no significant difference in oIPSC PPR of various inter-pulse intervals between SA and MK groups, which indicates that Pv interneuron-mediated GABAergic release probability is not affected in my NMDAR hypofunction model (Figure 2.7b). I further examined intrinsic excitability of PNs and Pv interneurons in SA and MK groups. Current-firing curve in PNs and Pv interneurons showed no differences between SA and MK group, respectively (Figure 2.8). This evidence collectively elucidate that reduced AMPAR synaptic strength (less inputs) onto Pv interneurons mediated by NMDAR hypofunction results in disinhibition (less outputs) onto L5 PNs, ultimately leading to hyperexcitability of PL network as E/I imbalance in my NMDAR hypofunction model.

Modulation of PV expression is implicated in regulation of AMPAR synaptic strength distinctively in Pv interneurons.

Of note, expression of PV protein is modulated by peroxisome proliferator activated receptor gamma coactivator 1α as a transcriptional coactivator, highly expressed in Pv interneurons.[65] Transcription of PGC-1α is also NMDAR-mediated Ca^{2+} influx-dependent, and in concert with other proteins, PGC-1α increases the transcription of PV.[46,66]

To test if NMDAR hypofunction causes loss of PV by reducing PGC-1α in Pv interneurons, I examined the level of PV and PGC-1α by Prelimbic (PL)-isolated western blot assay. Mice in SA or MK group were sacrificed a day after last injection. Consequently, MK group revealed significant reduction in PV associated with a considerable decrease in PGC-1α compared to SA group (Figure 3.1).

Psychiatric disease mouse models associated with Pv interneuronal dysfunction have suggested that a reduction in the levels of PV was the results of a decrease in PV immunoreactivity or loss of the number of Pv interneurons.[48,54,67,68]

I thus investigated if NMDAR hypofunction in Pv interneurons results in reduction in PV expression but is not likely to affect Pv interneuronal viability as toxicity which would alter the number of Pv interneurons. To test this, I examined immunohistochemistry to estimate the number of PV-positive cells and *Vicia Villosa Agglutinin* (VVA)-positive cells. VVA as a lectin has been applied to identify perineuronal nets (PNNs) which enclose Pv interneurons in a sheath, and VVA staining has been used as reliable marker for Pv interneuronal subpopulation.[69–72]

The number of PV-positive neurons showed a significant reduction in MK compared to SA group, although there is no difference in the number of VVA-positive neurons between SA and MK group. The difference in the number of double-labeled cells between SA and MK group was also notable (Figure 3.2b). Although most Pv interneurons are enwrapped with PNNs, PV and VVA overlapping does not always occur.[71,73] I thus determined the percentage of PV-positive neurons in VVA-positive pool. This indicates that identified PV-positive neurons are highly overlapped with VVA-positive neurons in normal SA group on average 80 % while MK group accounted for significantly 2-fold decrease in percentage (42 %) of PV-positive neurons in VVA-positive fraction compared to SA group (Figure 3.2b). These results suggest that NMDAR hypofunction downregulates PV protein by reduction in PGC-1α, which is a key component of Pv interneuronal dysfunction in my model.

Considering that my NMDAR hypofunction in Pv interneurons downregulated synaptic activity of AMPAR highly associated with reduction in PV, NMDAR function in Pv interneurons would be consequently the condition monitored by PV expression to regulate AMPAR-mediated synaptic changes.

To this end, we further hypothesized that synaptic changes of AMPAR in Pv interneurons are strongly modulated by the level of PV expression associated with NMDAR function. To investigate this hypothesis, I attempted to modulate PV expression by PL region specific overexpression or knockdown of PV through microinjection of adeno-associated viruses (AAVs) expressing pAAV-Ef1α-DIO-anti{mCherry-T2A-mPvalb) (stop)} (OX) or pAAV-U6-loxp-EGFP-loxp-mPalb-shR36-CFP (KD) respectively in Pv-cre mice. AAVs expressing empty vector

(pAAV-Ef1α-DIO-anti {mCherry (stop)}) (EM) or scrambled vector (pAAV-U6-loxp-CMV-EGFP-loxp-SCR-CMV-mcherry) (SCR) were used as a control. I examined PV quantification by PL-isolated western blot assay 3 weeks after virus injection, indicating that the levels of PV expression are regulated by PV OX as an increase (Figure 3.3a) or PV KD as a decrease (Figure 3.4a), respectively compared to PV EM or PV SCR as control.

I investigated whether recovery of PV expression might reverse impairments in NMDAR hypofunction. To elucidate this, PV OX viruses were administered to mice (bilateral injection into the PL) and then 2 weeks later (before complete expression of viruses), NMDAR hypofunction was induced by repetitive i.p injection of saline (SA) or mk-801 (MK) once-daily for a week. Reduced PV expression level in MK (EM_MK) was considerably restored to within normal range compared to SA group upon PV overexpression (OX_MK) (Figure 3.3d). Interestingly, ANOVA analysis revealed that this PV restoration markedly improved amplitude of AMPAR synaptic strength in Pv interneurons in OX_MK compared to EM_MK (no overexpression of PV) without affecting frequency of AMPAR (Figure 3.3d). These results explicate that reduction in PV induced by NMDAR hypofunction is associated with a decrease in AMPAR amplitude, which is enhanced by overexpression of PV without alteration of NMDAR activity.

In accordance with impairments in NMDAR hypofunction, I further addressed whether PV deficiency is sufficient to impair regulation of AMPA synaptic strength in Pv interneurons without affecting NMDAR function. I first examined if NMDAR function is affected by PV deficiency. The ratio of NMDAR- and AMPAR- mediated

evoked EPSCs (NMDA/AMPA ratio) showed no difference between PV SCR and KD group (Figure 3.4b). In AMPAR-mediated sEPSC, however, PV KD revealed a significant decrease in the amplitude without affecting the frequency compared to PV SCR group (Figure 3.4d). These results collectively demonstrate that regulation of AMPAR-mediated synaptic activity at postsynaptic sites of Pv interneurons exquisitely depends on the levels of PV expression, which is regardless of NMDAR function.

Modulation of PV expression is required to maintain PPI modulation in mPFC.

My NMDAR hypofunction (MK) and PV deficiency (PV KD) models shared a substantial decrease in AMPAR synaptic strength in Pv interneurons, which were significantly reversed to normal states each by overexpression of PV (in MK). Therefore, I investigated if improvement of AMPAR synaptic strength in Pv interneurons is associated with recovery of PPI deficits in my NMDAR hypofunction.

PV EM or OX viruses were administered to mice (bilateral injection into the PL) and then 2 weeks later (before complete expression of viruses), NMDAR hypofunction was induced by repetitive i.p injection of saline (SA) or mk-801 (MK) once-daily for a week (Figure 3.5a). Interestingly, this PV restoration (OX_MK) markedly improved PPI deficits compared to NMDAR hypofunction group with PV EM virus expression (EM_MK) although PPI in EM or OX group without NMDAR hypofunction was not affected (Figure 3.5b). Moreover, in accordance with PPI deficits in NMDAR hypofunction model (MK), PV KD mice indicated PPI impairments compared to PV SCR group (Figure 3.6). Taken together, these data elucidate that physiological role of PV expression involves PPI modulation, accompanied by synaptic changes of AMPAR in Pv interneurons.

Figure 1.1 NMDAR hypofunction model indicated several behavioral impairments.

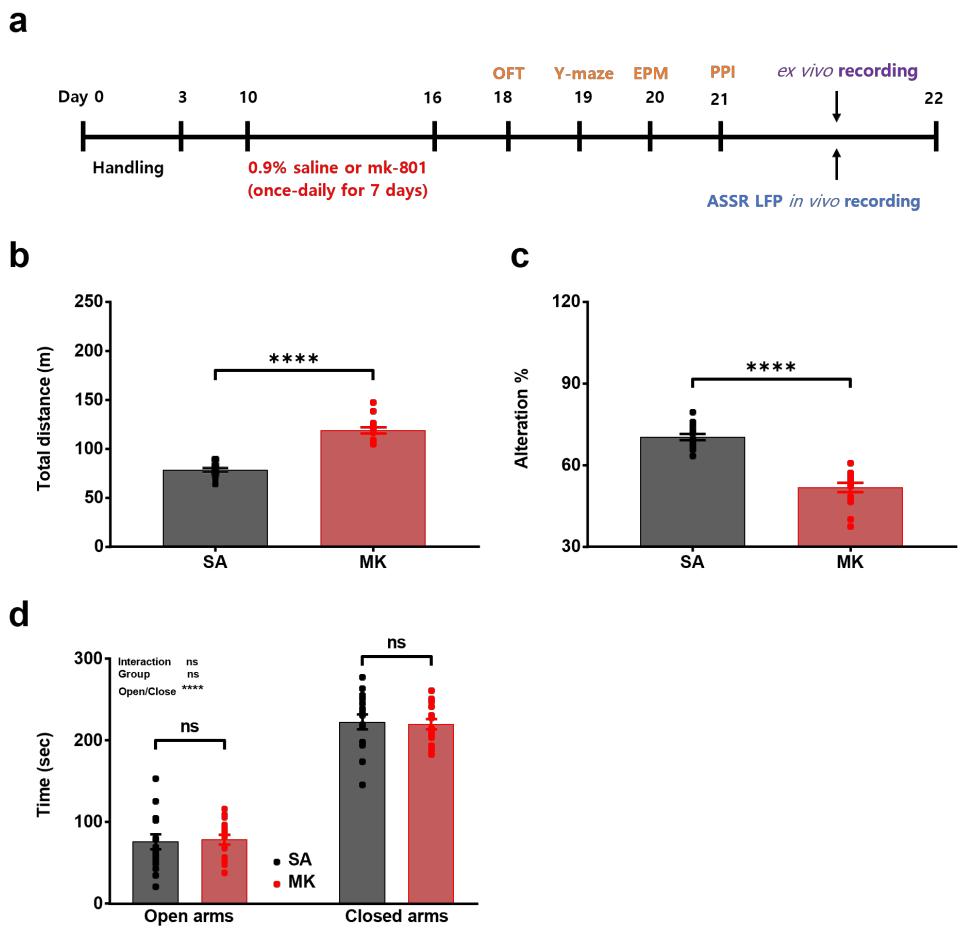

(a) Schematic experiment schedule in SA and MK group indicating after 0.9 % saline or mk-801 (1.0 mg/kg) once-daily for 7days were injected to mice, sequential several behavior assays were examined. Electrophysiological recording or *in vivo* LFP recording was performed after behavior screening.

(b-d) Bar graphs indicating open field test for locomotion activity as calculated by total distance moved (b), y-maze assay for working memory index as measured by proportion (%) of spontaneous alteration (c) and elevated plus

maze for anxiety levels as determined by difference of time spent between open- and closed- arms (d). Note that MK group showed hyperlocomotion activity and reduced spontaneous alteration % as impairments of working memory compared to SA group without affecting anxiety levels. (n= 15 mice [SA], n=15 mice [MK], SA-MK: open field test (p=<0.0001), y-maze (p=<0.0001), Unpaired t test, Two-tailed, Elevated plus maze: Interaction F (1, 28) = 0.05612, p=0.8145, Group F (1, 28) = 1.026, p=0.3197, open or close F (1, 28) = 167.7, p<0.0001, open arms (p=0.9690), closed arms (p=0.9613), Two-way repeated measures of ANOVA with Sidak's multiple comparisons test, ****p < 0.0001, ns, not significant, [bar graph]).

Figure 1.2 NMDAR hypofunction mice showed PPI impairments with normal ASR

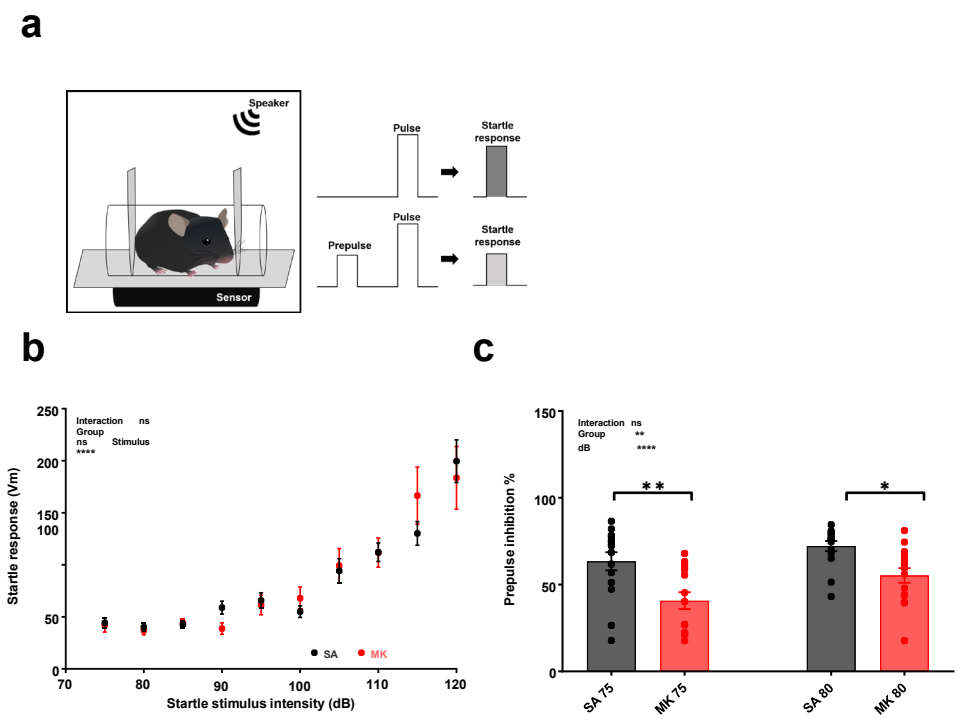

(a) Schematic diagram showing assay for acoustic startle response (ASR) with single pulse and pre-pulse inhibition (PPI) of ASR with pre-pulse.

(b) Basal ASR assay test across various stimulus intensities between 0.9 % saline [SA] or mk-801 (1.0 mg/kg) [MK] intraperitoneally (i.p) injected group once a day for 7 days. No significant difference between SA and MK group at various startle stimulus intensities as shown by mean-startle response (Vm). (n=13 mice [SA] and n=12 mice [MK], Interaction F (9, 98) = 1.319, p=0.2369, Group F (1, 12) = 0.008536, p=0.9279, Stimulus F (9, 108) = 32.42, p<0.0001, ****p < 0.0001, ns, not significant, Mixed-effects analysis with Sidak's multiple comparisons test [xy graph]).

(c) Bar graph comparing proportions (%) of PPI corresponding to each 75- or 80-dB pre-pulse in SA and MK group. Reduction of PPI %, meaning of increased response to pulse with pre-pulse, in MK group either to 75- or 80-dB pre-pulse. (n=15 mice [SA] and n=15 mice [MK], Interaction F (1, 28) = 1.395, p=0.2475, Group F (1, 28) = 11.97, p=0.0018, dB F (1, 28) = 23.26 , p<0.0001, SA vs. MK (75): p=0.0012, SA vs. MK (80): p=0.0168, *p < 0.05, **p < 0.01, ****p < 0.0001, ns, not significant, Repeated measures of Two Way ANOVA with Sidak's multiple comparisons test [bar graph])

Figure 1.3 Pv interneuronal function is implicated in PPI compared to ASR.

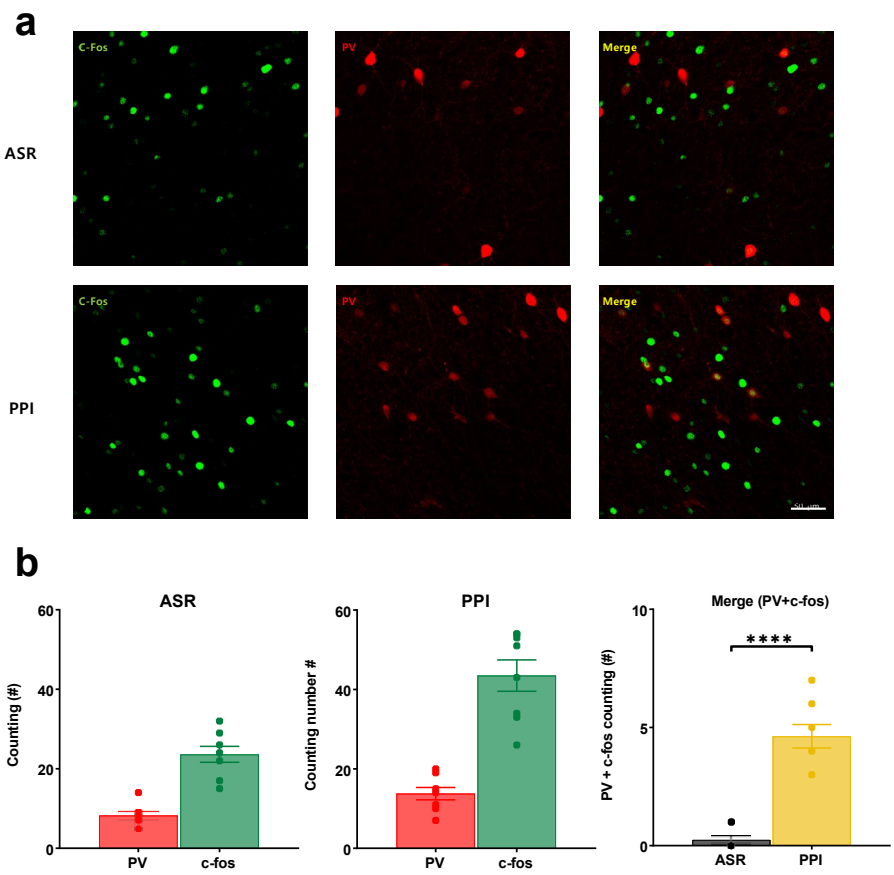

(a) Representative mPFC images showing c-fos positive(c-fos+)-neurons (A, D green), parvalbumin positive (PV+)-neurons (B, E, red), and merged images (C, F, yellow) from normal mice either with ASR (A, B, C, upper row) or PPI (D, E, F, lower row) session, respectively. Scale bar: 50 μm (A-F).

(b) Bar graphs showing counting estimation of PV+ and c-fos+ neurons in ASR session (left) and PPI session (middle) and double labeled neurons comparing between ASR and PPI session (right). Increased number of PV+ and c-fos+ neurons in PPI compared to ASR session, resulting in a

substantial increase in the number of double labeled neurons in PPI. (n=8 mice [PV] and n=8 mice [c-fos], ASR vs. PPI: p=<0.0001, ****p < 0.0001, Unpaired t test, Two-tailed, [bar graph])

Figure 1.4 NMDA hypofunction disrupts PPI-related regulatory Pv interneuronal function.

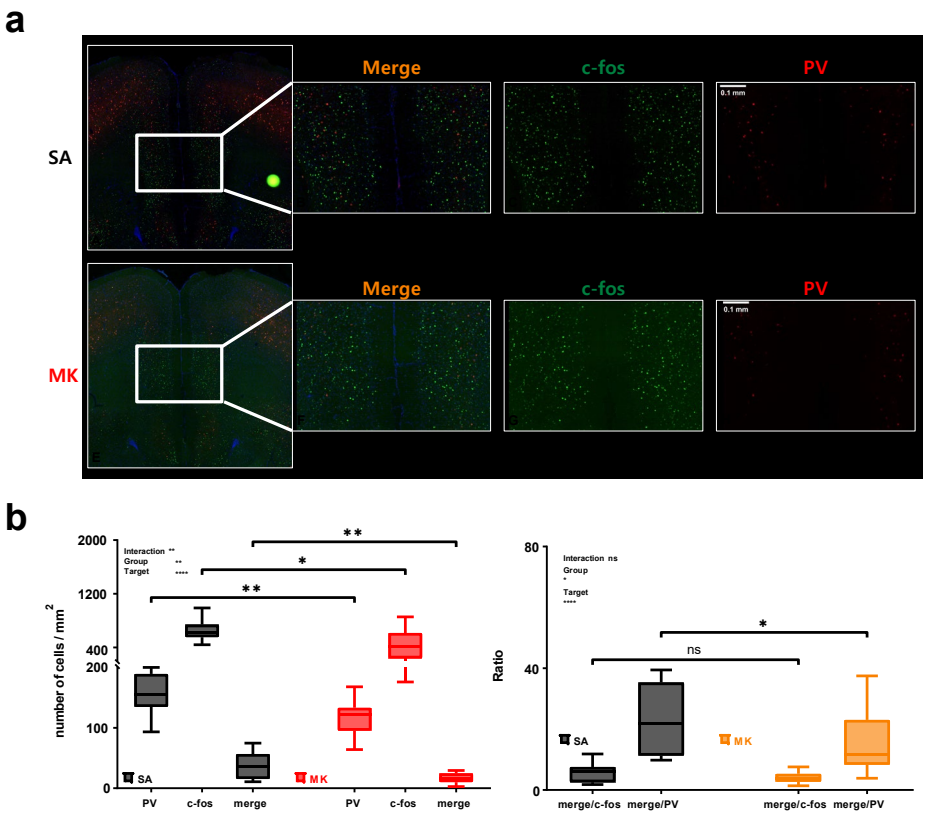

(a) Representative mPFC images (A, B) and prelimbic (PL)-targeted images indicating c-fos positive(c-fos+)-neurons (C, G green), parvalbumin positive (PV+)-neurons (D, H red), and merged images (B, F, yellow) between SA and MK group with PPI session. Scale bar: 100 μm (B-D, F-H).

(b) Decreased number of PV+, c-fos+, and double labeled neurons in MK group compared to SA group (top) (n=14 mice [PV] and n=14 mice [c-fos], Interaction F (2, 52) = 5.894, p=0.0049, Group F (1, 26) = 11.87, p=0.0020, Target F (1.024, 26.63) = 156.8, P<0.0001, SA-MK: PV (p=0.0056), c-fos

(p=0.0288), merge (p=0.0088), *p < 0.05, **p < 0.01, ****p < 0.0001, Repeated measures of Two Way ANOVA with Sidak's multiple comparisons test [bar graph]). Bar graph showing proportion (%) of double labeled neurons in each c-fos+ (merge/c-fos) or PV+ (merge/PV) pool as ratio. (bottom) A notable decrease in merge/PV ratio in MK group without affecting merge/c-fos ratio compared to SA group. (n=14 mice [merge/c-fos] and n=14 mice [merge/PV], Interaction F (1, 26) = 3.414, p=0.0761, Group F (1, 26) = 4.932, p=0.0353, Target F (1, 26) = 68.43, p<0.0001, SA-MK: merge/c-fos (p=0.7870), merge/PV (p=0.0113), *p < 0.05, ****p < 0.0001, ns, not significant, Repeated measures of Two Way ANOVA with Sidak's multiple comparisons test [bar graph])

Figure 1.5 Pv interneuronal function is required to modulate PPI in mPFC.

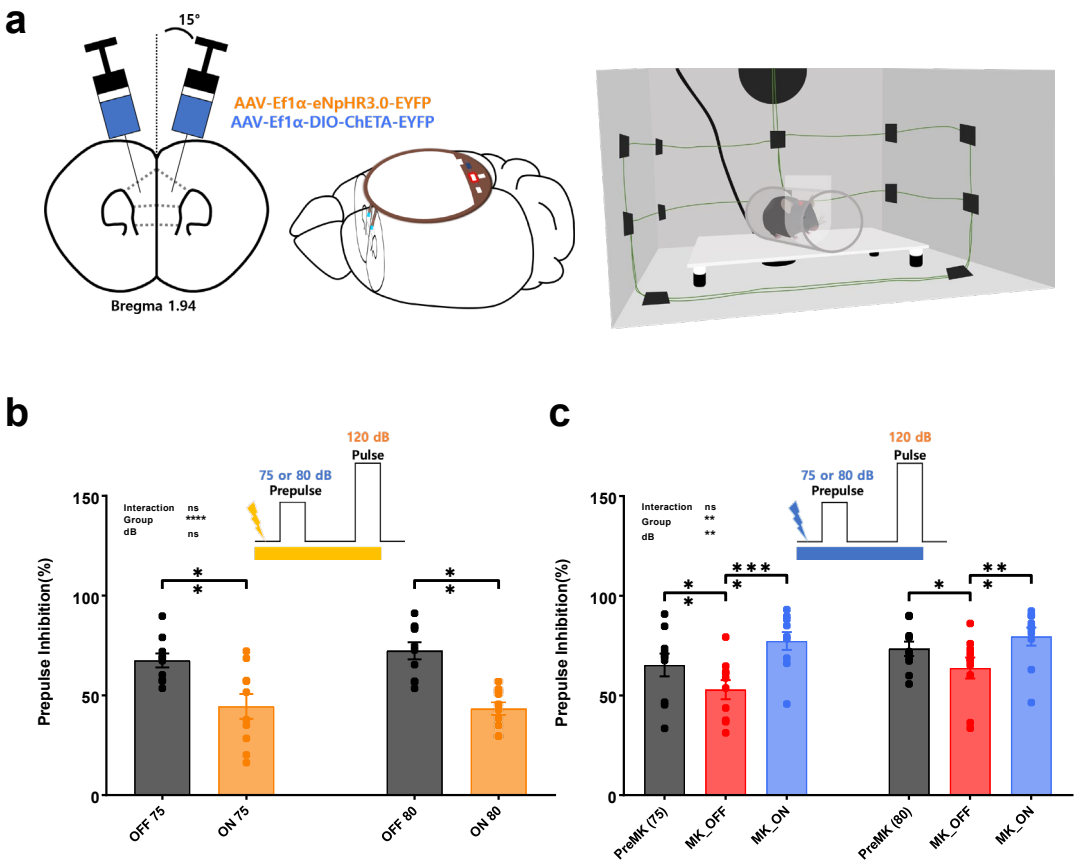

(a) Schematic diagram indicating virus injection of AAV-Ef1α-DIO-eNpHR3.0 for optogenetic suppression or AAV-Ef1α-DIO-ChETA for optogenetic excitation in PL-mPFC and wireless optogenetic modulation during PPI assay.

(b) Bar graph comparing PPI proportion (%) between LED OFF and ON (full length of one PPI trial) for optogenetic suppression of Pv interneurons in the same mouse during PPI session either with 75- or 80 dB pre-pulse.

Significantly decreased PPI % in LED ON group with 75- or 80-dB pre-pulse compared to LED OFF groups, respectively. (n=10 mice [OFF] and n=10 mice [ON], Interaction F (1, 9) = 0.5577 p=0.4742, Group F (1, 9) = 70.21, dB F (1, 9) = 0.3989, p=0.5434, OFF 75 vs. ON 75: p=0.0058, OFF 80 vs. ON 80: p=0.0013, **p < 0.01, ****p < 0.0001, ns, not significant, Two-way repeated measures of ANOVA with Sidak's multiple comparisons test [bar graph]).

(c) Bar graph comparing PPI proportion (%) to PreMK, MK_OFF, and MK_ON during PPI sessions either with 75- or 80 dB pre-pulse. PreMK described as mice before mk-801 repeated injection. MK_OFF or MK_ON represented as mice after mk-801 repeated injection, respectively with LED OFF or ON (full length of one PPI trial) for optogenetic excitation of Pv interneurons in the same mouse during PPI session. Note that MK_OFF showed a substantial decrease in PPI % compared to PreMK, which is considerably enhanced in MK_ON compared to MK_OFF. (n=10 mice [PreMK], n=10 mice [MK_OFF], and n=10 mice [MK_ON], Interaction F (2, 18) = 2.317, p=0.1272, Group F (2, 18) = 7.177, p=0.0051, dB F (1, 9) = 20.54, p=0.0014, PreMK 75 vs. MK_OFF: p=0.0014, MK_OFF 75 vs. MK_ON: p=<0.0001, PreMK 80 vs. MK_OFF: p=0.0112, MK_OFF 80 vs. MK_ON: p=0.0001, *p < 0.05, **p < 0.01, ****p < 0.0001, ns, not significant, Two-way repeated measures of ANOVA with Sidak's multiple comparisons test [bar graph]).

Figure 1.6 Lack of Pv interneuronal excitation aggravated PPI modulation.

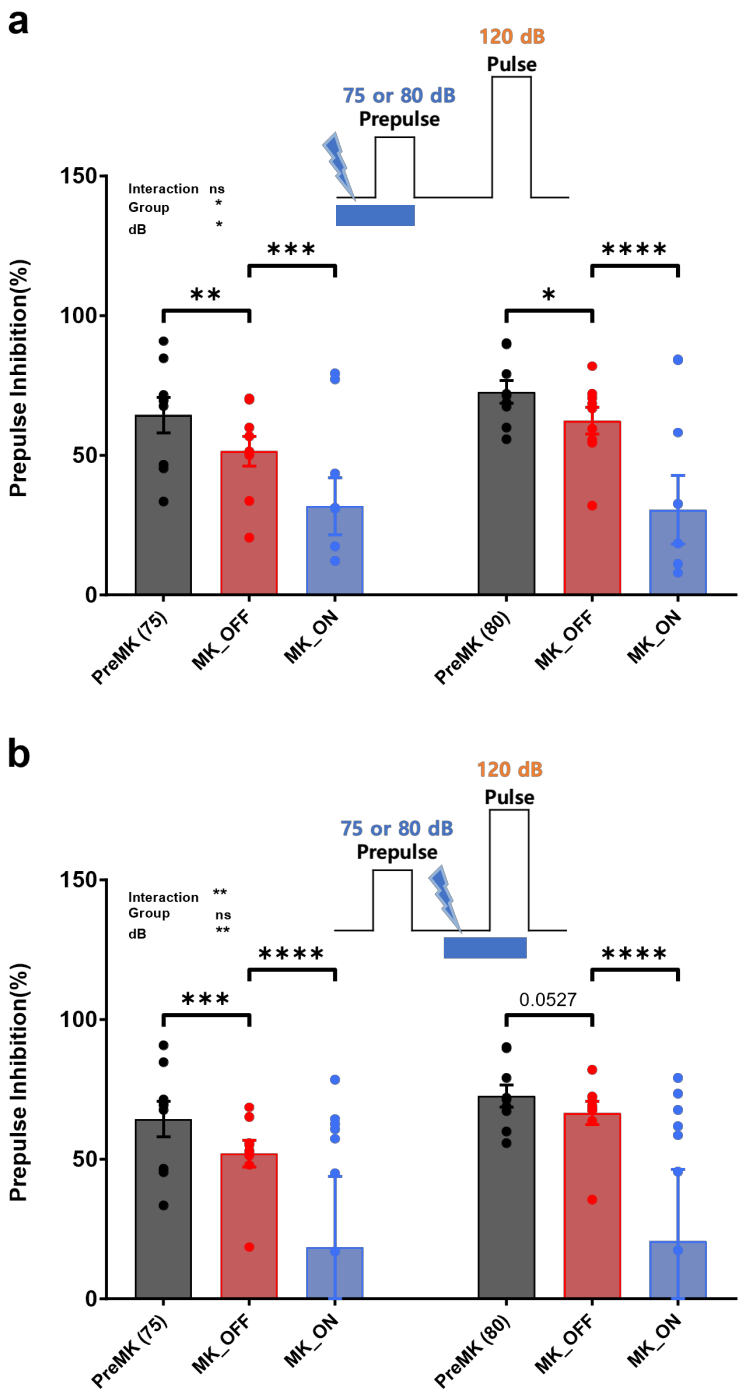

(a) Bar graph comparing PPI proportion (%) to PreMK, MK_OFF, and MK_ON during PPI sessions either with 75- or 80 dB pre-pulse. PreMK described as mice before mk-801 repeated injection. MK_OFF or MK_ON represented as mice after mk-801 repeated injection, respectively with LED OFF or ON (length of pre-pulse in each PPI trial) for optogenetic excitation of Pv interneurons in the same mouse during PPI session. Note that MK_OFF showed a substantial decrease in PPI % compared to PreMK, which is considerably aggravated in MK_ON compared to MK_OFF. (n= 9 mice [PreMK], n=9 mice [MK], n=9 mice [MK_ON], Interaction F (2, 16) = 3.106, p=0.0725, Group F (2, 16) = 5.725, p=0.0133, dB F (1, 8) = 5.435, p=0.0481, PreMK 75 vs. MK_OFF: p=0.0082, MK_OFF 75 vs. MK_ON: p=0.0002, PreMK 80 vs. MK_OFF: p=0.0357, MK_OFF 80 vs. MK_ON: p=<0.0001, *p < 0.05, **p < 0.01, ***p < 0.001, ****p < 0.0001, ns, not significant, Two-way repeated measures of ANOVA with Sidak's multiple comparisons test, [bar graph]).

(b) Bar graph comparing PPI proportion (%) to PreMK, MK_OFF, and MK_ON during PPI sessions either with 75- or 80 dB pre-pulse. MK_OFF or MK_ON represented as mice after mk-801 repeated injection, respectively with LED OFF or ON (length of followed pulse in each PPI trial) for optogenetic excitation of Pv interneurons in the same mouse during PPI session. Note that MK_OFF showed a substantial decrease in PPI % with 75- dB pre-pulse (subtle reduction in PPI % with 80-dB pre-pulse) compared to PreMK, which is notably deteriorated in MK_ON compared to MK_OFF. (n= 9 mice [PreMK], n=9 mice [MK], n=9 mice [MK_ON],

Interaction F (2, 16) = 7.001, p=0.0065, Group F (2, 16) = 2.711, p=0.0968, dB F (1, 8) = 21.26, p=0.0017, PreMK 75 vs. MK_OFF: p=0.0002, MK_OFF 75 vs. MK_ON: p=<0.0001, PreMK 80 vs. MK_OFF: p=0.0527, MK_OFF 80 vs. MK_ON: p=<0.0001, **p < 0.01, ****p < 0.0001, ns, not significant, Two-way repeated measures of ANOVA with Sidak's multiple comparisons test, [bar graph]).

Figure 1.7 C-fos expression in Pv interneurons was increased by wireless optogenetic Pv interneuronal excitation in mPFC.

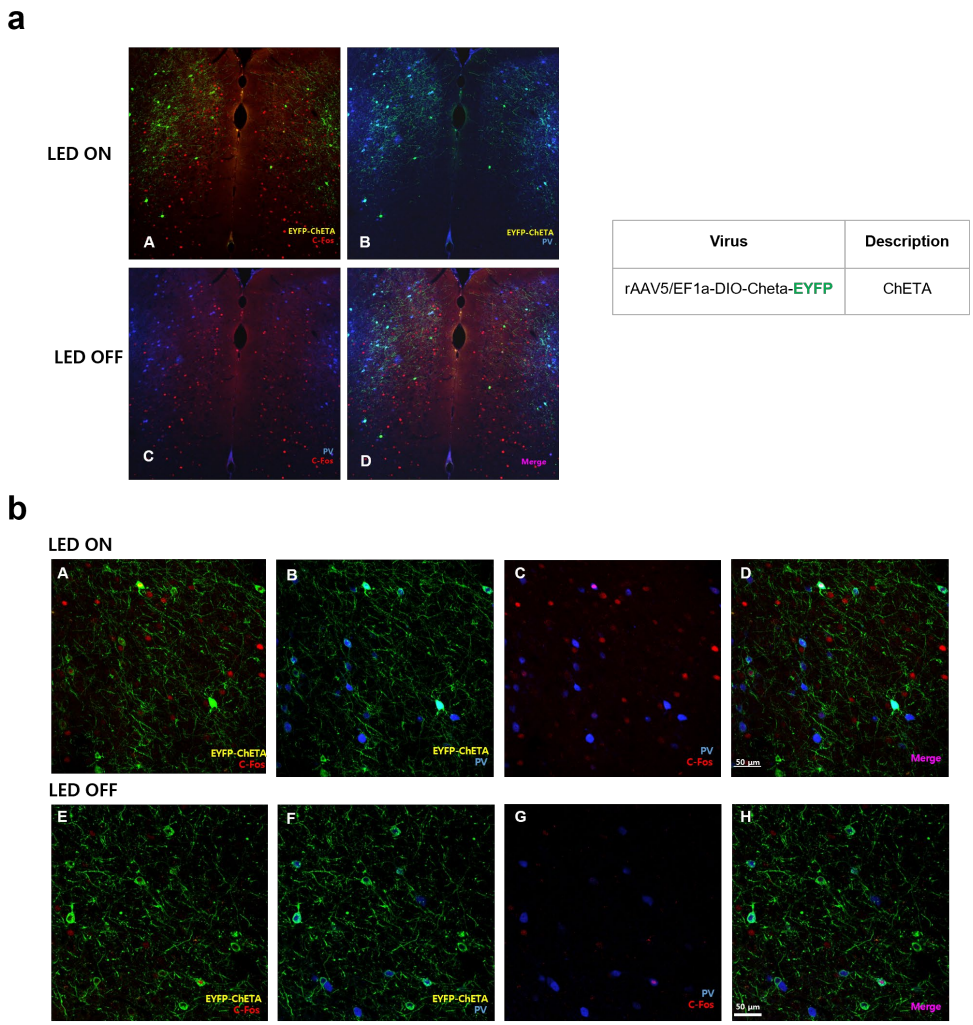

(a) After wireless optogenetic Pv excitation during PPI session, to validate whether Pv interneurons in the prelimbic region (PL) were activated with optogenetic Pv excitation, I examined c-fos expression in Pv interneurons in PL 1hr after LED ON compared to LED OFF (without optogenetic Pv excitation). Representative mPFC images (A-D) indicating ChETA positive (ChETA+) neurons double labeled with c-fos positive (c-fos+) (A) or

parvalbumin positive (PV+) (B) neurons, co-labeling of PV+ and c-fos+ neurons (C), and merged with ChETA+, PV+, and c-fos+ neuron (D).

(b) Prelimbic (PL)-targeted images (A-H) indicating ChETA positive (ChETA+) neurons double labeled with c-fos positive (c-fos+) (A, E) or parvalbumin positive (PV+) (B, F) neurons, co-labeling of PV+ and c-fos+ neurons (C, G), and merged with ChETA+, PV+, and c-fos+ neuron (D, H) in LED ON (upper row) and LED OFF (bottom row) with PPI session. Scale bar: 50 μm (A-H).

Figure 1.8 NMDAR antagonisms induced NMDAR hypofunction specifically, in Pv interneurons.

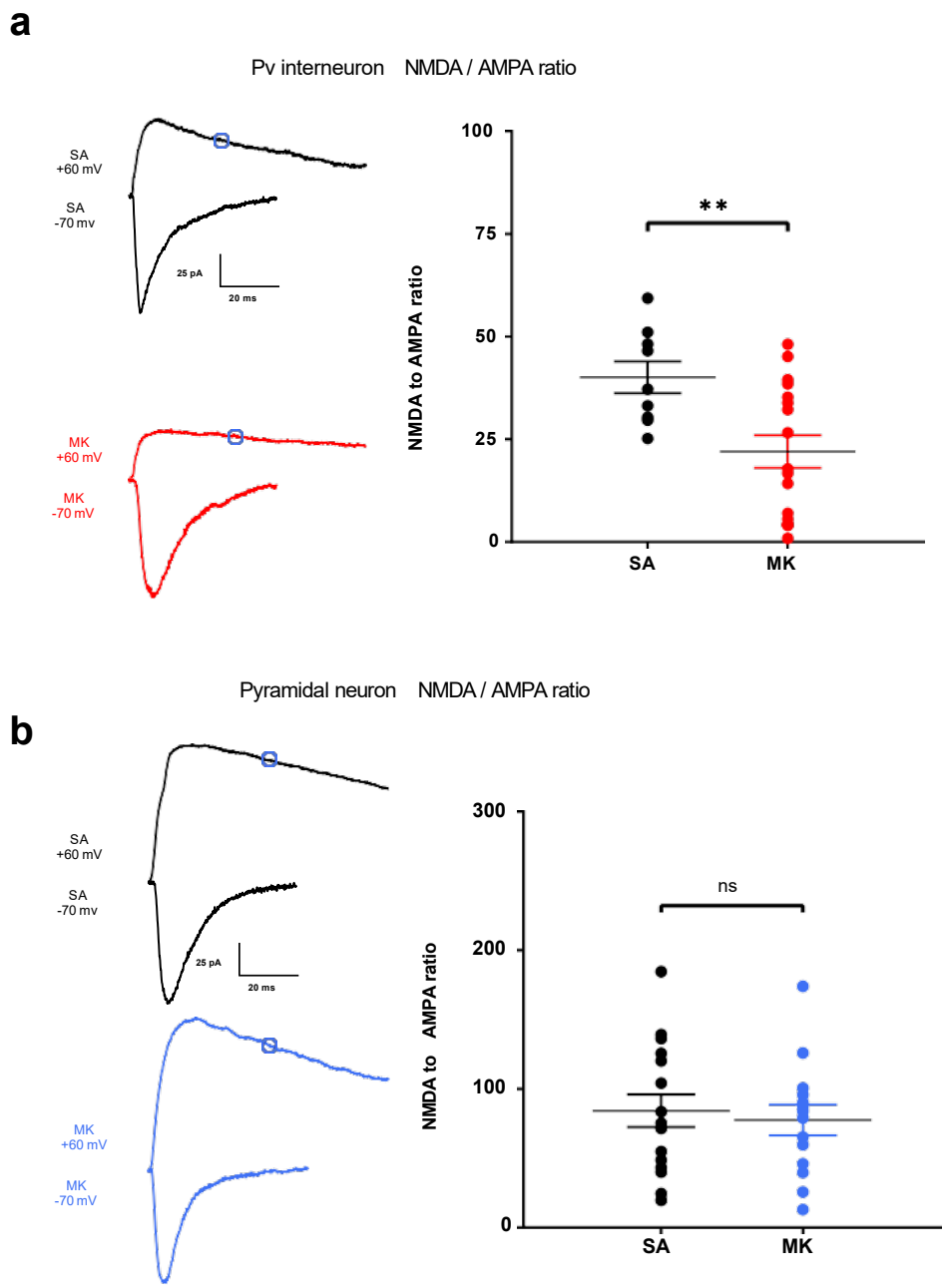

(a) Representative traces of NMDAR- and AMPAR- mediated evoked EPSC during voltage clamp respectively at + 60 mV and -70 mV in SA and MK

groups (left). Bar graph indicating decreased ratio of NMDA- and AMPAR-mediated evoked EPSCs in Pv interneuron in MK compared to SA group. (n=9 [SA], n=17 [MK], SA vs. MK: p=0.0071, **p < 0.01, Unpaired t test, Two-tailed [bar graph]).

(b) Representative traces of NMDAR- and AMPAR- mediated evoked EPSC during voltage clamp respectively at + 60 mV and -70 mV in SA and MK groups (left). Normal ratio of NMDA- and AMPAR- mediated evoked EPSCs in PNs in MK compared to SA group. (n=16 [SA], n=14 [MK], SA vs. MK: p=0.689, ns, not significant, Unpaired t test, Two-tailed [bar graph]).

Figure 1.9 NMDAR hypofunction in Pv interneurons impaired AMPAR regulation without affecting AMPAR of PNs.

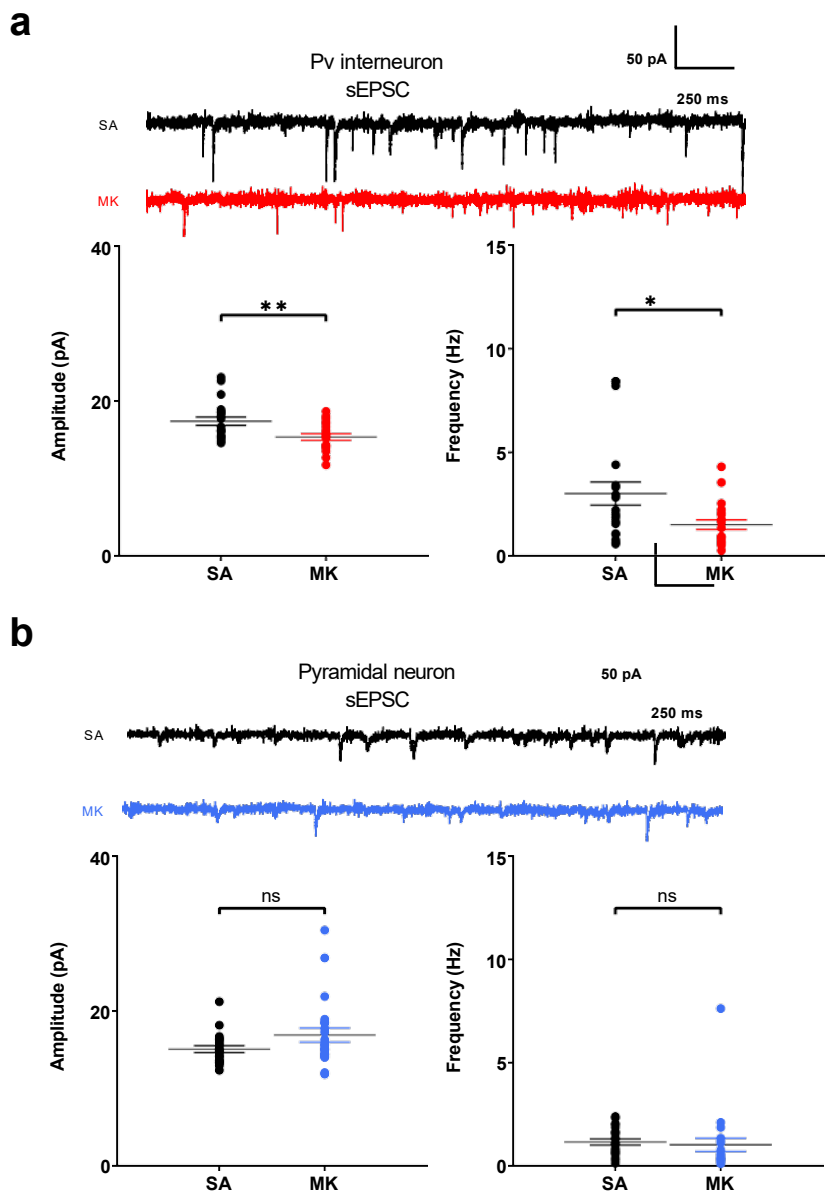

(a) Representative traces of AMPAR-mediated sEPSC at -70 mV voltage clamp recording in Pv interneurons between SA and MK group (top). Bar graphs

showing a significant decrease in the amplitude and frequency of AMPAR-mediated sEPSC in MK compared to SA group. (n=20 [SA], n=20 [MK], SA vs. MK (amplitude): p=0.0092, SA vs. MK (frequency): p=0.0223, *p < 0.05, **p < 0.01, Mann Whitney test, Two-tailed [bar graph]).

(b) Representative traces of AMPAR-mediated sEPSC at -70 mV voltage clamp recording in PNs between SA and MK group (top). Bar graphs showing no difference in the amplitude and frequency of AMPAR-mediated sEPSC between SA and MK group (n=22 [SA], n=23 [MK], SA vs. MK (amplitude): p=0.1013, SA vs. MK (frequency): p=0.063, ns, not significant, Mann Whitney test, Two-tailed [bar graph]).

Figure 1.10 NMDAR hypofunction impaired evoked AMPAR synaptic strength without affecting release probability of AMPAR.

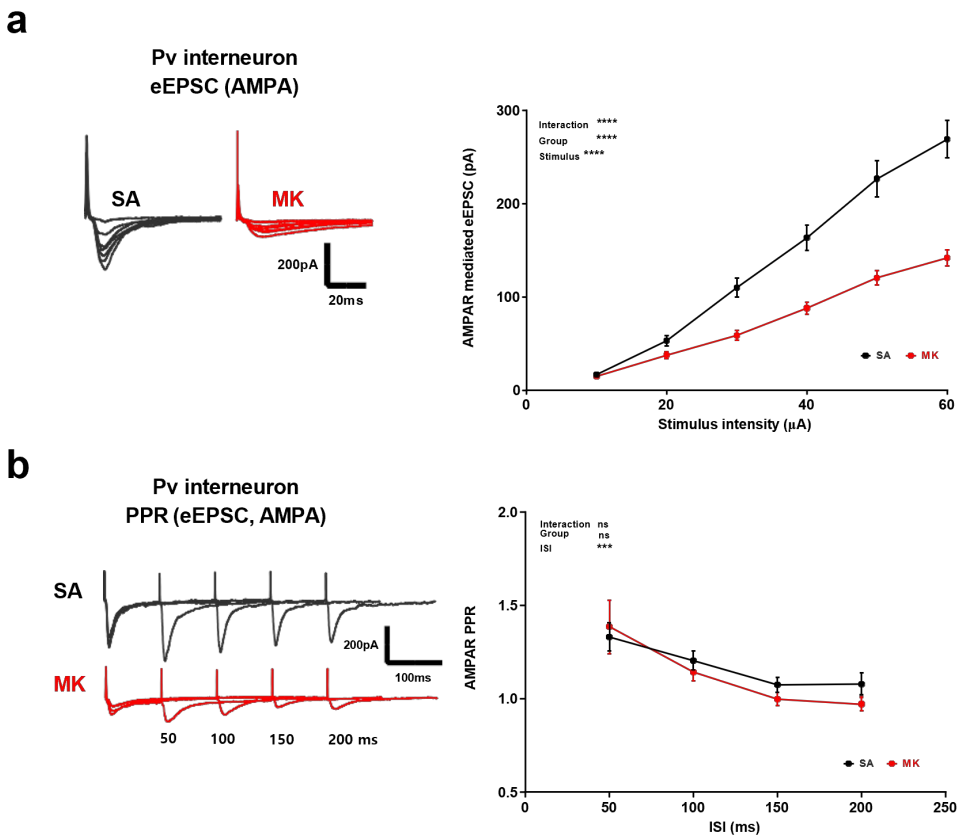

(a) Representative traces of AMPAR-mediated evoked EPSC (eEPSC) during voltage clamp at -70 mV in SA and MK group (top). Amplitude input-output (I/O) curve of AMPAR-mediated eEPSC elicited lower slope in MK compared with SA group (bottom). (n= 22 [SA], n=40 [MK] Interaction F (5, 300) = 30.16, p<0.0001, Group F (1, 60) = 39.53, p<0.0001, intensity F (5, 300) = 265.9, p<0.0001, ****p < 0.0001, Two-way repeated measures of ANOVA with Sidak's multiple comparisons test, [xy graph]).

(b) Representative traces of AMPAR-mediated eEPSC in response to paired-

pulse stimulation at the 50, 100, 150, or 200 ms inter-stimulus interval (ISI) (top). Calculation of paired-pulse ratio (2^{nd} / 1^{st} eEPSC) in each ISIs showed no difference between SA and MK group (bottom). (n= 22 [SA], n=40 [MK] Interaction F (3, 144) = 0.3807, p=0.7670, Group F (1, 48) = 0.4196, p=0.5202, Interval F (3, 144) = 7.401, p=0.0001, ***p < 0.001, ns, not significant, Two-way repeated measures of ANOVA with Sidak's multiple comparisons test, [xy graph]).

Figure 1.11 Pv interneuronal disinhibition onto PNs leads to E/I imbalance.

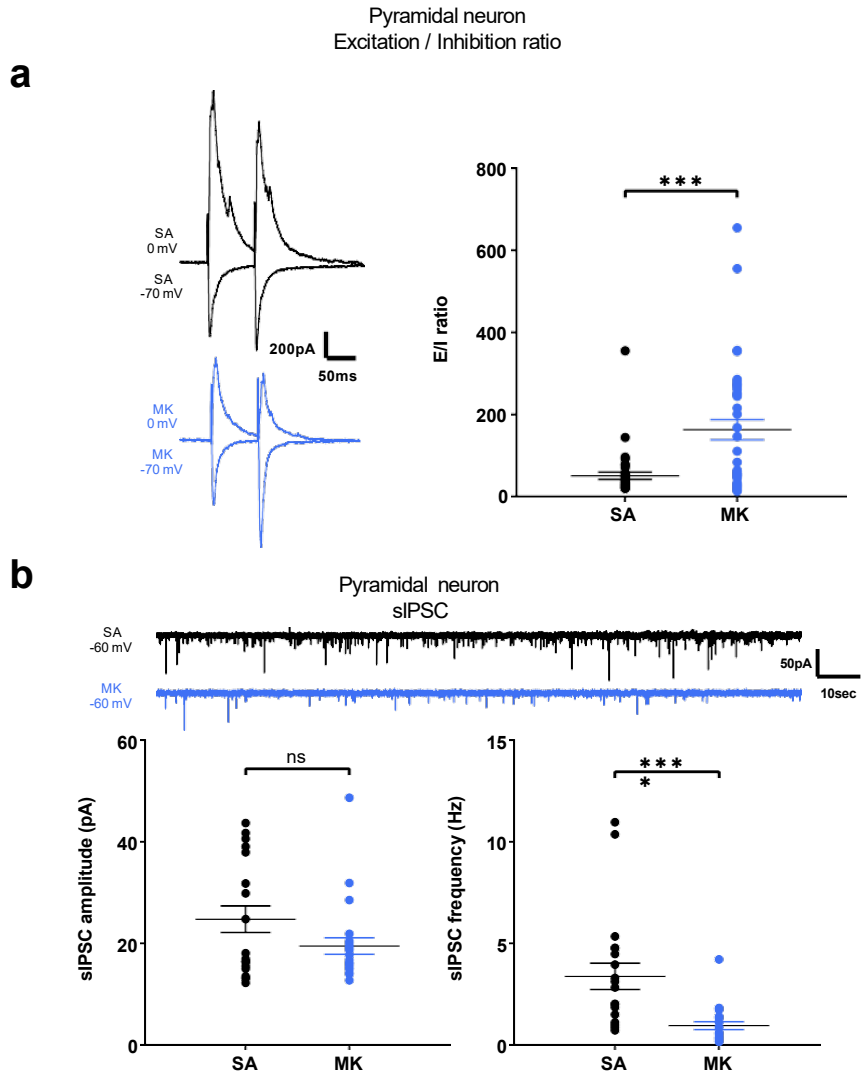

(a) Representative traces of evoked EPSCs to evoked IPSCs sequences at each -70 and 0 mV holding potential in voltage clamp recording in PNs between SA and MK group (left). Average excitation-inhibition (E-I) ratio in PNs was substantially increased in MK compared to SA (left). (n=39 [SA], n=39

[MK], SA vs. MK: p=0.0001, ***p < 0.001, Mann Whitney test, Two-tailed [bar graph]).

(b) Representative traces of sIPSC from PNs in voltage clamp at -60 mV between SA and MK group (top). Bar graphs displaying the frequency but not the amplitude of sIPSC in PNs was notably reduced in MK compared to SA group (bottom). (n=20 [SA], n=23 [MK], SA vs. MK (amplitude): p=0.4048, SA vs. MK (frequency): p=<0.0001, ****p < 0.0001, ns, not significant, Mann Whitney test, Two-tailed [bar graph]).

Figure 1.12 NMDAR hypofunction had no effect on GABA release probability and GABA receptor property onto PNs.

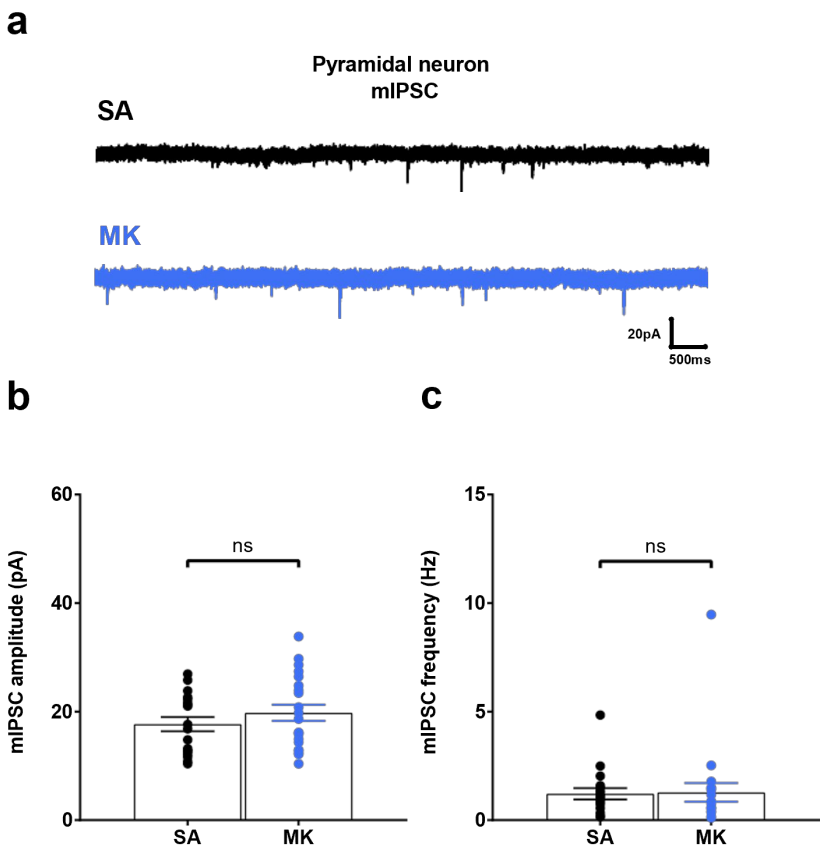

(a) Representative traces of miniature IPSC (mIPSC) from PNs in voltage clamp at -60 mV without network activity by TTX (1μM) application between SA and MK group.

(b) Normal amplitude of sIPSC from PNs in MK. (n=18 [SA], n=21 [MK], SA vs. MK: p=0.3245, ns, not significant, Mann Whitney test, Two-tailed, [bar graph]).

(c) Normal frequency of sIPSC from PNs in MK. (n=18 [SA], n=21 [MK], SA vs. MK: p=0.5349, ns, not significant, Mann Whitney test, Two-tailed, [bar

graph]).

Figure 1.13 Validation of Pv interneuronal optogenetic suppression by NpHR 3.0

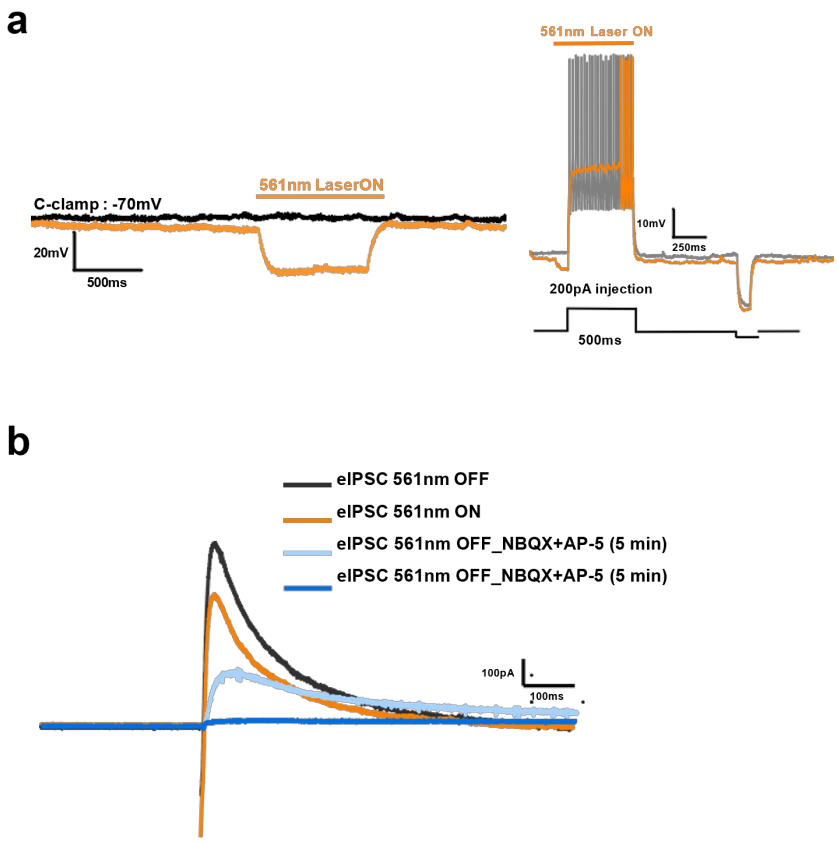

(a) Hyperpolarization in NpHR 3.0 expressing Pv interneurons evoked by yellow (λ = 561 nm) light-on (yellow) or not by light-off (black) at -70 mV current clamp (left). Reduced firing discharges induced by depolarization of 200 pA injection in NpHR 3.0 expressing Pv interneurons evoked by yellow (λ = 561 nm) light-on (yellow) or not by light-off (black) at -70 mV current clamp (right).

(b) Representative traces of di-synaptic eIPSCs in PNs at 0 mV voltage clamp in response to electrical stimulation of L 2/3 (black). Di-synaptic IPSCs

were slightly decreased by silencing Pv interneurons with yellow light-on (yellow) and were fully blocked by bath application of NBQX and AP-5 (blue).

Figure 1.14 In NMDAR hypofunction, Pv interneuronal inhibitory synaptic output onto PNs was reduced without affecting GABA release probability.

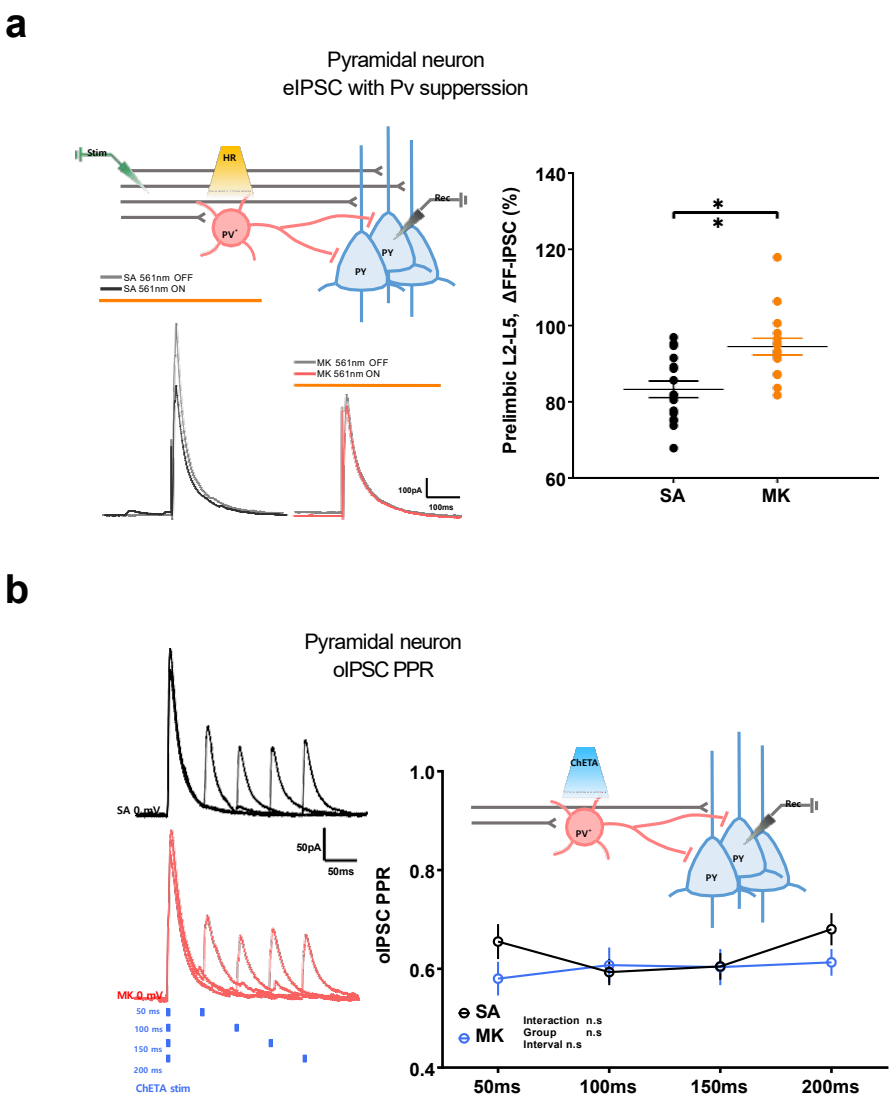

(a) Schematic diagram of evoked IPSC (eIPSC) from PNs with optogenetic suppression of Pv interneurons (left, top). Representative traces of di-synaptic evoked IPSCs from PNs with 0 mV holding potential induced by layer 2-3 electrical stimulation in SA and MK group either with yellow

light-off (OFF) or light-on (ON) (left, bottom). Bar graph showing proportion (%) of attenuated amplitudes of di-synaptic evoked IPSCs from PNs by silencing Pv interneurons in SA and MK group (right). Note that MK group showed an increase in percent of attenuated amplitudes, indicating that Pv interneuron-mediated eIPSCs were significantly weaken in MK compared to SA group. (n=16 [SA], n=16 [MK], SA vs. MK: p=0.0011, **p < 0.01, Unpaired t test, Two-tailed [bar graph]).

(b) Schematic diagram of optogenetically evoked IPSC (oIPSC) from PNs with optogenetic excitation of Pv interneurons (left, inlet). Representative traces of oIPSC from PNs at 0 mV holding potential in response to paired-pulse optical stimulation of Pv interneurons at the 50, 100, 150, or 200 ms inter-stimulus interval (ISI) in SA and MK group (right). Calculation of paired-pulse ratio (2^{nd} / 1^{st} eEPSC) (PPR) of Pv interneuron-mediated oIPSC each at 50, 100, 150, 200 ms ISI showed no difference between SA and MK group (left). (n=14 [SA], n=19 [MK], Interaction F (3, 93) = 1.599, p=0.1949, Group F (1, 31) = 0.8248, p=0.3708, interval F (2.846, 88.22) = 1.368, p=0.2585, ns, not significant, Repeated measures of Two-Way ANOVA with Sidak's multiple comparison [xy graph]).

Figure 1.15 Intrinsic excitability of PNs and Pv interneurons was not affected by NMDAR hypofunction.

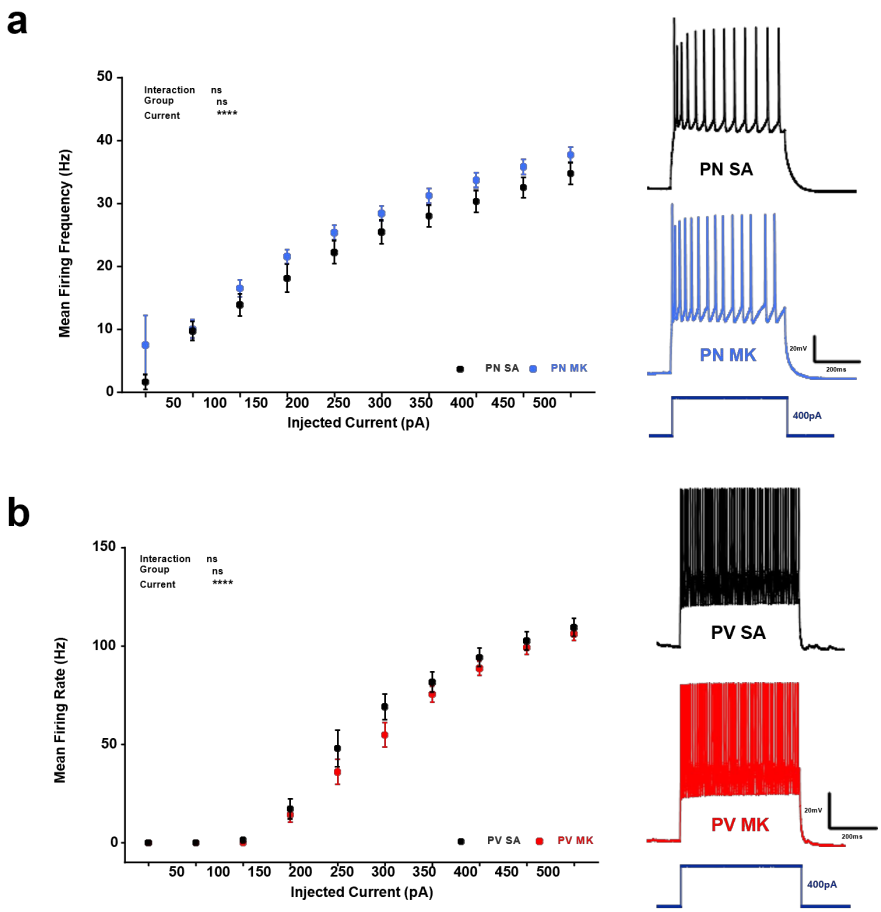

(a) Input / output (I/O) curve of mean firing frequency (Hz) from PNs across injected current steps, indicating no difference between SA and MK group (left). (n=15 [SA], n=20 [MK], Interaction F (9, 297) = 0.4957, p=0.8771, Group F (1, 33) = 2.522, p=0.1218, Current F (2.017, 66.57) = 127.9, p<0.0001, ****p < 0.0001, ns, not significant, Two-way repeated measures of ANOVA with Sidak's multiple comparisons test, [xy graph]). Representative traces of voltage response to 400pA current injection during

500ms in PNs in SA and MK group (right).

(b) Input / output (I/O) curve of mean firing frequency (Hz) from Pv interneurons across injected current steps, indicating no difference between SA and MK group (left). (n=22 [SA], n=22 [MK], Interaction F (9, 378) = 0.9698, p=0.4646, Group F (1, 42) = 1.273, p=0.2657, Current F (1.652, 69.40) = 323.7, p<0.0001, ****p < 0.0001, ns, not significant, Two-way repeated measures of ANOVA with Sidak's multiple comparisons test, [xy graph]). Representative traces of voltage response to 400pA current injection during 500ms in Pv interneurons in SA and MK group (right).

Figure 1.16 NMDAR hypofunction reduced PV protein levels through PGC-1α deficit.

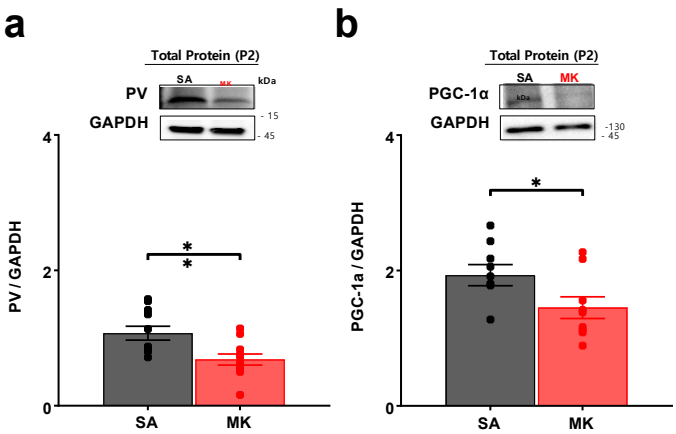

(a) Immunoblot analysis of PV protein levels in mPFC prepared from SA and MK group. Bar graphs indicating summary of quantification of PV protein levels. Note that MK group showed a substantial decrease in PV levels compared to SA group. (PV, n=11 [SA], n=11 [MK], SA vs. MK: p=0.0076, **p < 0.01, Unpaired t test, Two-tailed [bar graph]).

(b) Immunoblot analysis of PGC-1α protein levels in mPFC prepared from SA and MK group. Bar graphs indicating summary of quantification of PGC-1α protein levels. Note that MK group showed a substantial decrease PGC-1α levels compared to SA group. (PGC-1α, n=9 [SA], n=9 [MK], SA vs. MK: p=0.0477, *p < 0.05, Unpaired t test, Two-tailed [bar graph]).

Figure 1.17 Reduction of PV expression but not loss in the number of Pv interneurons in NMDAR hypofunction.

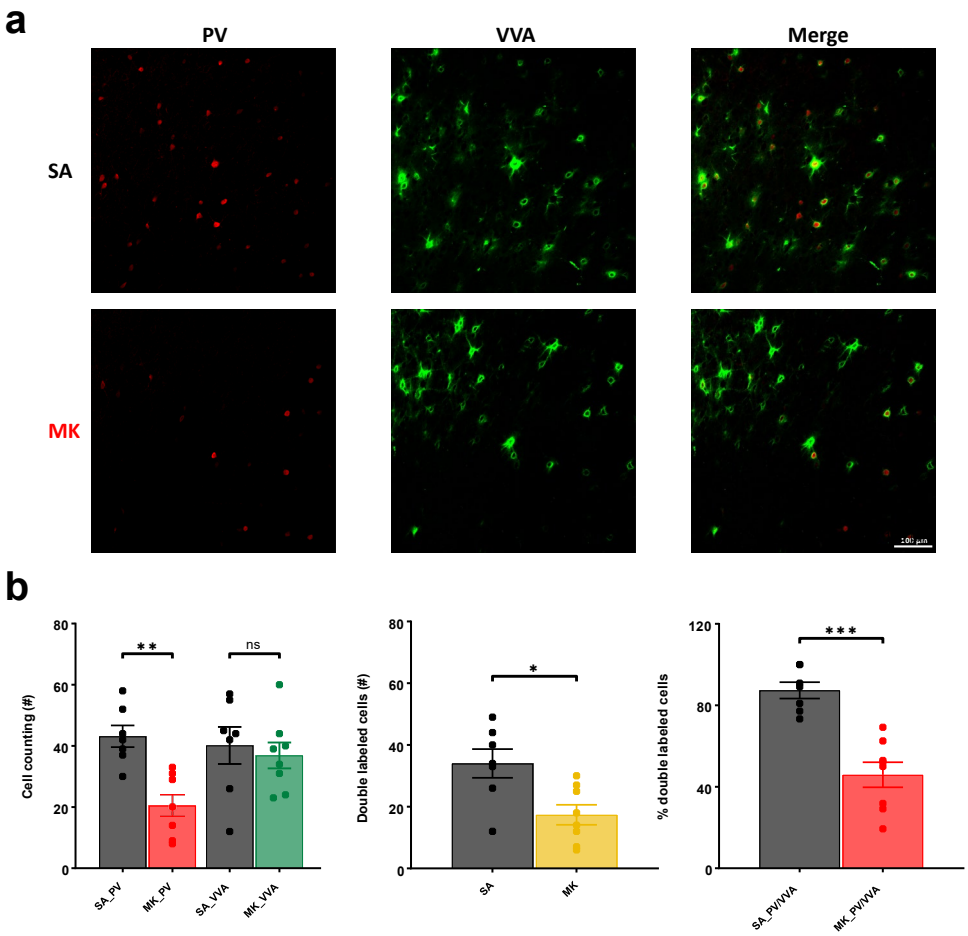

(a) Representative mPFC images showing PV positive (PV+)-neurons (A, D red), VVA positive (VVA+)-neurons (B, E, green), and merged images (C, F, yellow) between SA (A-C, upper row) and MK group (D-F, middle row). Scale bar: 100 μm (A-F).

(b) Bar graphs showing counting estimation of PV+ or VVA+ neurons (right, bottom row), double labeled neurons (middle, bottom row), and proportion

(%) of PV+ neurons in VVA+ neurons (right, bottom row). Note that MK group revealed a substantial decrease in the number of PV+ and double labeled neurons except VVA+ neurons compared to SA group (n=7 mice [SA], n=8 mice [MK], SA_PV vs. MK_PV: p=0.006, SA_VVA vs. MK_VVA: p=0.9519, Ordinary one-way ANOVA with Tukey's multiple comparisons test F (3, 26) = 5.465, SA vs. MK (double labeled neurons): p=0.0104, Unpaired t test, Two-tailed, *p < 0.05, **p < 0.01, ns, not significant [bar graph]), resulting in reduced percent of PV+ neurons in VVA+ neuron pool in MK. (n=7 mice [SA], n=8 mice [MK], SA_PV/VVA vs. MK_PV/VVA: p=0.0001, ***p < 0.001, Unpaired t test, Two-tailed [bar graph]).

Figure 1.18 PV overexpression enhanced AMPA regulation in NMDAR hypofunction model.

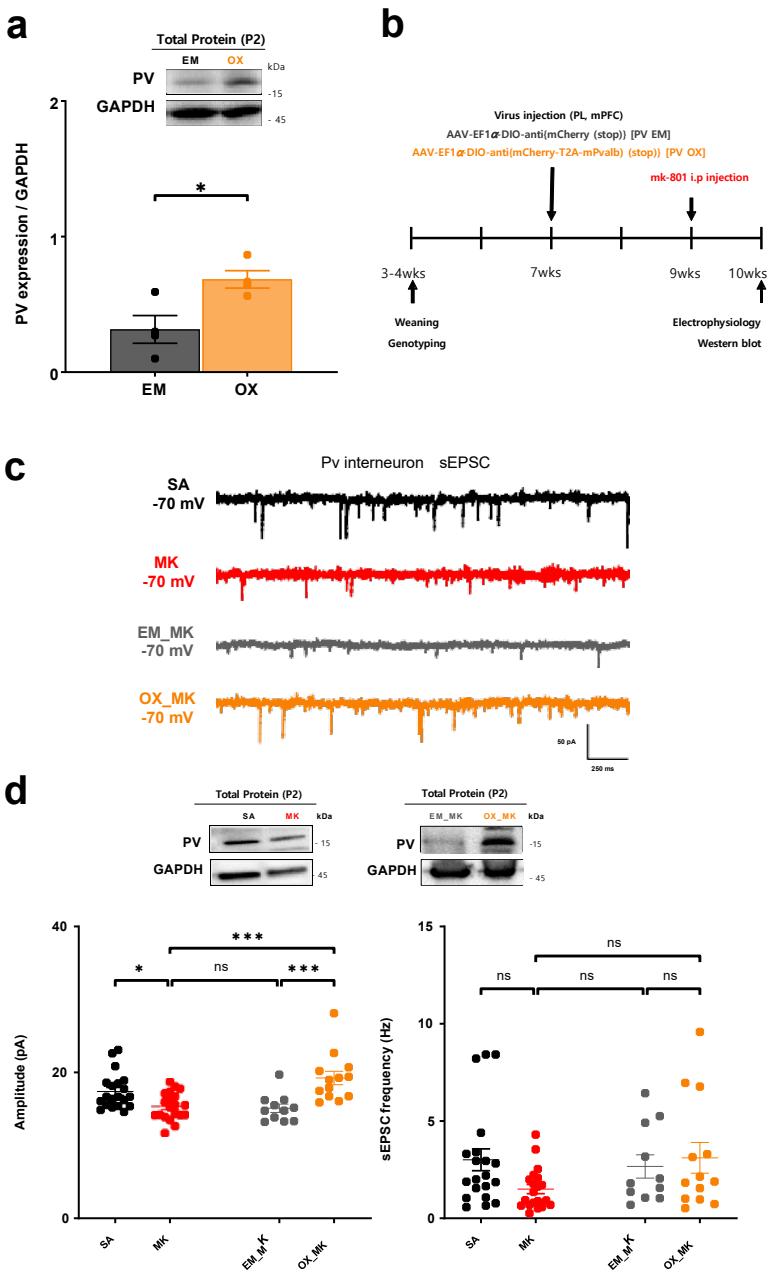

(a) For PV modulation, Pv-Cre mice were infected in the mPFC with AAV-Ef1α-DIO-anti {mCherry (stop)} for empty vector (EM) or AAV-Ef1α-

DIO-anti {mCherry-T2A-mPvalb) (stop)} for PV overexpression vector (OX) for 3 weeks. Immunoblot analysis of PV (inlet) protein levels in mPFC prepared from EM and OX group. Bar graphs indicating summary of quantification of PV protein levels. Note that PV OX group showed a notable increase in PV protein levels compared to PV EM group. (n=4 [EM], n=4 [OX], EM vs. OX: p=0.0222, *p < 0.05, Unpaired t test, Two-tailed [bar graph]).

(b) Schematic electrophysiology experiment schedule (left, top), indicating that mk-801 injection for 1 week as NMDAR hypofunction (MK) was examined before complete expression of EM (EM_MK) or OX (OX_MK) vector for 3 weeks to investigate PV EM or OX effects on NMDAR hypofunction mice.

(c) Representative traces of sEPSC from Pv interneurons in voltage clamp at -70 mV in SA, MK, EM_MK, and OX_MK group (left, bottom).

(d) Representative immunoblot of PV displaying that PV protein levels were reduced in MK and EM_MK group compared to SA group, which was enhanced in OX_MK group (right, inlet). Bar graphs indicating the amplitude and frequency of AMPAR-mediated sEPSC in Pv interneurons in four different groups (right, bottom). Note that the amplitude was reduced in MK and EM_MK compared to SA group, which was dramatically improved in OX_MK without affecting the frequency of AMPAR-mediated sEPSC in Pv interneurons. (n=20 [SA], n=20 [MK], n=11 [EM_MK], n=13 [OX_MK], *p < 0.05, ***p < 0.001, ns, not significant, amplitude: Ordinary one-way ANOVA with Holm-Sidak's multiple comparisons test F (3, 60) =

9.087, frequency: Kruskal-Wallis test with Dunn's multiple comparisons test, [bar graph]).

Figure 1.19 PV deficiency solely impaired AMPAR regulation in Pv interneurons.

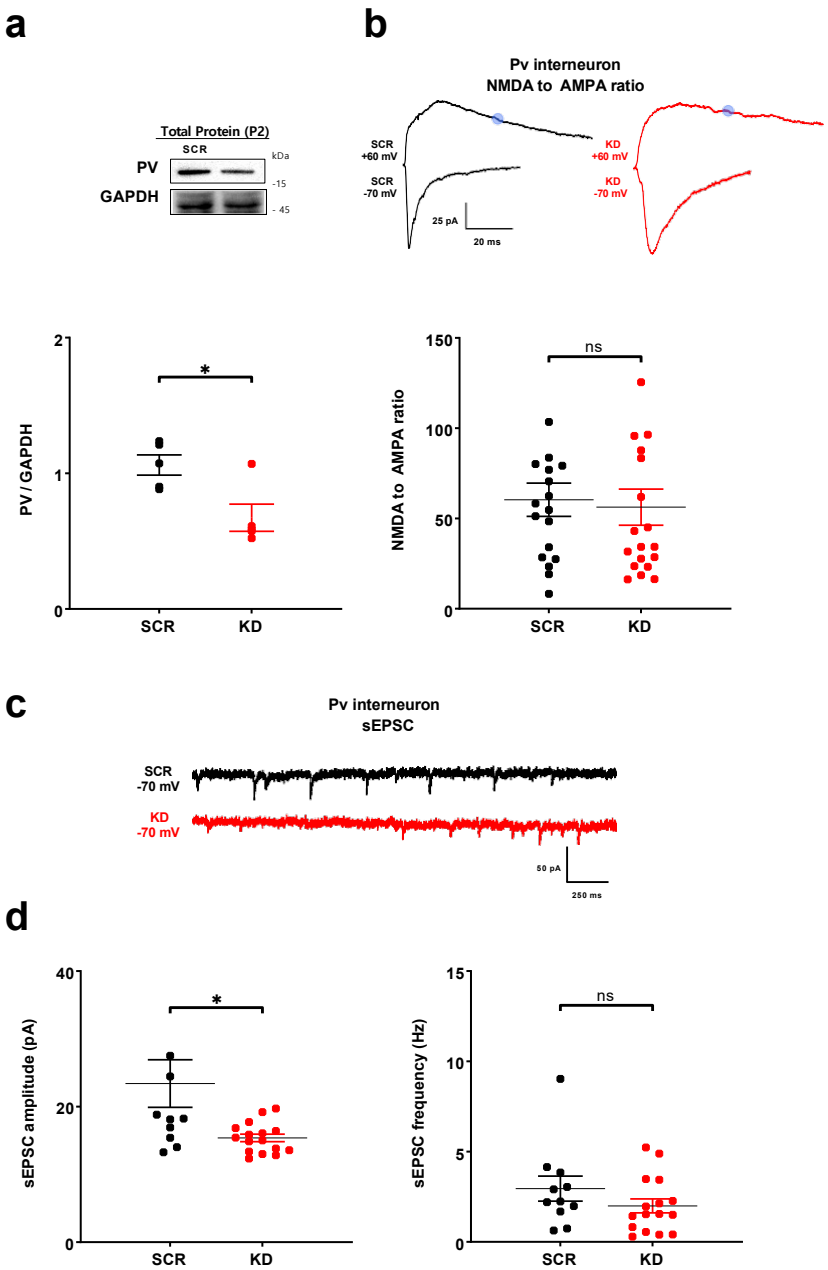

(a) For PV modulation, Pv-Cre mice were infected in the mPFC with AAV-U6-loxp-CMV-EGFP-loxp-SCR-CMV-mcherry for PV scrambled vector (SCR)

or AAV-U6-loxp-EGFP-loxp-mPalb-shR36-mcherry for PV knockdown vector (KD) for 3 weeks. Immunoblot analysis of PV (inlet) protein levels in mPFC prepared from PV SCR and KD group. Bar graphs indicating summary of quantification of PV protein levels. Note that PV KD group showed a considerable decrease in PV protein levels compared to PV SCR group. (n=5 [SCR], n=5 [KD], SCR vs. KD: p=0.0145, *p < 0.05, Unpaired t test, Two-tailed [bar graph]).

(b) Representative traces of NMDAR- and AMPAR- mediated evoked EPSC from Pv interneurons during voltage clamp respectively at + 60 mV and -70 mV in PV SCR and KD group (top). Normal ratio of NMDA- and AMPAR-mediated evoked EPSCs in Pv interneurons in PV KD compared to SCR group. (n=18 [SCR], n=19 [KD], SCR vs. KD: p=0.599, *ns, not significant, Mann Whitney test, Two-tailed [bar graph]).

(c) Representative traces of AMPAR-mediated sEPSC at -70 mV voltage clamp recording in Pv interneurons between PV SCR and KD group.

(d) Bar graphs showing a substantial decrease in the amplitude but not frequency of AMPAR-mediated sEPSC in PV KD compared to SCR group (n=11 [SCR], n=16 [KD], SCR vs. KD (amplitude): p=0.0171, SCR vs. KD (frequency): p=0.1623, *p < 0.05, ns, not significant, Mann Whitney test, Two-tailed [bar graph]).

Figure 1.20 PV overexpression improved PPI deficits in NMDAR hypofunction model.

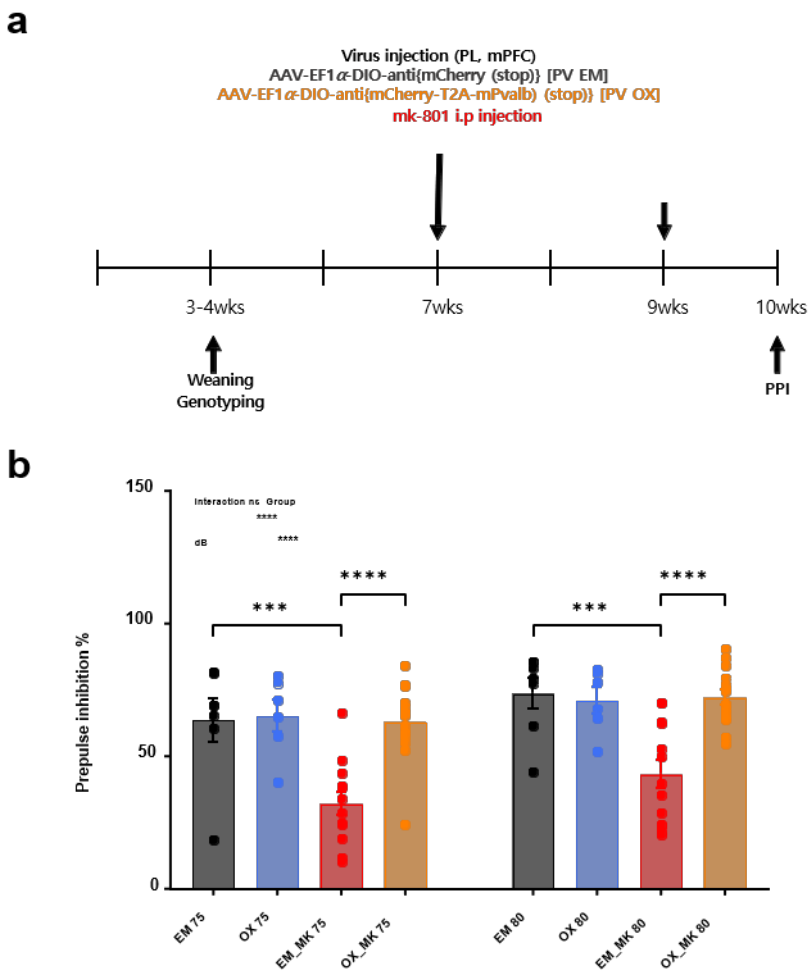

(a) Schematic PPI assay experiment schedule (left), indicating that PV EM or OX virus was injected to Pv-cre mice (bilateral injection into the PL) and then 2 weeks later (before complete expression of viruses), saline or mk-801 was repetitively administered to mice.

(b) EM or OX group described as mice injected with EM or OX virus with additional administration of saline for 1week. EM_MK or OX_MK group

represented as mice injected with additional administration of mk-801 for 1week (left). Bar graphs comparing proportion (%) of PPI between PV EM and OX group each within saline or mk-801 effects in PPI assay either with 75- or 80- dB pre-pulse (right). Note that EM_MK group showed a substantial decrease in PPI % both with 75- or 80-dB pre-pulse compared to EM or OX group, which is significantly enhanced in OX_MK group. (n=7 mice[EM], n=13 mice [EM_MK], n= 6 mice [OX], n=14 mice [OX_MK], Interaction $F(3, 36) = 0.4102$, $p=0.7466$, dB $F(3, 36) = 12.54$, $p<0.0001$, Group $F(1, 36) = 28.49$, $p<0.0001$, EM 75 vs. EM_MK: $p=0.0003$, EM_MK 75 vs. OX_MK: $p=<0.0001$, EM 80 vs. EM_MK: $p=0.0005$, EM_MK 80 vs. OX_MK: $p=<0.0001$, ***$p < 0.001$, ****$p < 0.0001$, ns, not significant, Repeated measures of Two Way ANOVA with Sidak's multiple comparisons test [bar graph]).

Figure 1.21 PV deficiency mice showed PPI deficits, comparable to NMDAR hypofunction model.

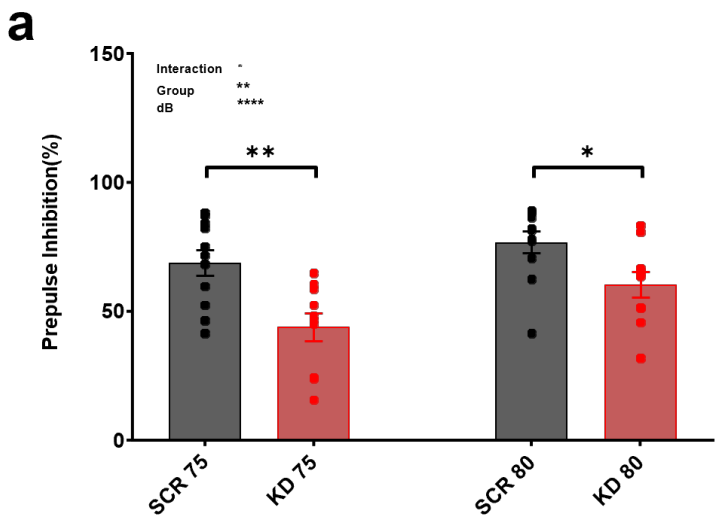

(a) For PPI assay in PV SCR and KD mice, Pv-Cre mice were infected in the mPFC with AAV-U6-loxp-CMV-EGFP-loxp-SCR-CMV-mcherry for PV scrambled vector (SCR) or AAV-U6-loxp-EGFP-loxp-mPalb-shR36-mcherry for PV knockdown vector (KD) for 3 weeks. Bar graph showing proportion (%) of PPI between PV SCR and KD group. Robust decrease in PPI % in PV KD group both in 75- or 80-dB pre-pulse compared to PV SCR group. (n= 11 mice [SCR], n=10 mice [KD], Interaction F (1, 19) = 4.547, p=0.0462, Group F (1, 19) = 9.494, p=0.0061, dB F (1, 19) = 39.02, p<0.0001, SCR 75 vs. KD: p=0.0020, SCR 80 vs. KD: p=0.0472, *p < 0.05, **p < 0.01, ****p < 0.0001, Repeated measures of Two Way ANOVA with Sidak's multiple comparisons test, [bar graph]).

DISCUSSION

In this chapter I, my main conclusion is that PV deficiency induced by NMDAR hypofunction is a key factor to impair Pv interneuronal functions of regulation of AMPAR synaptic strength, leading to sensorimotor gating deficits.

- **NMDAR hypofunction with downregulated AMPAR activity in mPFC network imbalance and PPI deficits.**

In addition to confirming PPI deficits in my NMDAR hypofunction mice, my results demonstrate how NMDAR hypofunction impairs PPI-related Pv interneuronal function in mPFC. My results suggest that NMDAR hypofunction specifically in Pv interneurons induces downregulation of AMPAR, leading to E/I imbalance. Equalizing E/I ratio modulated by proportional Pv interneuronal inhibition plays a role in information processing in mPFC microcircuits.[59,60,62,63] In line with this, my results indicate that the concomitant reduction of NMDAR and AMPAR activity in Pv interneurons is sufficient to impair Pv interneuronal function, leading to dysfunction of mPFC network for PPI processing. Therefore, considering that AMPAR and NMDAR are tightly coregulated by activity at synapses at which they are both expressed,[93] it is critical for NMDAR function to modify proper AMPAR-mediated synaptic changes in Pv interneurons in maintaining PPI modulation.

- **NMDAR function-dependent PV expression in modification of AMPAR synaptic strength for PPI**

My NMDAR hypofunction results in loss of PV expression due to lack of PGC-1α without affecting the number of Pv interneurons in prelimbic (PL) mPFC. Loss of PV protein has been identified as biomarker for psychiatric diseases including SZ, which represent one of the key components to cause Pv neuron dysfunction.[41,43–45,48,54] Of note, PV knockout mice ($PV^{-/-}$) indicate impairments of short-term plasticity in Pv interneurons[54–56] accompanied by SZ-related phenotypes including defects of acoustic startle response and PPI.[54,57] However, it has not been extensively investigated whether and how specific Pv interneuronal mechanisms underlying the causes and consequences of PV deficiency are implicated in sensorimotor gating deficits.

Notably, my results demonstrate that PV deficiency induced by NMDAR hypofunction is strongly associated with downregulation of AMPAR in Pv interneurons, which is reversed by boosting PV expression levels (PV OX group) while NMDAR function is still decreased. Importantly, this modulation of PV expression underlies PPI effects in NMDAR hypofunction mice. In addition to identifying PV absence in NMDAR hypofunction mice, loss of PV alone is sufficient to cause reduction of AMPAR synaptic strength without affecting NMDAR function. This finding contrasts with the evidence that there is no effect on basal synaptic transmission in $PV^{-/-}$ mice.[55,56] This genetical ablation of PV may be of differences in developmental and compensatory effects when compared to suppressing PV in young adult mice by PL region-specific knock-down viruses. Moreover, my PV deficiency mice indicate considerable PPI deficit accompanied by abnormal evoked gamma oscillation while other baseline behaviors were not disturbed.

NMDAR hypofunction model (MK group) and PV deficiency model with intact NMDAR activity (PV KD group) share a substantial decrease in AMPAR synaptic strength specifically in Pv interneurons associated with PPI deficits. Therefore, my study connects these two Pv interneuronal dysfunction models, suggesting that Pv interneuronal signaling that extends from NMDAR function to PV expression is important key mechanism underlying elaborate regulation of AMPAR-mediated synaptic activity to modulate PPI in mPFC.

■ Implication of this study

In the end, my data suggest that Pv interneuron-specific neuronal mechanisms for coupling NMDAR activity to physiological role of PV expression, which is implicated in modification of AMPAR synaptic strength and its-related PPI effects. PV deficiency induced by NMDAR hypofunction is the key causation to impair AMPAR synaptic strength, thereby leading to sensorimotor gating deficits. My study is highly relevant to the pathophysiology of psychiatric diseases such as schizophrenia in a way that a decrease in NMDAR function and PV expression relates to sensorimotor gating deficits respectively in our NMDAR hypofunction and PV deficiency mouse models as core features of SZ-phenotypes.[1,2,10,94,108–110] This leads to huge discrepancy from genetical NMDAR ablation mouse models such as NR1 knockout mice. NMDAR expression in Pv interneurons is developmentally regulated. NMDAR is highly expressed in immature Pv interneurons at early postnatal stages in the brain but gradually decrease to a lower level found in mature Pv interneurons in adult. [111–116] Schizophrenia is regarded as progressive mental illness because symptoms such as cognitive impairment worsen with age.[117–120] If the

progression of NMDAR hypofunction (not NMDAR ablation itself) would be more relevant to pathogenesis of positive symptoms including PPI, knockout of NMDAR from Pv interneurons precludes developmental importance before full removal of NMDAR at approximately young adult.

■ Conclusion

In conclusion, my study provides the physiological role of PV proteins, underpinning exquisite regulation of AMPAR which is adaptive to network alteration such as NMDAR activity. This coupling NMDAR function to PV expression for synaptic regulation specifically in Pv interneurons contributes to advancements in my understanding of PPI-related Pv interneuronal mechanisms.

Chapter II. Distinctive AMPAR regulation by PV-mediated AC 5 signaling in Pv interneurons is required for sensorimotor gating

Introduction

Multiple lines of evidence have suggested that function of PV as Ca^{2+} binding proteins is important in intracellular modulation of Ca^{2+} transients (dynamics) in cell body and dendrites and thus promote facilitation and depression as short-term synaptic plasticity.[46,55,57,74,75] In chapter I, I address that the physiological role of PV proteins, besides Ca^{2+} buffer function, plays a significant role in AMPAR-mediated synaptic regulation in Pv interneurons, which is implicated in modulation of PPI. However, how this specific Pv interneuronal mechanisms underlying consequences of PV deficiency are implicated in downregulation of AMPAR, leading to sensorimotor gating deficits remains unclear.

Accumulating evidence have suggested that AMPARs are modulated primarily through NMDAR-dependent mechanisms in which several molecular players are mediated by calcium influx through NMDAR to elicit synaptic modification.[39] Previous studies have investigated that NMDAR-mediated synaptic activity to regulate AMPAR requires increased cAMP signaling.[97,121–124] This leads to notion that it would be important to investigate Pv interneuronal specific cAMP signaling for coupling NMDAR function to AMPAR synaptic regulation.

Adenylate cyclase (AC) that accounts for most of the synthesis of cyclic AMP (cAMP) has nine membrane-bound isoforms, each with different expression specificity and properties in neurons and brain regions.[81,82] AC isoforms differ in their functional properties for generating cAMP stimulated by NMDAR-mediated Ca^{2+} influx. While AC 1 and AC 8 are stimulated by Ca^{2+} through calmodulin,[125–129] AC 2, AC 4, and AC 5 are directly activated Ca^{2+} or through Ca^{2+}-mediated other protein kinases such as PKC and PKA.[97,130]

Of note, AMPAR-mediated synaptic strength is dynamically attuned by phosphorylation of it in which many different kinases in response to Ca^{2+} transients are activated.[39] Of various kinases, while CaMKII and/or PKC-mediated phosphorylation of AMPAR is primarily implicated in long-term potentiation (LTP) or long-term depression (LTD), PKA-dependent phosphorylation of AMPAR considerably coordinates synaptic changes adaptive to network activity, indicating scaling-up and down.[76] Of various downstream effectors, cAMP mainly targets PKA signaling. Given that subsequent activation of cAMP dependent PKA signaling contributes to modulate AMPAR trafficking, AC activity is also implicated in synaptic changes.[83,84]

To this end, based on the chapter I results that the level of PV expression controlled by NMDAR function (Ca^{2+} influx through NMDAR) is in an ideal position to regulate synaptic activity of AMPAR specifically in Pv interneurons, I hypothesized that activity of Pv interneuron-specific AC isoform would exquisitely arrange PKA modulation for synaptic regulation of AMPAR, which is associated with maintaining PPI modulation. Proper synaptic changes in Pv interneurons are important in GABAergic signaling to modulate excitation/inhibition (E/I) balance in neural networks by inhibitory gating of local excitatory neurons.[59–61] Synchrony of Pv interneurons generate high frequency (30-80 Hz: gamma) neuronal oscillation.[131,132] In mPFC, normal gamma oscillation is implicated in diverse cognitive processes including PPI.[90,91,133,134] Of note, gamma oscillation dysfunctions are observed in PPI deficit mice with elevating spontaneous gamma power and reduced sensory-evoked gamma response.[14,15] To this end, it is significant to

investigate Pv interneuronal mechanisms in mPFC underlying PPI deficits associated with abnormal gamma oscillation, which are represented in psychiatric diseases. Stimulus-evoked gamma frequency oscillation (not spontaneous oscillation) is highly correlated with PPI in cortical circuits and exhibits PPI.[90,91] To examine stimulus-evoked gamma oscillations, I examined auditory steady-state response (ASSR) paradigms which are measured with electroencephalography (EEG) in response to a repeated sound at a fixed rate or frequency.[92] Given that ASSR is entrained to auditory sensory evoked neuronal oscillations of a resonant frequency at maximal 40 Hz, ASSR measurements reflect evoked-gamma frequency synchronization at neuronal circuits for auditory sensory processing. Moreover, as a key biomarker, reduced ASSR in the 40 Hz is prevalent in psychiatric disorders.

In the chapter II study, I revealed that AC 5 was highly enriched specifically on Pv interneurons and PV deficiency disrupted AC 5 modulation. Activation of AC 5-PKA signaling increased synaptic strength at excitatory synapses onto Pv interneurons in my parvalbumin (PV) knockdown model, leading to PPI effects. Moreover, my NMDAR hypofunction mice and PV deficiency mice shared disruption of stimulus-evoked gamma frequency oscillation through ASSR, correlated to PPI deficits. This gamma frequency abnormality was rescued by re-activation of AC 5 signaling, which is consistent with improved AMPAR and PPI effects.

These results suggest that synaptic regulation of AMPAR modulated by PV expression through Pv interneuronal distinct mechanisms (AC 5-PKA signaling) are required to maintain PPI modulation correlated with network activity in mPFC.

Materials and Methods

Animals

All inbred mouse strains, Pv-Cre, Pv-Cre;Ai14. SOM-Cre, and SOM-Cre;Ai14 were obtained from the Jackson laboratories and GAD65-GFP was obtained from a colony of Korean Institute for Science and Technology (KIST). All strains were maintained in a C57B/6J or 129S2/SV background (> N10 backcross). All experimental procedures were performed on male mice with P55-70. All the mice were maintained under standard temperature controls with housing up to five animals per cage under 12/12h light/dark cycle. Animals received water and food ad libitum. All experiments including behavioral tests, electrophysiological experiments, and biochemistry were done in littermate males at 8-10 weeks of age. For mk-801 & saline mouse model, mice were treated with mk-801 (1.0 mg/kg, intraperitoneally [i.p.], daily) or 0.9% saline as vehicle control for 7 consecutive days from P55 to P60. I modified mk-801 model dosage based on previous publication (Xi, D., Zhang and Gao, W.-J. et.al 2009). Animal procedures were approved by the Institutional Animal Care and Use committee of Seoul National University (SNU) and Institute for Basic Science (IBS).

In vivo surgery

P50-55 mice were anesthetized with 8 mg/ml ketamine (16% by volume) and xylazine (2.8% by volume) in saline solution by intraperitoneal injection and were mounted stereotactic frame (David Kopf Inc., USA) with a heating pad for maintenance of core body temperature at 36℃. For electrophysiology or behavioral

experiments, a volume of about 0.5 µl virus solution was bilaterally injected into the dorsal region of medial prefrontal cortex (AP 1.94mm; ML 0.8mm; DV 1.75mm; 15-degree angle relative to Bregma) by 20 psi pressure with 5 msec duration (Picospritzer III, Parker Hannifin Corp.). The injection glass pipette was then removed after 10-15min for diffusion. The optic fiber (Doric Lenses Inc., 100µm core, 0.22 NA, ZF 1.25, DFL) was targeted to the same position as virus injection coordination. Cell-type-specific expression of virus was obtained using the following Cre-dependent AAV: AAV5-EF1a-DIO-eNpHR3.0-mcherry-WPRE (UNC vector core), AAV9-Ef1a-DIO-ChETA(E123T/H134R)-eYFP-WPRE-hGH (Penn vector core). Local prelimbic micro-infusions with cannula (28-gauge bilateral cannula, 1.75 mm) (Plastics One Inc., USA) was implanted, targeting prelimbic region (AP 1.94mm; ML 0.8mm; DV 1.75mm relative to Bregma). After implantation, cannula was inserted with dummy cannula to prevent being blocked. Before infusion, dummy cannula was removed, and then internal cannula was bilaterally inserted and attached to a 25-ul Hamilton syringe (Hamilton, USA). All prelimbic micro-infusions (1 ul, 0.05 ul per min) of saline-containing vehicle or PKA activator forskolin (2.5 ug/ul) were simultaneously infused into the left and right hemispheres using infusion pump (USA). bilateral injections of DAMGO (15 ng on each side) All infusions were performed in freely moving mice in an empty cage. After infusion, internal cannula remained in place for 2min for drug diffusion. After cannula implantation, medical glue and dental cement were coated under the cannula pedestal. Mice were under recovery period at least 4days.

Local field potential recording

Local field potential (LFP) evoked by auditory steady-state response (ASSR) was recorded with a INTAN RHD2132 16-channel amplifier and Open Ephys acquisition board using Insulated tungsten wire (130/180 um in bare/coated diameter, A-M Systems, USA) attached to the cannula. The electrode was implanted at 1.94 mm anterior, 0.8mm lateral, and 1.75 ventral from bregma. The electrode impedance was approximately 20 kΩ. The ground and reference electrodes were implanted at the skull on cerebellum using micro screws (stainless steel, 3mm in length and 1mm in diameter, Asia Bolt, Korea). Mice underwent a recovery period at least 4 days.

Preparation of mice brain lysate, solubilization

The brain tissues were added to homogenization buffer (0.32-M sucrose in phosphate-buffered saline solution) and homogenized using a homogenizer. The lysate was centrifuged for 10 min at 1400 × *g* at 4 °C. The pellet was saved as P1. The supernatant (S1) was collected and spun again at 13,800 × *g* for 10 min at 4 °C. The second supernatant (S2) and pellet (P2) were saved. Solubilization buffer was made with PBS by freshly adding p0.5% Triton X-100, 0.5 mM EDTA, 0.5 mM EGTA, protease inhibitor mixture, and additional detergents as indicated for each experiment. The P2 was resuspended in solubilization buffer, mixed gently for 60 min at 4 °C on a rotator, and spun down at 14,000 × *g* for 15 min to collect the supernatant including solubilized proteins.

Co-immunoprecipitation

The brain tissue was solubilized with PBS including 1% Triton X-100 followed with IP using pv antibodies. For immunoprecipitation (IP), 100ug of pv antibody

(swant) was used, respectively. Antibodies were bound to Protein A-Sepharose beads (Amersham Biosciences) by incubating at 4 °C for 90 min. The solubilized proteins were first incubated with protein A-Sepharose beads for 90 min as a preclearing process and then incubated with the antibody-protein A-Sepharose beads at 4 °C for 3 h on a rotator. After washing the beads three times with three-bed volumes of ice-cold PBS, proteins bound to the antibodies were eluted with the protein gel loading buffer (2% SDS, 1% β-mercaptoethanol, 0.005% bromphenol blue, 2% glycerol, and 0.05 M Tris-HCl, pH 6.8) and applied to SDS-PAGE (sodium dodecyl sulfate polyacrylamide gel electrophoresis) followed by Western blot analysis.

Brain slice preparation

P63-80 mice were anesthetized with isoflurane and decapitated. After brain dissection, coronal slices of medial prefrontal cortex (300μm) were cut in ice-cold oxygenated sucrose-based cutting solution containing (in mM): 75 Sucrose, 76 NaCl, 2.5 KCl, 25 $NaHCO_3$, 25 Glucose, 1.25 NaH_2PO_4, 7 $MgSO_4$, 0.5 $CaCl_2$ with pH 7.3, and 310 mOsm by using vibratome 7000smz-2 (Campden instruments, England), and then recovered in the same solution for 30min at 33-34 °C. Slices were then transferred to a incubation chamber filled with oxygenated artificial cerebral spinal fluid (ACSF) containing (in mM): 124 NaCl, 2.5 KCl, 1.3 $MgCl_2$, 2.5 $CaCl_2$, 1.0 NaH_2PO_4, 26.2 $NaHCO_3$, 20 Glucose with pH 7.4 and 310 mOsm at room temperature and slices were kept in less than 7hrs before recordings.

Auditory steady-state electroencephalogram (ASSR)

To habituate mice, mice were seated in a transparent cylinder (17 cm in diameter

and 21 cm in height) in a dark and quite cage for 30 min during 2-3 consecutive days. Sound was presented in a train consisted of four different frequencies (19, 27, 34 and 41 Hz) pulse with random order. Each pulse length is 500ms with 10ms duration. The interstimulus between pulses was 1000ms. The sound trains lasted for 40min. The sound train was delivered binaurally through general speaker (80dB, sound pressure level). The sound was generated by PULSE PAL (developed by Josh Sanders at Cold Spring Harbor) and controlled by customized C++ written code (Visual studio 2015). The LFP at the frontal cortex was recorded with the sampling rate 1kHz using the Open Ephys GUI. Baseline was also recorded for 30min with no sound. For ex vivo recording, slices were transferred to a recording chamber perfused with oxygenated ACSF at 30-32℃ controlled by a peristaltic pump.

Electrophysiology

Cells in prelimbic region were visualized with 80x and 20x magnification objective (Olympus) on the stage of upright microscope (BX61W1, Olympus) equipped with infrared-differential interference contrast optics in combination with digital camera (AquaCAM Pro/S3) and equipped with sCMOS camera for fluorescence imaging (Zyla, ANDOR). Patch microelectrodes were pulled from borosilicate glass (O.D.:1.5mm, I.D.: 1.10mm, WPI) on a Flaming-Brown micropipette puller model P-1000 (Sutter Instruments, USA). Patch microelectrodes had a resistance of 4-8MΩ. Signals were recorded using a patch-clamp amplifier (Multiclamp 700B, Axon Instruments, USA) and digitized with Digidata 1550A (Axon Instruments, USA) using Clampex software. Signals were amplified, sampled at 10 kHz, and filtered to 2 or 5 kHz. Pyramidal neurons were identified by large

apical dendrites, and SOM & Pv interneurons were identified by tdTomato, YFP, or mcherry fluorescence expression. During current-clamp recordings for intrinsic excitability and EPSP summation, membrane potential was held at -70mV with intracellular solution (in mM): 135 K-gluconate, 7 NaCl, 10 HEPES, 0.5 EGTA, 2 Mg-ATP, 0.3 Na_2-GTP, 10 Na-phosphocreatine with pH 7.3 and 295 mOsm. Current-clamp experiments were recorded 5min after obtaining whole-cell configuration. Action potentials (APs) were generated by injecting 500 ms current steps increasing by 50 pA. During voltage-clamp recordings for eEPSC eIPSC, sEPSC, and mEPSC, Cell membrane potential was kept at -70mV for AMPAR mediated EPSC, +40mV for NMDAR mediated EPSC, and 0mV for eIPSC with the following intracellular solution (in mM): 135 CsMS, 10 CsCl, 10 HEPES, 0.2 EGTA, 4 Mg-ATP, 0.4 Na_2-GTP with pH 7.3 and 295 mOsm. sIPSC and mIPSC were recorded at -60mV membrane holding potential with normal chloride intracellular solution (in mM): 110 CsMS, 40 CsCl, 2 $MgCl_26H_2O$, 0.1 $CaCl_22H_2O$, 10 HEPES, 1 EGTA, 2 Na-ATP, 0.4 Na-GTP and with high chloride intracellular solution (in mM): 150 CsCl, 2 $MgCl_26H_2O$, 0.1 $CaCl_22H_2O$ 10 HEPES, 1 EGTA, 2 Na-ATP, 0.4 Na-GTP respectively. Cells were voltage or current-clamped at each holding potential with liquid-junction potential correction of estimated 10.5 mV. During EPSC recording, to block inhibitory synaptic responses, 20 μM SR95531 (GABAzine, Tocris) was bath applied but for IPSC recording, 10 μM NBQX and 50 μM AP-5 (Tocris) were bath applied to block excitatory synaptic responses. For mEPSC and mIPSC, 1 μM tetrodotoxin (TTX, Abcam) was added to bath. To isolate NMDAR mediated EPSC, 10 μM NBQX (Tocris) was added to bath to block AMPAR mediated synaptic responses.

Optogenetics

In vitro slice stimulation: When virus for eNpHR3.0 was specifically expressed in Pv interneurons 4weeks after virus injection as described in viral targeting method, acute coronal slices of prelimbic in mPFC were prepared. Pv interneurons were identified by fluorescence labeling for optogenetic cellular manipulations. Di-synaptic inhibitory postsynaptic currents (IPSC) in pyramidal neurons were isolated by holding cells at 0mV and abolished by not only GABAA receptor antagonist GABAzine but also combination of AMPAR receptor antagonist NBQX and NMDA receptor antagonist AP-5. While electrically evoked di-synaptic IPSC were obtained, Pv interneuron mediated IPSC was isolated by calculating differentiation between total IPSC with and without 561 nm light-evoked suppression of Pv interneurons. In addition to this, while EPSP temporal summation in pyramidal neurons was recorded by 20 or 50Hz repetitive electrical stimulation, 561 nm light was delivered to suppress Pv interneurons to figure out its effect on excitation and inhibition temporal summation of excitatory neurons. 561 nm light pulse was delivered for 300-500ms with 1.5mW intensity.

Behavioral procedures

Open field test

The open field was composed of a white PVC enclosed area (40 X 40 X 40 cm) with stable lightning conditions (20 LUX). Mice were placed individually into the center of the arena and allowed to explore for 1 or 3 hrs. Total distance moved and

velocity were recorded, video-tracked, and analyzed by using EthoVision software.

Y maze spontaneous alteration test

Y maze consisted of Y-shaped maze with three white and opaque PVC made arms at a 120° angle from each other. Mice were placed at the end of one arm and then allowed to freely explore the three arms with recording. All the arm entries and behavior trials were recorded to analyze the percentage of alternation included three consecutive entries to a different arm.

Elevated plus maze

Elevated plus maze was composed of plus-shaped maze with two closed arms surrounded opaque walls and two open arms. The maze was elevated 150cm from the floor. Mice were placed at the center zone of the maze and then permitted to freely explore for 10min. All the arm entries were recorded and analyzed to calculate time stayed in open and closed arms by using Ethovision software.

Acoustic startle response and pre-pulse inhibition

Acoustic startle response (ASR) was described by an exaggerated flinching response of mice when unexpected auditory stimulus was delivered. This response was attenuated when preceded by a weaker stimulus, underlying pre-pulse inhibition (PPI). ASR and PPI were measured using the SR-Lab system (San Diego Instruments, USA) During all trials, background was delivered at 65 dB white noise. Each ASR trial consisted of a single 40-ms startle pulse of 75, 80, 85, 90, 95, 100, 105, 110, 115 or 120 dB with ten times in pseudorandom order. Trials were delivered with a

variable intertrial interval (ITI) of 10-25 s. PPI was composed of 5min acclimation period followed by 2 types of trials presented 10times in pseudorandom order. Each PPI trial had 5 sec backgrounds followed by 20 ms pre-pulse (75 or 80 dB), 80 ms interval, and 40 ms startle response with 120 dB intensity. PPI trials were presented with a variable ITI of 10-25 s. For calculating ASR and PPI, at the beginning of each startle pulse, maximum velocity (Vmax) in arbitrary units was recorded every 1ms for 65ms. The Vmax in trials was averaged for analysis. PPI was calculated as the difference between Vmax after 20 ms pre-pulse (Vmax ppi) and Vmax after 120 dB startle response alone from ASR tests (Vmax-ctrl), which was expressed as a percentage of PPI = ((Vmax-ctrl) - (Vmax ppi))/(Vmax-ctrl))*100.

Data analysis

All waveforms were analyzed in pClamp or LabVIEW with custom written scripts. All graphs were made with Prism 9. Synaptic currents were analyzed by pClamp. To make epochs, continuous LFP time series was segmented based on stimulus frequency (20, 30, 40 and 50 Hz) with pre-stimulus of 500ms and a 1000ms of the stimulus period. To be screened for artifacts, the epoch was rejected when the amplitude of epoch exceeded. The mean stimulus power was computed by averaging the power of each stimulus epochs. After base epochs were extracted from baseline period, the mean base power also was computed by averaging the power of each base epochs. ASSR index was defined by ratio between mean stimulus power and mean base power at stimulus frequency. All analysis was done by MATLAB and all codes were customized-written.

RESULTS

AC 5-PKA signaling modulated by PV expression mediated regulation of AMPAR synaptic strength specifically in Pv interneurons.

Considering that the levels of PV expression regulate AMPAR synaptic strength in response to network activity represented as NMDAR-mediated Ca^{2+} transients in Pv interneurons, PKA signaling would orchestrate AMPAR phosphorylation as an intermediary role for regulation synaptic changes in the crosstalk between PV and AMPAR. Therefore, I examined the level of AMPAR subunits (GluR 1/4) and PKA expression in Pv interneurons as performing PL-isolated western blot assay in PV SCR and KD mice. To extract those proteins specifically in Pv interneurons, I utilized co-immunoprecipitation (co-IP) assay which can identify physiologically relevant protein to protein interaction. Interestingly, as pulling down with PV, I determined its interaction proteins including AMPAR subunits (GluR1 and 4), PKA, and AC 5. In addition to this, CaMKII and $GABA_AR$ were not pulled by PV proteins as negative control (Figure 1.1b). This significantly implies that besides Ca^{2+} binding buffer, PV proteins would function as signal transduction by physiological interaction between AMPAR subunits and PKA. Consequently, co-IP assay indicated that GluR4, PKA, and AC 5 expression were significantly reduced in PV KD compared to PV SCR group, although there is no difference in the levels of proteins in total input assay between PV SCR and KD group except PV proteins (Figure 1.1b). Consistent with a decrease in AMPAR synaptic currents in PV KD, expression of GluR 4, preferentially enriched in Pv interneurons[77–79], was reduced in

PV KD compared to SCR group (Figure 1.1b). These results elicit that PV deficiency causes downregulation of PV-binding PKA expression (not total PKA proteins), leading to disrupt phosphorylation of AMPAR subunits (GluR 4) in Pv interneurons.

I further addressed that re-activation of PKA signaling might improve reduced AMPA synaptic strength in Pv interneurons. To test this, I investigated alteration of AMPAR-mediated sEPSC in Pv interneurons with bath application of PKA activator forskolin on brain slices between PV SCR and KD group. Forskolin treatment substantially increased AMPAR-mediated amplitude and frequency of Pv interneurons in PV KD group without affecting PV SCR group (Figure 1.2). This indicates that PKA signaling may be elaborately controlled to limit overactivation of PKA activity in normal states.[80] Together, these data suggest that as a downstream effector mediated by PV expression with physiological interaction, PKA signaling has a significant role in modulating AMPAR-mediated synaptic activity in Pv interneurons.

To investigate which AC isoform is highly enriched in Pv interneurons, I performed laser-capture microdissection (LCM) which is used to analyze RNA transcripts in certain neuronal populations within heterogeneous brain slices.[85–87] For PL slice, brains were harvested from Pv-Cre mice which are crossed with Cre-dependent $^{R26LSL\text{-}tdTomato}$ (Ai 14) reporter line to label Pv interneurons. Using an inverted fluorescence microscope in LCM instrument, I visualized Pv interneurons with a red fluorescent protein in PL brain slice. Nuclei staining by cresyl violet was used to procure non-Pv neurons (majority of excitatory neurons) with large cell bodies. Each RNA sample from Pv interneurons or non-Pv neurons were collected and then

prepared to perform real-time RT-PCR, respectively (Figure 1.3a). RNA quantification assay revealed that in a family of AC enzymes, AC 5 isoform is strongly expressed in Pv interneurons compared to the other neurons with higher values of fold change (~ 5-fold) (Figure 1.3b). Consistent with RNA expression of AC 5 highly enriched in Pv interneurons, PV KD showed a remarkable decrease in AC 5 expression compared to PV SCR group both in total input and co-IP assay by PV pulling down (Figure 1.1b). Intriguingly, this also confirmed that AC 5 has a physiological interaction with PV proteins. These results strongly support that PV deficiency causes downregulated AC 5 expression in Pv interneurons.

In accordance with improvement of AMPAR synaptic strength by re-activation of PKA signaling, I further addressed whether the observed downregulation of AMPAR synaptic strength in PV KD mice may be rescued by activation of AC 5 in Pv interneurons. However, there is no directly working activator for AC 5 pharmacologically used. Alternatively, there is little evidence that activation of AC 5 is mediated by μ opioid receptor agonist DAMGO through $G_{i/o}$ alpha subunits, leading to increased activity of cAMP-dependent protein kinase.[88,89] Therefore, I investigated effects of AMPAR-mediated sEPSC in Pv interneurons with bath application of DAMGO on brain slices between PV SCR and KD group. Interestingly, DAMGO treatment significantly increased AMPAR-mediated amplitude of Pv interneurons without affecting frequency in PV KD group while PV SCR mice were not affected by DAMGO in AMPA synaptic currents (Figure 1.4).

Overall, these data demonstrate that PV expression delicately arranges subsequent modulation of AC 5-dependent PKA signaling which is important in synaptic regulation of AMPAR distinctively in Pv interneurons.

Robust increase in AC 5-PKA signaling promotes to improve PPI deficits associated with recovery of network activity.

The chapter I and above results described thus far demonstrate that PV deficiency downregulated AC 5-PKA signaling, leading to reduction in AMPAR-mediated synaptic strength specifically in Pv interneurons even without affecting NMDAR function. Of note, my NMDAR hypofunction (MK) with loss of PV expression and PV deficiency (PV KD) models shared a substantial decrease in AMPAR synaptic strength in Pv interneurons, which was significantly reversed to normal states each by overexpression of PV (in MK) or by re-activation of AC 5-PKA signaling (in PV KD). In addition to this, consistent with PPI impairment either in NMDAR hypofunction or PV deficiency mice, AC 5 knock out mice (AC 5 $^{-/-}$) significantly showed PPI deficit with no effects on other baseline behaviors compared to wild-type (WT) and even to hetero-type (HT) (Figure 2.1). These results suggest that not only the levels of PV in Pv interneurons but also AC 5 itself play a notable role in modulation of PPI.

To this end, I investigated if improvement of AMPAR synaptic strength by AC 5-PKA signaling in Pv interneurons is associated with recovery of PPI deficits in PV deficiency models. To test this, I performed microinjection of forskolin (FK, PKA activator) or DAMGO (DM, AC 5 mediator) into the PL, 3 weeks after administration of PV SCR or KD viruses (Figure 2.2a (forskolin), 2.4a (DAMGO)). To exclude acute effects of drugs, I examined PPI assay a day after microinjection. Intriguingly, ANOVA analysis revealed that reduced PPI % in PV KD was restored to within normal range comparable to PV SCR group by forskolin treatment

(KD_FK) (Figure 2.2b) or by DAMGO treatment (KD_DM) (Figure 2.4b), although PV SCR mice were not significantly affected by forskolin or DAMGO treatment. In contrast to this, other behaviors (locomotion activity and working memory) were not significantly affected by forskolin and DAMGO effects in PV SCR (subtle changes in locomotion activity by forskolin and KD mice except anxiety levels determined by time spent in center-zone during open field test (Figure 2.3 (forskolin), 2.5 (DAMGO)). Taken together, these data explicate that physiological role of PV expression or AC 5-PKA signaling is implicated in PPI modulation, which is accompanied by exquisite regulation of AMPAR synaptic strength in Pv interneurons.

Stimulus-evoked gamma frequency oscillation (not spontaneous oscillation) is highly correlated with PPI in cortical circuits and exhibits PPI.[90,91] I thus investigated if my PV deficiency model (PV KD) would disrupt network activity of stimulus-evoked gamma oscillations and then consistent with PPI recovery, this abnormality would be rescued by re-activation of AC 5 signaling. To test this, I examined auditory steady-state response (ASSR) paradigms which are measured with electroencephalography (EEG) in response to a repeated sound at a fixed rate or frequency.[92] Given that ASSR is entrained to auditory sensory evoked neuronal oscillations of a resonant frequency at maximal 40 Hz, ASSR measurements reflect evoked-gamma frequency synchronization at neuronal circuits for auditory sensory processing (Figure 2.6a). When local field potential (LFP) was recorded at PL mPFC in freely moving mice, 500 ms auditory trains at four different frequencies (19, 27, 34, and 41 Hz) with random order were delivered to PV SCR and KD mice (Figure 2.6b). PV KD mice showed a significant reduction in fast

fourier transform (FFT) amplitudes at different frequencies except 19 Hz, compared to PV SCR mice. DAMGO treatment in PV KD mice through microinjection into PL substantially enhanced FFT amplitudes at 27, 34, and 41 Hz, which are comparable to PV SCR mice, although PV SCR mice were not affected by DAMGO effect (Figure 2.7a). As a key biomarker prevalent in psychiatric disorders, reduced ASSR in the 40 Hz (gamma frequency oscillation) is highly associated with cognitive dysfunction. I thus calculated oscillation power at 41 Hz normalized to baseline. ANOVA analysis indicated that a decrease in power of PV KD mice was reversed to the normal states comparable to PV SCR mice by DAMGO effects, although there is no difference in power between PV SCR and PV SCR_DM group (Figure 2.7b). These results suggest that PPI-related auditory stimulus-evoked oscillation as network activity in PL mPFC is modulated by AC 5 signaling, which is in line with AC 5 effects on PPI modulation.

Figure 2.1 PV deficiency downregulated PV-binding PKA and GluR 4 protein levels.

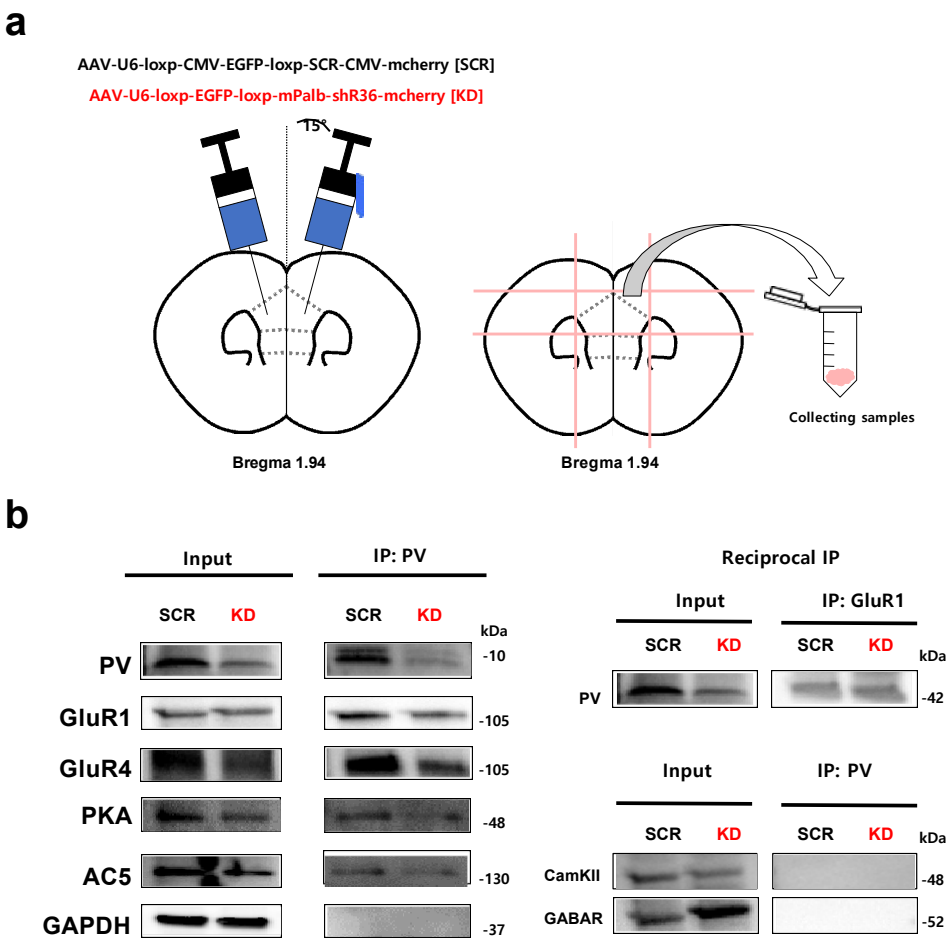

(a) Schematic diagram showing virus injection of AAV-U6-loxp-CMV-EGFP-loxp-SCR-CMV-mcherry for PV scrambled vector (SCR) or AAV-U6-loxp-EGFP-loxp-mPalb-shR36-mcherry for PV knockdown vector (KD) and preparation of PL-isolated proteins 3 weeks after injection of viruses.

(b) Representative immunoblots of PL-isolated protein from PV SCR and KD group for total western and co-IP assay pulling down with PV proteins, which are selected from two different sets of my data. Note that PV protein

levels were decreased in KD group within total and co-IP assay. Levels of GluR 4, PKA, and AC 5 proteins biding to PV proteins were also significantly reduced in KD group within co-IP assay compared to SCR group, although there is no significant difference in several protein levels except PV and AC 5 between PV SCR and KD group within total western assay. Reciprocal binding of GluR 1 to PV was determined in PV SCR and KD group (right, top). A few proteins such as CaMKII and GABAR had no physiological interaction with PV proteins both in PV SCR and KD group (right, bottom).

Figure 2.2 Re-activation of PKA signaling with forskolin improved AMPAR synaptic strength in Pv interneurons.

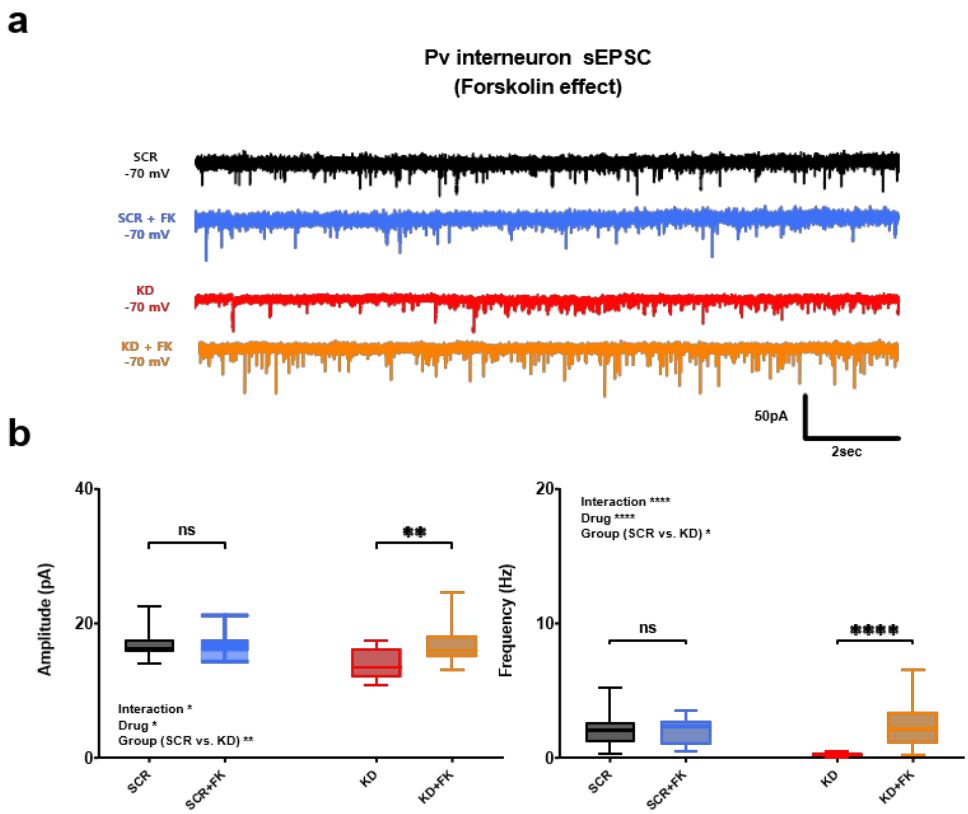

(a) For PKA activator effects on AMPAR-mediated sEPSC in Pv interneurons, forskolin 20 μM was bath applied to brain slices at least 20 min in PV SCR and KD group. Representative traces of AMPAR-mediated sEPSC at -70 mV voltage clamp recording from Pv interneurons before and after forskolin treatment in PV SCR (SCR vs. SCR+FK) and KD (KD vs. KD+FK) groups.

(b) Bar graphs comparing the amplitude or frequency of AMPAR-mediated sEPSC within PV SCR or KD group before and after forskolin treatment. Note that forskolin effects enhanced the amplitude and frequency of sEPSC in PV KD without affecting sEPSC in PV SCR. (amplitude, n=18 [SCR],

n=18 [SCR+FK], n=17 [KD], n=17 [KD+FK], Interaction F (1, 33) = 6.795, p=0.0136, Drug F (1, 33) = 6.020, p=0.0196, Group F (1, 33) = 8.326, p=0.0068, SCR vs. SCR+FK: p>0.9999, KD vs. KD+FK: p=0.0025, *p < 0.05, **p < 0.01, ns, not significant, Repeated measures of Two Way ANOVA with Bonferroni's test [bar graph]) (frequency, n=18 [SCR], n=18 [SCR+FK], n=17 [KD], n=17 [KD+FK], Interaction F (1, 33) = 23.59, p<0.0001, Drug F (1, 33) = 22.66, p<0.0001, Group F (1, 33) = 4.764, p=0.0363, SCR vs. SCR+FK: p=0.9970, KD vs. KD+FK: p<0.0001, *p < 0.05, ****p < 0.0001, ns, not significant, Repeated measures of Two Way ANOVA with Sidak's multiple comparisons test [bar graph]).

Figure 2.3 Adenylate cyclase 5 were enriched specifically in Pv interneurons.

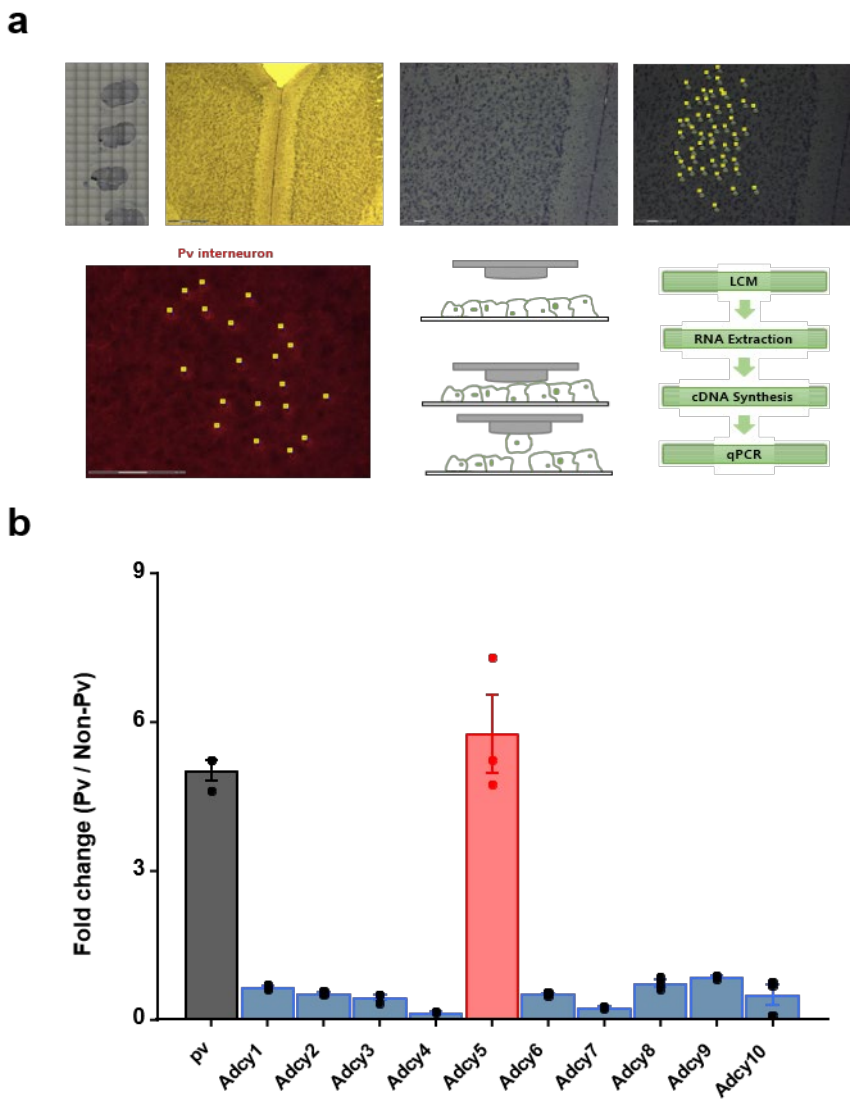

(a) Schematic diagram for laser-capture microdissection (LCM) to examine RNA transcripts assay specifically in Pv interneuronal population from normal mice. Real-time quantitative PCR (RT-PCR) was assessed for a family of adenylate cyclase (AC) isoforms. RNA samples were collected

from Pv interneurons and Non-Pv interneurons in the PL through LCM.

(b) Summary of mRNA expression in Pv interneurons as a fold change compared with non-Pv interneurons for AC 1-10 isoforms and pv genes. Note that AC 5 is the most highly enriched in Pv interneurons compared to other isoforms of AC, associated with prominent expression of PV.

Figure 2.4 AC 5 mediator, DAMGO, enhanced AMPAR synaptic strength in Pv interneurons.

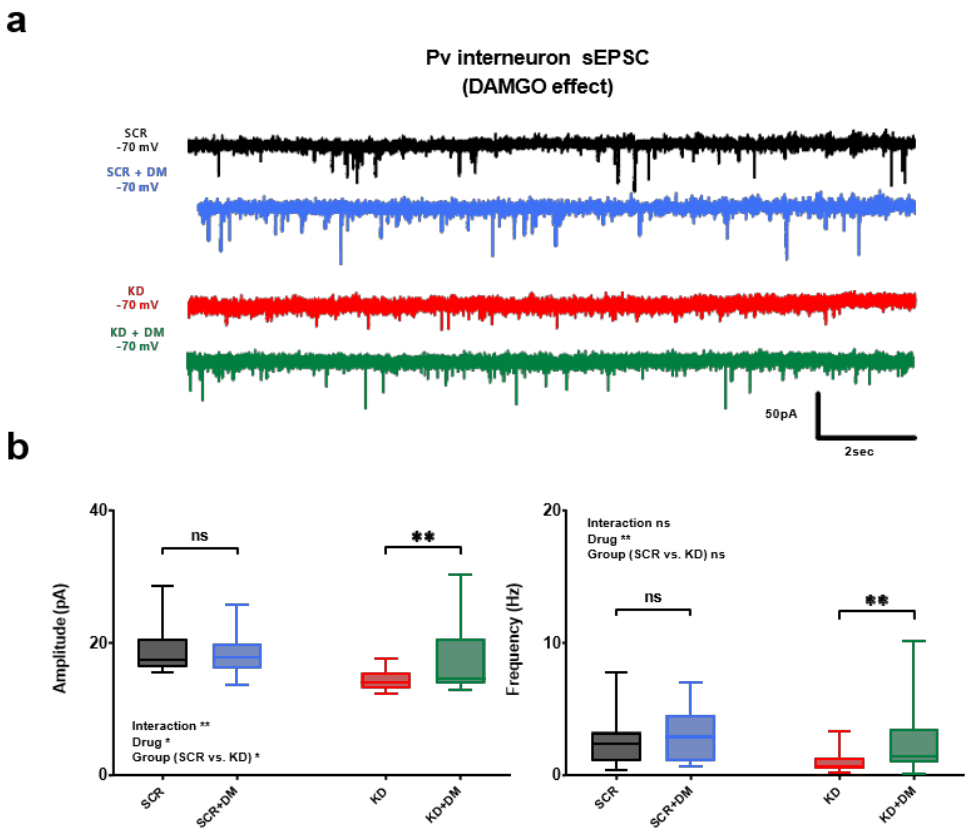

(a) For AC 5 mediator effects on AMPAR-mediated sEPSC in Pv interneurons, DAMGO 1 μM was bath applied to brain slices at least 25 min in PV SCR and KD group. Representative traces of AMPAR-mediated sEPSC at -70 mV voltage clamp recording from Pv interneurons before and after DAMGO treatment in PV SCR (SCR vs. SCR+DM) and KD (KD vs. KD+DM) groups.

(b) Bar graphs comparing the amplitude or frequency of AMPAR-mediated sEPSC within PV SCR or KD group before and after DAMGO treatment

(SCR vs. SCR+DM and KD vs. KD+DM). Note that DAMGO effects enhanced the amplitude but not frequency of sEPSC in PV KD without affecting sEPSC in PV SCR. (amplitude, n=17 [SCR], n=17 [SCR+DM], n=17 [KD], n=17 [KD+DM], Interaction F (1, 32) = 9.603, p=0.0040, Drug F (1, 32) = 4.250, p=0.0475, Group F (1, 32) = 6.645, p=0.0148, SCR vs. SCR+DM: p=0.7176, KD vs. KD+DM: p=0.0019, *p < 0.05, **p < 0.01, ns, not significant, Repeated measures of Two Way ANOVA with Bonferroni's test [bar graph]) (frequency, n=17 [SCR], n=17 [SCR+DM], n=17 [KD], n=17 [KD+DM], Interaction F (1, 32) = 1.595, p=0.2158, Drug F (1, 32) = 9.270, p=0.0046, Group F (1, 32) = 2.699, p=0.1102, SCR vs. SCR+DM: p=0.3865, KD vs. KD+DM: p=0.0092, **p < 0.01, ns, not significant, Repeated measures of Two Way ANOVA with Sidak's multiple comparisons test [bar graph]).

Figure 2.5 AC 5 KO (AC 5 $^{-/-}$) mice indicated PPI deficits with normal behavior phenotypes.

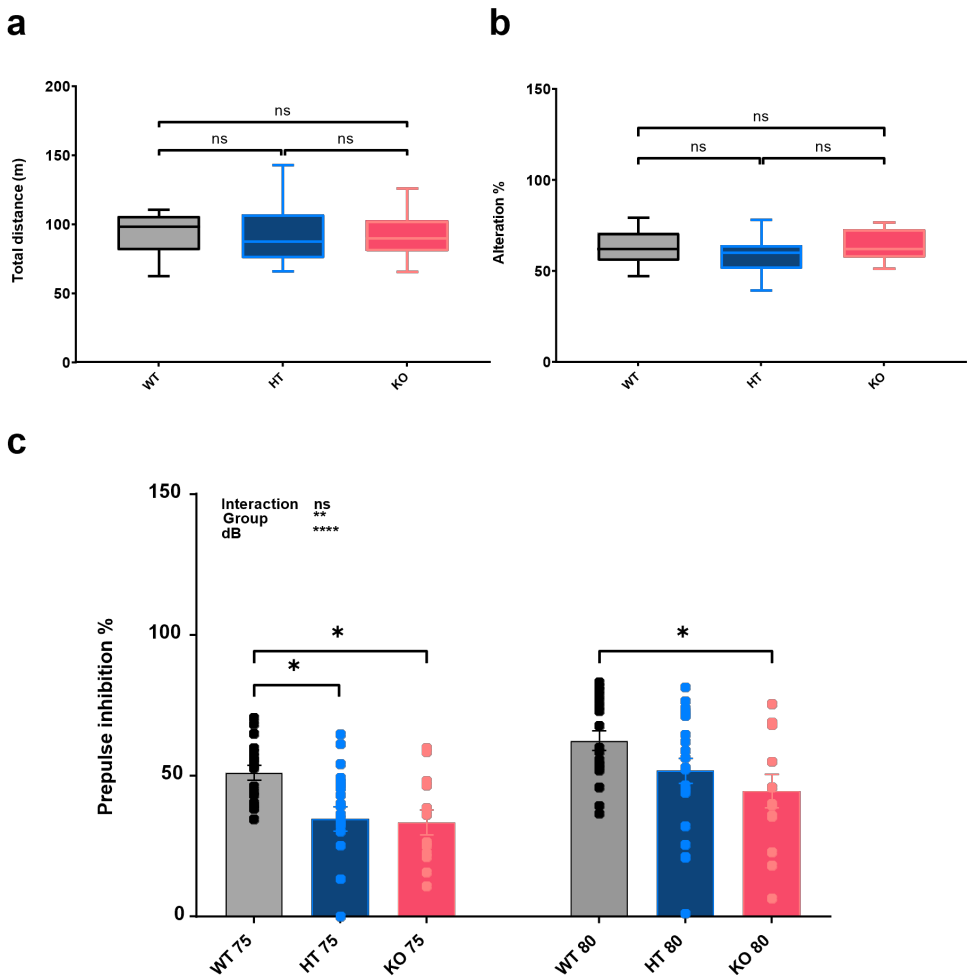

(a) Bar graph showing open field test for locomotion activity as calculated by total distance moved. Normal locomotion activity between AC 5 wild-type (AC 5 $^{+/+}$, AC 5 WT), AC 5 hetero-type (AC 5 $^{+/-}$, AC 5 HT), and AC 5 knock out (AC 5 $^{-/-}$, AC 5 KO) mice. (n=18 [WT], n=23 [HT], n=15 [KO], F 0.004537, WT vs. HT: p=0.9997, WT vs. KO: p=0.9997, HT vs. KO: p=0.9997, ns, not significant, Ordinary one-way ANOVA with Holm-

Sidak's multiple comparisons test, [bar graph]).

(b) Y-maze assay for working memory index as measured by proportion (%) of spontaneous alteration. Normal spontaneous alteration % between AC 5 WT, HT, and KO mice. (n=18 [WT], n=23 [HT], n=15 [KO], F 2.596, WT vs. HT: p=0.2383, WT vs. KO: p=0.5125, HT vs. KO: p=0.1014, ns, not significant, Ordinary one-way ANOVA with Holm-Sidak's multiple comparisons test, [bar graph])

(c) Bar graph comparing PPI proportion (%) to AC 5 AC 5 WT, HT, and KO mice during PPI sessions either with 75- or 80 dB pre-pulse. Note that AC 5 KO mice showed significant reduction in PPI % compared to AC 5 WT mice both in 75- and 80-dB pre-pulse with AC 5 HT mice showing subtle reduction in PPI % in 75-dB pre-pulse. (n=18 [WT], n=23 [HT], n=15 [KO], Interaction F (2, 51) = 1.148, p=0.3254, Group F (2, 51) = 5.132, p=0.0093, dB F (1, 51) = 45.00, p<0.0001, WT 75 vs. HT: p=0.0135, WT 75 vs. KO: p=0.0234, WT 80 vs. KO: p=0.0215, *p < 0.05, **p < 0.01, ****p < 0.0001, ns, not significant, Two-way repeated measures of ANOVA with Tukey's multiple comparisons test, [bar graph]).

Figure 2.6 Forskolin improved PPI deficits in PV deficiency model.

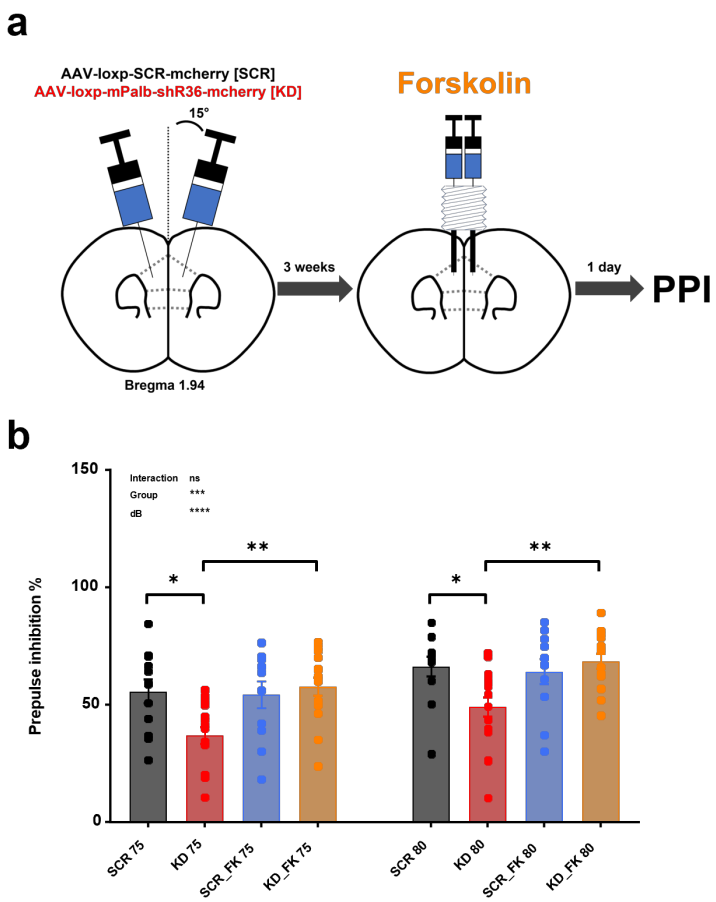

(a) Schematic diagram for sequential experiments indicating that bilateral microinjection of vehicle or drug (forskolin 2.5 µg/µl) into each prelimbic region was examined in Pv-cre mice infected either with PV SCR or PV KD viruses for 3 weeks to investigate drug effects on PPI assay. SCR or KD described as mice injected PV SCR or PV KD viruses with microinjection of vehicle. SCR_FK or KD_FK represented as mice injected PV SCR or PV KD viruses with microinjection of each drug (FK, forskolin).

(b) Bar graphs comparing proportion (%) of PPI between PV SCR and KD

group each within vehicle or forskolin effects in PPI assay either with 75- or 80- dB pre-pulse. Note that PV KD group showed a substantial decrease in PPI % both with 75- or 80-dB pre-pulse compared to SCR group, which is significantly enhanced in KD_FK group with no forskolin effects on SCR group. (n= 12 mice [SCR], n=11 mice [SCR_FK], n=17 mice [KD], n=15 mice [KD_FK], Interaction F (3, 51) = 0.05811, p=0.9814, dB F (1, 51) = 25.51, p<0.0001, Group F (3, 51) = 7.087, p=0.0005, SCR 75 vs. KD: p=0.0131, KD 75 vs. KD_FK: p=0.0021, SCR 80 vs. KD: p=0.0282, KD 80 vs. KD_FK: p=0.0047, *p < 0.05, **p < 0.01, ***p < 0.001, ****p < 0.0001, ns, not significant, Repeated measures of Two Way ANOVA with Sidak's multiple comparisons test, [bar graph]).

Figure 2.7 Reactivation of PKA signaling had no effect on basal behavior phenotypes in PV deficiency model.

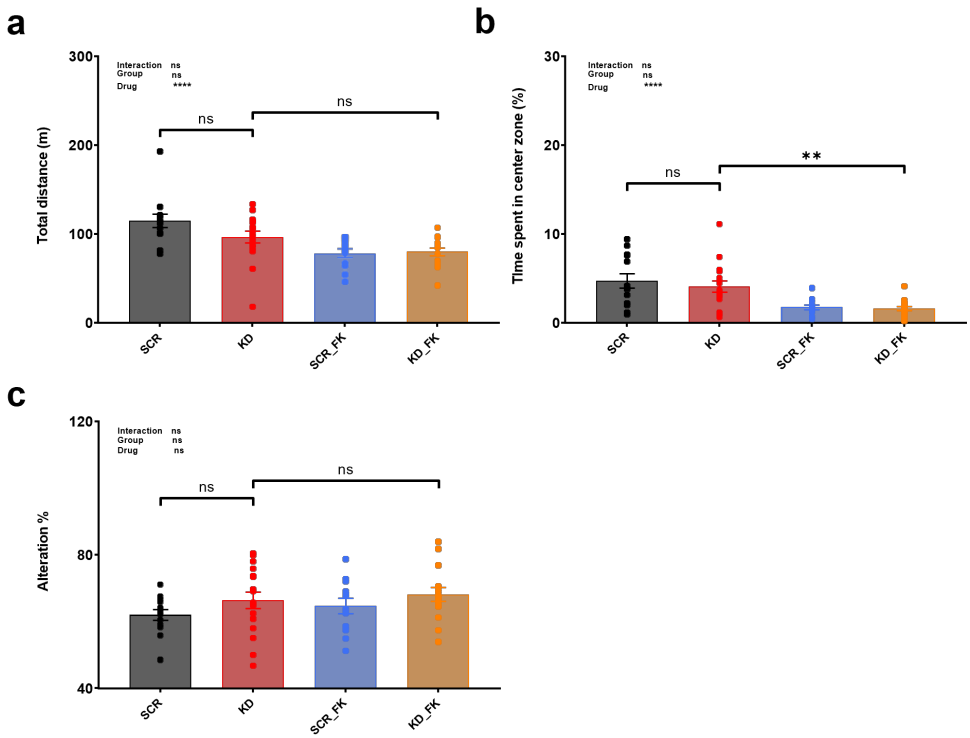

(a) Bar graph showing open field test for locomotion activity as calculated by total distance moved. Normal locomotion activity between PV SCR and KD group with no forskolin (FK) effects in PV SCR (SCR_FK) and KD (KD_FK) group. (n=13 [SCR], n=12 [SCR_FK], n=17 [KD], n=15 [KD_FK] Interaction F (1, 53) = 2.702, p=0.1062, Group F (1, 53) = 1.774, p=0.1886, Drug F (1, 53) = 18.42, p<0.0001, SCR vs. KD: p=0.0696, KD vs. KD_FK: p=0.0992, **p < 0.01, ****p < 0.0001, ns, not significant, Two-way ANOVA with Sidak's multiple comparisons test, [bar graph]).

(b) In open field test, anxiety levels as determined by the time spent in the first 5 min in center-zone, indicating increased anxiety levels with less time spent

in center-zone. Note that there is no difference in anxiety levels between PV SCR and KD group, with significant forskolin (FK) effects on anxiety levels both in PV SCR (SCR_FK) and KD (KD_FK) group. (n=13 [SCR], n=12 [SCR_FK], n=17 [KD], n=15 [KD_FK] Interaction F (1, 53) = 0.2167, p=0.6435, Group F (1, 53) = 0.5135, p=0.4768, Drug F (1, 53) = 22.80, p<0.0001, SCR vs. KD: p=0.6340, KD vs. KD_FK: p=0.0040, **p < 0.01, ****p < 0.0001, ns, not significant, Two-way ANOVA with Sidak's multiple comparisons test, [bar graph]).

(c) Y-maze assay for working memory index as measured by proportion (%) of spontaneous alteration. Normal spontaneous alteration % between PV SCR and KD group without forskolin (FK) effects in PV SCR (SCR_FK) and KD (KD_FK) group. (n=13 [SCR], n=12 [SCR_FK], n=17 [KD], n=15 [KD_FK] Interaction F (1, 53) = 0.05222, p=0.8201, Group F (1, 53) = 3.078, p=0.0851, Drug F (1, 53) = 0.9742, p=0.3281, SCR vs. KD: p=0.2880, KD vs. KD_FK: p=0.8147, ns, not significant, Two-way ANOVA with Sidak's multiple comparisons test, [bar graph]).

Figure 2.8 DAMGO reversed PPI deficits in PV deficiency model.

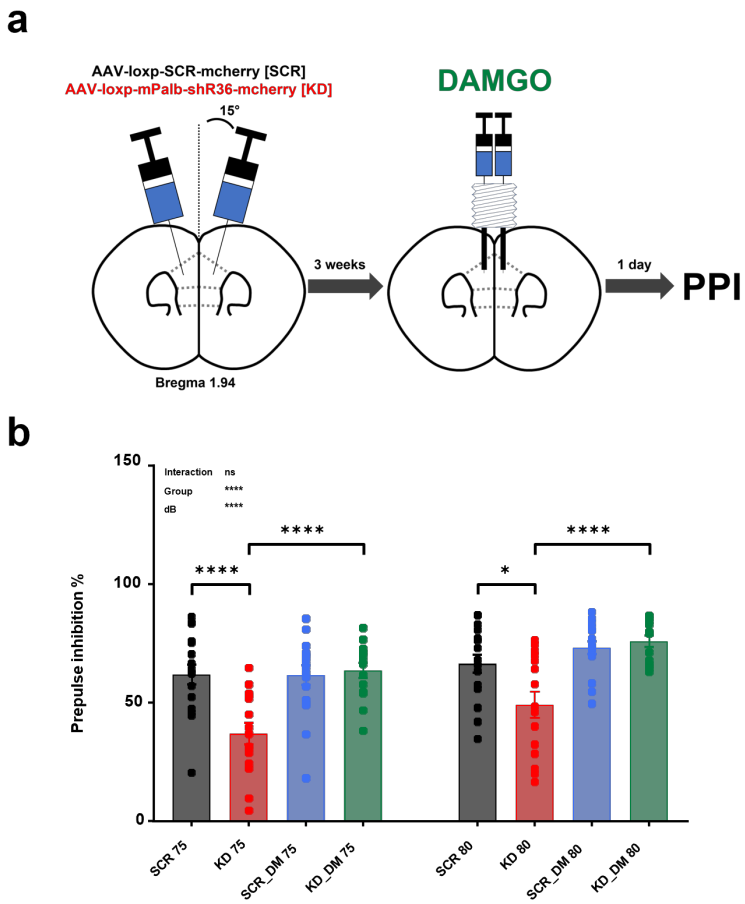

(a) Schematic diagram for sequential experiments indicating that bilateral microinjection of vehicle or drug (DMAGO 10 ng/µl) into each prelimbic region was examined in Pv-cre mice infected either with PV SCR or PV KD viruses for 3 weeks to investigate drug effects on PPI assay. SCR or KD described as mice injected PV SCR or PV KD viruses with microinjection of vehicle. SCR_DM or KD_DM represented as mice injected PV SCR or PV KD viruses with microinjection of each drug (DM, DAMGO).

(b) Bar graphs indicating comparison of PPI proportion (%) between PV SCR

and KD group each within vehicle or DAMGO effects on PPI assay either with 75- or 80- dB pre-pulse. Note that PV KD group showed a considerable decrease in PPI % both with 75- or 80-dB pre-pulse compared to SCR group, which is substantially improved in KD_DM group without DAMGO effects on SCR group. (n= 17 mice [SCR], n=17 mice [SCR_DM], n=17 mice [KD], n=14 mice [KD_DM], Interaction F (3, 59) = 1.672, p=0.1827, dB F (1, 59) = 47.92, p<0.0001, Group F (3, 59) = 10.71, p<0.0001, SCR 75 vs. KD: p=<0.0001, KD 75 vs. KD_DM: p=<0.0001, SCR 80 vs. KD: p=0.0116, KD 80 vs. KD_DM: p=<0.0001, *p < 0.05, ****p < 0.0001, ns, not significant, Repeated measures of Two Way ANOVA with Tukey's multiple comparisons test, [bar graph]).

Figure 2.9 AC 5 mediator, DAMGO, had no effect on basal behavior phenotypes in PV deficiency model.

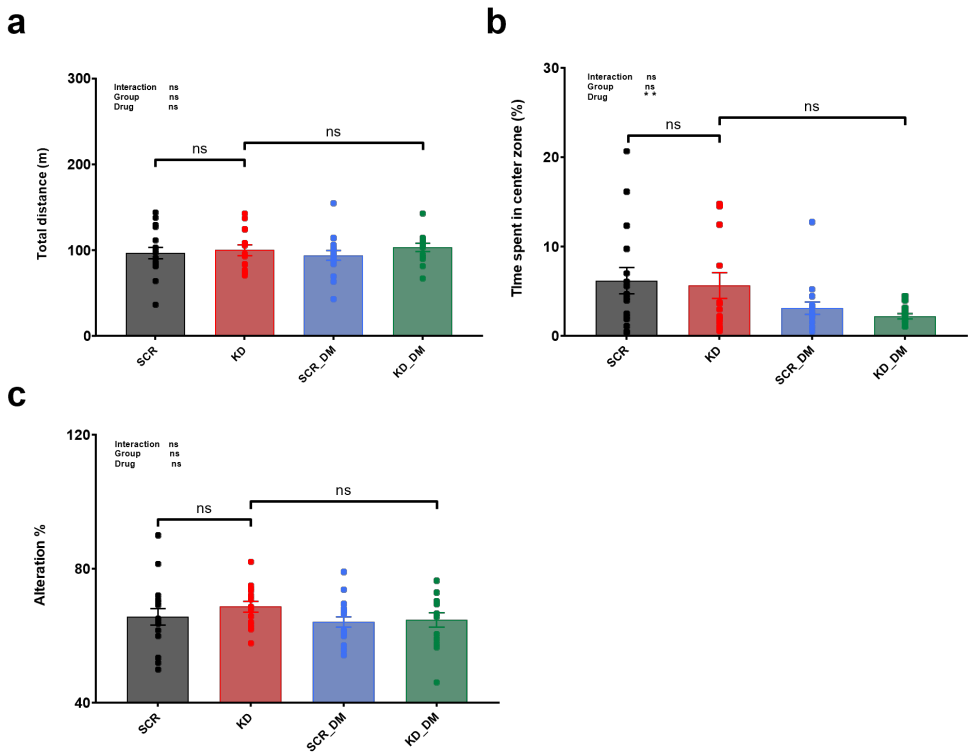

(a) Bar graph indicating open field test for locomotion activity. Normal locomotion activity between PV SCR and KD group with no DAMGO (DM) effects in PV SCR (SCR_DM) and KD (KD_DM) group. (n=17 [SCR], n=17 [SCR_DM], n=15 [KD], n=14 [KD_DM], Interaction F (1, 59) = 0.2600, p=0.6121, Group F (1, 59) = 1.079, p=0.3032, Drug F (1, 59) = 2.152e-007, p=0.9996, SCR vs. KD: p=0.9143, KD vs. KD_DM: p=0.9269, ****p < 0.0001 ns, not significant, Two-way ANOVA with Sidak's multiple comparisons test, [bar graph]).

(b) Bar graph displaying anxiety levels in open field test. Note that there is no difference in anxiety levels between PV SCR and KD group with no

DAMGO (DM) effect both in PV SCR (SCR_DM) and KD (KD_DM) group. (n=17 [SCR], n=17 [SCR_DM], n=15 [KD], n=14 [KD_DM], Interaction F (1, 53) = 0.2167, p=0.6435, Group F (1, 53) = 0.5135, p=0.4768, Drug F (1, 53) = 22.80, p<0.0001, SCR vs. KD: p=0.9255, KD vs. KD_DM: p=0.0681, ns, not significant, Two-way ANOVA with Sidak's multiple comparisons test, [bar graph]).

(c) Bar graph showing proportion (%) of spontaneous alteration. Normal spontaneous alteration % between PV SCR and KD group without DAMGO (DM) effects in PV SCR (SCR_DM) and KD (KD_DM) group. (n=17 [SCR], n=17 [SCR_DM], n=15 [KD], n=14 [KD_DM], Interaction F (1, 59) = 0.3510, p=0.5558, Group F (1, 59) = 0.7807, p=0.3805, Drug F (1, 59) = 1.905, p=0.1728, SCR vs. KD: p=0.5049, KD vs. KD_DM: p=0.8147, ns, not significant, Two-way ANOVA with Sidak's multiple comparisons test, [bar graph]).

Figure 2.10 Auditory steady-state response induced evoked gamma oscillation in mPFC.

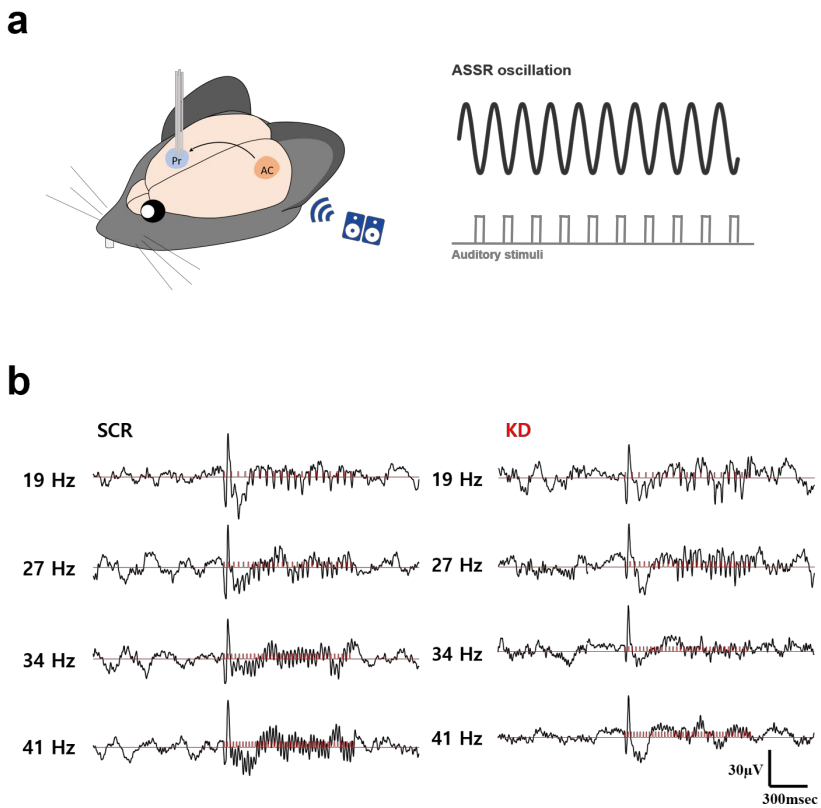

(a) Schematic diagram for auditory steady-state response (ASSR)-mediated evoked gamma oscillation recording. When sound clicks were presented in a train with each frequency pulse, auditory sensory evoked neuronal oscillation of each resonant frequency was recorded as local field potential (LFP) in the PL-mPFC.

(b) Averaged traces of LFP activity (black lines) in PV SCR (top) and KD group (bottom) with band-pass filtered at each 19, 27, 34, or 41 Hz of auditory stimuli (red lines).

Figure 2.11 PV deficiency model showed reduction in ASSR-mediated evoked gamma oscillation, improved by DAMGO.

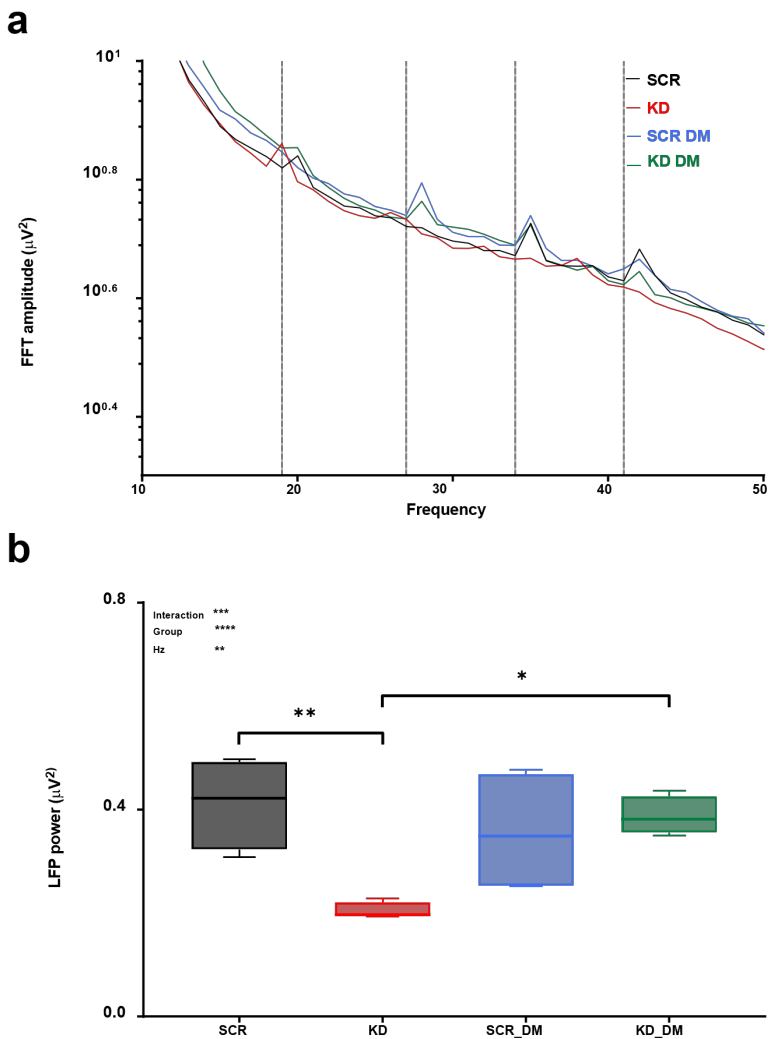

(a) Averaged fast fourier transform (FFT) amplitudes in PV SCR and KD group with or without DAMGO treatment through microinjection into PL-mPFC by cannula. Note that PV KD group showed reduced FFT amplitudes at 27, 34, and 41 Hz compared to PV SCR group, which were enhanced in PV KD group with DAMGO effects (KD_DM) without DAMGO effects on PV

SCR group.

(b) Bar graph indicating averaged relative power normalized to baseline at 41 Hz as gamma frequency oscillation in PV SCR and KD group with or without DAMGO treatment. Note that a significant decrease in power in PV KD was improved by DAMGO effects in PV KD_DM group without affecting PV SCR group. (n= 10 mice [SCR], n=9 mice [SCR_DM], n=20 mice [KD], n=7 mice [KD_DM], Interaction F (9, 126) = 3.581, p=0.0005, Group F (3, 42) = 5.913, p=0.0018, Hz F (2.322, 97.51) = 15.77, p<0.0001, SCR vs. KD: p=0.0071, KD vs. KD_DM: p=0.0175, *p < 0.05, **p < 0.01, ***p < 0.001, ****p < 0.0001, Repeated measures of Two Way ANOVA with Tukey's multiple comparisons test, [bar graph]).

Figure 2.12 ASSR-mediated evoked gamma oscillation was reduced in NMDAR hypofunction model.

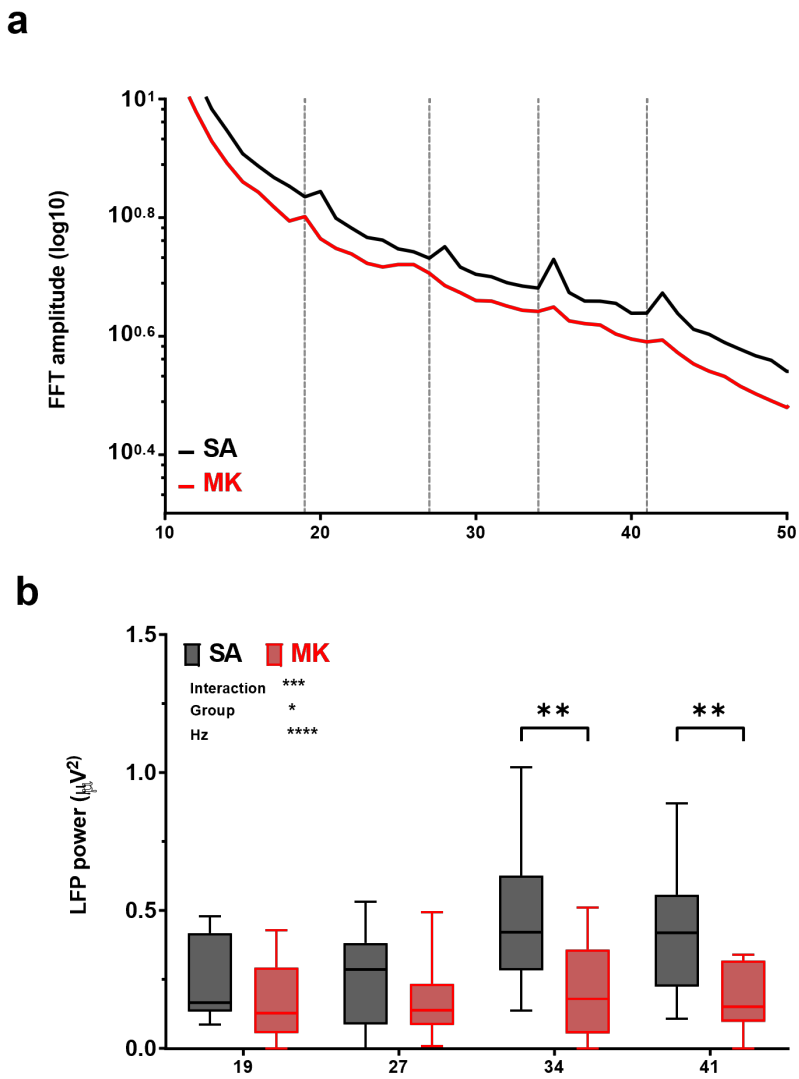

(a) Averaged fast fourier transform (FFT) amplitudes in SA and MK group. Note that MK group showed a substantial decrease in FFT amplitudes at 27, 34, and 41 Hz compared to SA group.

(b) Bar graph indicating averaged relative power normalized to baseline at 19, 27, 34, and 41 Hz in SA and MK group. Note that a significant decrease in

power at 34 and 41 Hz in MK group compared to SA group. (n=19 [SA], n=19 [MK], Interaction F (3, 72) = 7.366, p=0.0002, Group F (1, 24) = 7.465, p=0.0116, Group F (1, 24) = 7.465, p=0.0116, SA 19 vs. MK 19: p=0.7553, SA 27 vs. MK 27: p=0.7513, SA 34 vs. MK 34: p=0.0012, SA 41 vs. MK 41: p=0.0016, *p < 0.05, **p < 0.01, ***p < 0.001, ****p < 0.0001, ns, not significant, Two-way repeated measures of ANOVA with Sidak's multiple comparisons test, [bar graph]).

DISCUSSION

In chapter II, my main conclusion is that Pv interneuronal dysfunction, distinctively, of AC 5-PKA signaling-dependent regulation of AMPAR synaptic strength is caused by PV deficiency, leading to sensorimotor gating deficits.

Previous studies on Pv interneuronal dysfunction have suggested that limited NMDAR hypofunction mouse models revealed sensorimotor gating deficits.[25–27,31,33–37] Furthermore, parvalbumin (PV) deficiency mouse models have been associated with sensorimotor gating deficits.[54,57] In my study including chapter I & II, these two mechanisms are interconnected to demonstrate how NMDAR hypofunction-induced PV deficiency is implicated in sensorimotor gating deficits.

- **AC 5-mediated PKA signaling to regulate AMPAR distinctively in Pv interneurons for PPI modulation**

Intriguingly, my data indicate that PV deficiency causes reduction in PKA signaling which contributes to synaptic changes of AMPAR in Pv interneurons as determined by a significant decrease level of PKA and GluR 4 as pulling down with PV in PV KD mice. Furthermore, in terms of subsequent activation of cAMP dependent PKA signaling by adenylate cyclase (AC), of note, AC 5 isoform enriched in Pv interneurons is substantially reduced in my PV deficiency mice. This reduced modulation of PKA and AC 5 signaling in PV deficiency mice negatively regulates AMPAR synaptic strength and results in PPI deficits. Consistent with this, AC 5 knock out (AC 5 $^{-/-}$) also indicate PPI impairments. Re-activation of AC 5-PKA signaling moderately promotes an increase of AMPAR synaptic activity and

improvement of gamma oscillation power, thereby enhancing its-related PPI effects. Importantly, I demonstrate that distinct AC 5-mediated PKA signaling depends on PV expression, which is the key component to regulate AMPAR specifically in Pv interneurons for mPFC network activity to modulate PPI.

This finding contrasts with the phenotypes of increased synaptic plasticity and enhanced complex learning in AC 6 knock out mice (AC 6 $^{-/-}$).[96] However, consistent with the previous evidence that Ca^{2+}-stimulated AC 1 or AC 8 is essential for synaptic plasticity of AMPAR[97], a decrease in AC 5 modulation cause downregulation of AMPAR in Pv interneurons, leading to sensorimotor gating deficit. My finding is also in line with regulation of AMPAR by AC 5 signaling in non-neuronal mechanisms.[98] These results indicate that synaptic regulation of AMPAR may appear differently in various neuronal mechanisms depending on types of adenylate cyclase isoforms.

- **AMPAR-mediated synaptic changes in Pv interneurons are implicated in evoked gamma oscillation through ASSR**

Mice with deletion of NMDAR in Pv interneurons indicate a different pattern of an increase in spontaneous gamma oscillation but a decrease in evoked gamma oscillation associated with subtle behavioral effects.[34,35,37] These results demonstrate that there is a dissociation between the effects of NMDAR hypofunction on abnormal evoked gamma oscillation and cognitive deficits.[34,37] This leads to notion that NMDAR hypofunction itself with abnormal gamma oscillation could not be fully implicated in dysfunction of sensorimotor gating as one of complex cognitive

functions, which is insufficient to represent SZ-related phenotype model. In contrast to this, reduced excitatory recruitment of Pv interneurons by deletion of AMPAR GluR 4 subunit (not GluR 1) deteriorates induced gamma oscillation with corresponding defects in the cognitive function.[78] Therefore, as compared to reduction in NMDAR activity alone, I suggest NMDAR hypofunction in concert with downregulated AMPAR is more critical causation to impair evoked gamma oscillation determined as ASSR[94], leading to sensorimotor gating deficits as SZ-related cognitive dysfunction in my NMDAR hypofunction mice. Previous evidence explicates that deletion of NMDAR in interneurons is important to result in several schizophrenia-related phenotypes including PPI deficits accompanied by reduction in gamma oscillation power.[95] This is determined in NMDAR hypofunction in a mixed population of GABAergic interneurons including Pv interneurons. However, my model of NMDAR hypofunction specifically in Pv interneurons without affecting PNs suggests that the function of NMDAR activity in regulation of AMPAR is required to modulate PPI in mPFC.

■ Implication of this study

In the end, my data suggest that Pv interneuron-specific signal transduction for coupling NMDAR activity to PKA signaling is through PV-mediated AC 5, which is implicated in synaptic regulation of AMPAR to coordinate mPFC network activity and its-related PPI effects.

Previous results suggest that adenylate cyclases are activated by Ca^{2+} dependent kinases such as calmodulin (CaM) mostly in excitatory neurons.[97,99–101] In contrast,

inhibitory interneurons, specifically, are devoid of cytoplasmic CaM and its-dependent enzymes as a major Ca^{2+} signaling, yet CaM is localized in nuclei as CaM shuttling to trigger gene expression.[102,103] This leads to the absence of major forms of synaptic plasticity of AMPAR mediated by CaM and Ca^{2+}/CaM-dependent protein kinase II (CaMKII) in inhibitory neurons.[104–107] Therefore, I suggest the alternative mechanisms underlying modification of AMPAR synaptic activity by activating adenylate cyclases specifically in Pv interneurons. Ca^{2+} binding parvalbumin itself, distinctively in Pv interneurons, may be of function as activation of AC 5 to modulate cAMP levels to compensate lack of CaM and its-related Ca^{2+} signaling. This is supported by my results that PV deficiency alone causes significant loss of AC 5 expression, leading to downregulation of cAMP dependent AMPAR activity in Pv interneurons. From this point of view, importantly, PV deficiency induced by NMDAR hypofunction is the key causation to impair AMPAR synaptic strength, thereby leading to reduction in evoked gamma oscillation and sensorimotor gating deficits. This evidence suggests the need to further investigate Ca^{2+}-related mechanisms underlying how PV itself arranges subsequent modulation of AC 5-dependent PKA signaling distinctively in Pv interneurons in future studies.

My study is highly relevant to the pathophysiology of psychiatric diseases such as schizophrenia in a way that a decrease in evoked gamma oscillation associated with auditory steady-state response (ASSR) and sensorimotor gating deficits in my Pv interneuronal dysfunction models relate to SZ-phenotypes.[1,2,10,94,108–110]

■ Conclusion

In conclusion, my study provides the novel PV-AC 5 signal transduction for coupling NMDAR function to PKA signaling, underpinning regulation of AMPAR adaptive to network alteration such as NMDAR activity. This novel PV-AC 5 signaling for synaptic changes specifically in Pv interneurons contributes to advancements in my understanding of PPI-related Pv interneuronal mechanisms. My work reveals new links between dysfunction of Pv interneuronal mechanisms in synaptic modulation and sensorimotor gating deficits for the investigation of one dimension of pathophysiology in SZ-phenotypes, suggesting a new target for therapeutic effects.

Bibliography

1. Perry, W., Minassian, A., Lopez, B., Maron, L. & Lincoln, A. Sensorimotor Gating Deficits in Adults with Autism. *Biol Psychiat* **61**, 482–486 (2007).

2. Braff, D. L. & Geyer, M. A. Sensorimotor Gating and Schizophrenia. *Arch Gen Psychiat* **47**, 181 (1990).

3. Qi, R., Li, M., Ma, Y. & Chen, N. State-dependent changes in auditory sensory gating in different cortical areas in rats. *Plos One* **10**, e0126684 (2015).

4. Rohleder, C. *et al.* The Functional Networks of Prepulse Inhibition: Neuronal Connectivity Analysis Based on FDG-PET in Awake and Unrestrained Rats. *Front Behav Neurosci* **10**, 148 (2016).

5. Braff, D. L., Geyer, M. A. & Swerdlow, N. R. Human studies of prepulse inhibition of startle: normal subjects, patient groups, and pharmacological studies. *Psychopharmacology* **156**, 234–258 (2001).

6. Plakke, B. & Romanski, L. M. Auditory connections and functions of prefrontal cortex. *Front Neurosci-switz* **8**, 199 (2014).

7. Medalla, M. & Barbas, H. Specialized prefrontal "auditory fields" : organization of primate prefrontal-temporal pathways. *Front Neurosci-switz* **8**, 77 (2014).

8. Li, L., Du, Y., Li, N., Wu, X. & Wu, Y. Top–down modulation of prepulse inhibition of the startle reflex in humans and rats. *Neurosci Biobehav Rev* **33**, 1157–1167 (2009).

9. Tóth, A. *et al.* Neuronal coding of auditory sensorimotor gating in medial prefrontal cortex. *Behav Brain Res* **326**, 200–208 (2017).

10. Valsamis, B., Chang, M., Typlt, M. & Schmid, S. Activation of mGluR2/3 receptors in the ventro-rostral prefrontal cortex reverses sensorimotor gating deficits induced by systemic NMDA receptor antagonists. *Int J Neuropsychopharmacol Official Sci J Coll Int Neuropsychopharmacol Cinp* **17**, 303–12 (2014).

11. Geyer, M. A., Krebs-Thomson, K., Braff, D. L. & Swerdlow, N. R. Pharmacological studies of prepulse inhibition models of sensorimotor gating deficits in schizophrenia: a decade in review. *Psychopharmacology* **156**, 117–154 (2001).

12. Japha, K. & Koch, M. Picrotoxin in the medial prefrontal cortex impairs sensorimotor gating in rats: reversal by haloperidol. *Psychopharmacology* **144**, 347–354 (1999).

13. Ellenbroek, B. A., Budde, S. & Cools, A. R. Prepulse inhibition and latent inhibition: the role of dopamine in the medial prefrontal cortex. *Neuroscience* **75**, 535–542 (1996).

14. Jones, N. C. *et al.* Effects of aberrant gamma frequency oscillations on prepulse inhibition. *Int J Neuropsychopharmacol* **17**, 1671–1681 (2014).

15. Hudson, M. R., Rind, G., O'Brien, T. J. & Jones, N. C. Reversal of evoked gamma oscillation deficits is predictive of antipsychotic activity with a unique profile for clozapine. *Transl Psychiat* **6**, e784 (2016).

16. Lazarus, M. S., Krishnan, K. & Huang, Z. J. GAD67 Deficiency in Parvalbumin Interneurons Produces Deficits in Inhibitory Transmission and Network Disinhibition in Mouse Prefrontal Cortex. *Cereb Cortex* **25**, 1290–1296 (2015).

17. Brown, J. A. *et al.* Inhibition of parvalbumin-expressing interneurons results in complex behavioral changes. *Mol Psychiatr* **20**, 1499–507 (2015).

18. Volman, V., Behrens, M. M. & Sejnowski, T. J. Downregulation of Parvalbumin at Cortical GABA Synapses Reduces Network Gamma Oscillatory Activity. *J Neurosci* **31**, 18137–18148 (2011).

19. Nguyen, R. *et al.* Parvalbumin and GAD65 interneuron inhibition in the ventral hippocampus induces distinct behavioral deficits relevant to schizophrenia. *J Neurosci Official J Soc Neurosci* **34**, 14948–60 (2014).

20. Wang, H.-X. & Gao, W.-J. Development of calcium-permeable AMPA receptors and their correlation with NMDA receptors in fast-spiking interneurons of rat prefrontal cortex. *J Physiology* **588**, 2823–2838 (2010).

21. Xi, D., Zhang, W., Wang, H.-X., Stradtman, G. G. & Gao, W.-J. Dizocilpine (MK-801) induces distinct changes of N-methyl-D-aspartic acid receptor subunits in parvalbumin-containing interneurons in young adult rat prefrontal cortex. *Int J Neuropsychopharmacol Official Sci J Coll Int Neuropsychopharmacol Cinp* **12**, 1395–408 (2009).

22. Li, Q., Clark, S., Lewis, D. V. & Wilson, W. A. NMDA Receptor Antagonists Disinhibit Rat Posterior Cingulate and Retrosplenial Cortices: A Potential Mechanism of Neurotoxicity. *J Neurosci* **22**, 3070–3080 (2002).

23. Homayoun, H. & Moghaddam, B. NMDA Receptor Hypofunction Produces Opposite Effects on Prefrontal Cortex Interneurons and Pyramidal Neurons. *J Neurosci* **27**, 11496–11500 (2007).

24. Grunze, H. *et al.* NMDA-dependent modulation of CA1 local circuit inhibition. *J Neurosci* **16**, 2034–2043 (1996).

25. Wozniak, D. F., Olney, J. W., Kettinger, L., Price, M. & Miller, J. P. Behavioral effects of MK-801 in the rat. *Psychopharmacology* **101**, 47–56 (2013).

26. Rompala, G. R., Zsiros, V., Zhang, S., Kolata, S. M. & Nakazawa, K. Contribution of NMDA receptor hypofunction in prefrontal and cortical excitatory neurons to schizophrenia-like phenotypes. *Plos One* **8**, e61278 (2013).

27. Wegener, N. *et al.* Evaluation of brain pharmacokinetics of (+)MK-801 in relation to behaviour. *Neurosci Lett* **503**, 68–72 (2011).

28. Maxwell, C. R. *et al.* Ketamine Produces Lasting Disruptions in Encoding of Sensory Stimuli. *J Pharmacol Exp Ther* **316**, 315–324 (2005).

29. Seamans, J. Losing inhibition with ketamine. *Nat Chem Biol* **4**, 91–93 (2008).

30. Bakshi, V. P. & Geyer, M. A. Multiple Limbic Regions Mediate the Disruption of Prepulse Inhibition Produced in Rats by the Noncompetitive NMDA Antagonist Dizocilpine. *J Neurosci* **18**, 8394–8401 (1998).

31. Jackson, M. E., Homayoun, H. & Moghaddam, B. NMDA receptor hypofunction produces concomitant firing rate potentiation and burst activity reduction in the prefrontal cortex. *Proc National Acad Sci* **101**, 8467–8472 (2004).

32. Krystal, J. H. *et al.* Subanesthetic Effects of the Noncompetitive NMDA Antagonist, Ketamine, in Humans: Psychotomimetic, Perceptual, Cognitive, and Neuroendocrine Responses. *Arch Gen Psychiat* **51**, 199 (1994).

33. Featherstone, R. E. *et al.* Subchronic ketamine treatment leads to permanent changes in EEG, cognition and the astrocytic glutamate transporter EAAT2 in mice. *Neurobiol Dis* **47**, 338–346 (2012).

34. Carlén, M. *et al.* A critical role for NMDA receptors in parvalbumin interneurons for gamma rhythm induction and behavior. *Mol Psychiatr* **17**, 537–548 (2011).

35. Bygrave, A. M. *et al.* Knockout of NMDA-receptors from parvalbumin interneurons sensitizes to schizophrenia-related deficits induced by MK-801. *Transl Psychiat* **6**, e778–e778 (2016).

36. Hudson, M. R., Sokolenko, E., O'Brien, T. J. & Jones, N. C. NMDA receptors on parvalbumin-positive interneurons and pyramidal neurons both contribute to MK-801 induced gamma oscillatory disturbances: Complex relationships with behaviour. *Neurobiol Dis* **134**, 104625 (2019).

37. Billingslea, E. N. *et al.* Parvalbumin cell ablation of NMDA-R1 causes increased resting network excitability with associated social and self-care deficits. *Neuropsychopharmacol Official Publ Am Coll Neuropsychopharmacol* **39**, 1603–13 (2014).

38. Wang, H.-X. & Gao, W.-J. Prolonged exposure to NMDAR antagonist induces cell-type specific changes of glutamatergic receptors in rat prefrontal cortex. *Neuropharmacology* **62**, 1808–1822 (2012).

39. Voglis, G. & Tavernarakis, N. The role of synaptic ion channels in synaptic plasticity. *Embo Rep* **7**, 1104–1110 (2006).

40. Pérez-Otaño, I. & Ehlers, M. D. Homeostatic plasticity and NMDA receptor trafficking. *Trends Neurosci* **28**, 229–238 (2005).

41. Honeycutt, J. A. & Chrobak, J. J. Parvalbumin Loss Following Chronic Sub-Anesthetic NMDA Antagonist Treatment is Age-Dependent in the Hippocampus: Implications for Modeling NMDA Hypofunction. *Neuroscience* **393**, 73–82 (2018).

42. Hashemi, E., Ariza, J., Rogers, H., Noctor, S. C. & Martínez-Cerdeño, V. The Number of Parvalbumin-Expressing Interneurons Is Decreased in the Medial Prefrontal Cortex in Autism. *Cereb Cortex* **27**, 1931–1943 (2017).

43. Lauber, E., Filice, F. & Schwaller, B. Dysregulation of Parvalbumin Expression in the Cntnap2−/− Mouse Model of Autism Spectrum Disorder. *Front Mol Neurosci* **11**, 262 (2018).

44. Chung, D. W., Fish, K. N. & Lewis, D. A. Pathological Basis for Deficient Excitatory Drive to Cortical Parvalbumin Interneurons in Schizophrenia. *Am J Psychiat* **173**, 1131–1139 (2016).

45. Joshi, D., Catts, V. S., Olaya, J. C. & Weickert, C. S. Relationship between somatostatin and death receptor expression in the orbital frontal cortex in schizophrenia: a postmortem brain mRNA study. *Npj Schizophrenia* **1**, 14004 (2015).

46. Jiang, Z., Cowell, R. M. & Nakazawa, K. Convergence of genetic and environmental factors on parvalbumin-positive interneurons in schizophrenia. *Front Behav Neurosci* **7**, 116 (2013).

47. Steullet, P. *et al.* Oxidative stress-driven parvalbumin interneuron impairment as a common mechanism in models of schizophrenia. *Mol Psychiatr* **22**, 936–943 (2017).

48. Filice, F., Vörckel, K. J., Sungur, A. Ö., Wöhr, M. & Schwaller, B. Reduction in parvalbumin expression not loss of the parvalbumin-expressing GABA interneuron subpopulation in genetic parvalbumin and shank mouse models of autism. *Mol Brain* **9**, 10 (2016).

49. Jenkins, T. A., Harte, M. K. & Reynolds, G. P. Effect of subchronic phencyclidine administration on sucrose preference and hippocampal parvalbumin immunoreactivity in the rat. *Neurosci Lett* **471**, 144–147 (2010).

50. Abekawa, T., Ito, K., Nakagawa, S. & Koyama, T. Prenatal exposure to an NMDA receptor antagonist, MK-801 reduces density of parvalbumin-immunoreactive GABAergic neurons in the medial prefrontal cortex and enhances phencyclidine-induced hyperlocomotion but not behavioral sensitization to methamphetamine in postpubertal rats. *Psychopharmacology* **192**, 303–316 (2007).

51. Braun, I. *et al.* Alterations of hippocampal and prefrontal GABAergic interneurons in an animal model of psychosis induced by NMDA receptor antagonism. *Schizophr Res* **97**, 254–263 (2007).

52. Cochran, S. M. *et al.* Induction of Metabolic Hypofunction and Neurochemical Deficits after Chronic Intermittent Exposure to Phencyclidine: Differential Modulation by Antipsychotic Drugs. *Neuropsychopharmacol* **28**, 265–275 (2003).

53. Coleman, L. G., Jarskog, L. F., Moy, S. S. & Crews, F. T. Deficits in adult prefrontal cortex neurons and behavior following early post-natal NMDA antagonist treatment. *Pharmacol Biochem Be* **93**, 322–330 (2009).

54. Wöhr, M. *et al.* Lack of parvalbumin in mice leads to behavioral deficits relevant to all human autism core symptoms and related neural morphofunctional abnormalities. *Transl Psychiat* **5**, e525 (2015).

55. Caillard, O. *et al.* Role of the calcium-binding protein parvalbumin in short-term synaptic plasticity. *Proc National Acad Sci* **97**, 13372–13377 (2000).

56. Orduz, D., Bischop, D. P., Schwaller, B., Schiffmann, S. N. & Gall, D. Parvalbumin tunes spike-timing and efferent short-term plasticity in striatal fast spiking interneurons: Parvalbumin regulates striatal fast spiking interneuron function. *J Physiology* **591**, 3215–3232 (2013).

57. Popelář, J., Rybalko, N., Burianová, J., Schwaller, B. & Syka, J. The effect of parvalbumin deficiency on the acoustic startle response and prepulse inhibition in mice. *Neurosci Lett* **553**, 216–220 (2013).

58. Madisen, L. *et al.* A robust and high-throughput Cre reporting and characterization system for the whole mouse brain. *Nat Neurosci* **13**, 133–40 (2009).

59. Xue, M., Atallah, B. V. & Scanziani, M. Equalizing excitation-inhibition ratios across visual cortical neurons. *Nature* **511**, 596–600 (2014).

60. Ferguson, B. R. & Gao, W.-J. PV Interneurons: Critical Regulators of E/I Balance for Prefrontal Cortex-Dependent Behavior and Psychiatric Disorders. *Front Neural Circuit* **12**, 37 (2018).

61. Yizhar, O. *et al.* Neocortical excitation/inhibition balance in information processing and social dysfunction. *Nature* **477**, 171–8 (2011).

62. Nelson, S. B. & Valakh, V. Excitatory/Inhibitory Balance and Circuit Homeostasis in Autism Spectrum Disorders. *Neuron* **87**, 684–98 (2015).

63. Scholl, B. & Wehr, M. Disruption of balanced cortical excitation and inhibition by acoustic trauma. *J Neurophysiol* **100**, 646–56 (2008).

64. Roux, N. L., Amar, M., Baux, G. & Fossier, P. Homeostatic control of the excitation-inhibition balance in cortical layer 5 pyramidal neurons. *Eur J Neurosci* **24**, 3507–3518 (2006).

65. Dityatev, A. *et al.* Activity-dependent formation and functions of chondroitin sulfate-rich extracellular matrix of perineuronal nets. *Dev Neurobiol* **67**, 570–588 (2007).

66. Lucas, E. K. *et al.* Parvalbumin Deficiency and GABAergic Dysfunction in Mice Lacking PGC-1α. *J Neurosci* **30**, 7227–7235 (2010).

67. Zikopoulos, B. & Barbas, H. Altered neural connectivity in excitatory and inhibitory cortical circuits in autism. *Front Hum Neurosci* **7**, 609 (2013).

68. Gogolla, N. *et al.* Common circuit defect of excitatory-inhibitory balance in mouse models of autism. *J Neurodev Disord* **1**, 172–181 (2009).

69. Härtig, W., Brauer, K. & Brückner, G. Wisteria floribunda agglutinin-labelled nets surround parvalbumin-containing neurons. *Neuroreport* **3**, 869–872 (1992).

70. Celio, M. R. & Blumcke, I. Perineuronal nets — a specialized form of extracellular matrix in the adult nervous system. *Brain Res Rev* **19**, 128–145 (1994).

71. Haunsø, A. *et al.* Morphology of perineuronal nets in tenascin-R and parvalbumin single and double knockout mice. *Brain Res* **864**, 142–145 (2000).

72. Schwaller, B. *et al.* Parvalbumin deficiency affects network properties resulting in increased susceptibility to epileptic seizures. *Mol Cell Neurosci* **25**, 650–663 (2004).

73. Bitanihirwe, B. K. Y. & Woo, T.-U. W. Perineuronal nets and schizophrenia: The importance of neuronal coatings. *Neurosci Biobehav Rev* **45**, 85–99 (2014).

74. Baimbridge, K. G., Celio, M. R. & Rogers, J. H. Calcium-binding proteins in the nervous system. *Trends Neurosci* **15**, 303–308 (1992).

75. Müller, M., Felmy, F., Schwaller, B. & Schneggenburger, R. Parvalbumin Is a Mobile Presynaptic Ca2+ Buffer in the Calyx of Held that Accelerates the Decay of Ca2+ and Short-Term Facilitation. *J Neurosci* **27**, 2261–2271 (2007).

76. Diering, G. H., Gustina, A. S. & Huganir, R. L. PKA-GluA1 coupling via AKAP5 controls AMPA receptor phosphorylation and cell-surface targeting during bidirectional homeostatic plasticity. *Neuron* **84**, 790–805 (2014).

77. Catania, M. V. *et al.* AMPA receptor subunits are differentially expressed in parvalbumin- and calretinin-positive neurons of the rat hippocampus. *Eur J Neurosci* **10**, 3479–3490 (1998).

78. Fuchs, E. C. *et al.* Recruitment of Parvalbumin-Positive Interneurons Determines Hippocampal Function and Associated Behavior. *Neuron* **53**, 591–604 (2006).

79. Chang, M. C. *et al.* Narp regulates homeostatic scaling of excitatory synapses on parvalbumin-expressing interneurons. *Nat Neurosci* **13**, 1090–1097 (2010).

80. Maurice, D. H. *et al.* Advances in targeting cyclic nucleotide phosphodiesterases. *Nat Rev Drug Discov* **13**, 290–314 (2014).

81. Hanoune, J. & Defer, N. R EGULATION AND R OLE OF A DENYLYL C YCLASE I SOFORMS. *Annu Rev Pharmacol* **41**, 145–174 (2001).

82. Kheirbek, M. A., Beeler, J. A., Chi, W., Ishikawa, Y. & Zhuang, X. A molecular dissociation between cued and contextual appetitive learning. *Learn Memory* **17**, 148–154 (2010).

83. Lu, H.-C. *et al.* Adenylyl cyclase I regulates AMPA receptor trafficking during mouse cortical “barrel” map development. *Nat Neurosci* **6**, 939–947 (2003).

84. Cooper, D. M. F. & Crossthwaite, A. J. Higher-order organization and regulation of adenylyl cyclases. *Trends Pharmacol Sci* **27**, 426–431 (2006).

85. Espina, V. *et al.* Laser-capture microdissection. *Nat Protoc* **1**, 586–603 (2006).

86. Farris, S., Wang, Y., Ward, J. M. & Dudek, S. M. Optimized Method for Robust Transcriptome Profiling of Minute Tissues Using Laser Capture Microdissection and Low-Input RNA-Seq. *Front Mol Neurosci* **10**, 185 (2017).

87. Kihara, A. H., Moriscot, A. S., Ferreira, P. J. & Hamassaki, D. E. Protecting RNA in fixed tissue: An alternative method for LCM users. *J Neurosci Meth* **148**, 103–107 (2005).

88. Kim, K.-S. *et al.* Adenylyl cyclase type 5 (AC5) is an essential mediator of morphine action. *P Natl Acad Sci Usa* **103**, 3908–3913 (2006).

89. Avidor-Reiss, T., Nevo, I., Levy, R., Pfeuffer, T. & Vogel, Z. Chronic Opioid Treatment Induces Adenylyl Cyclase V Superactivation INVOLVEMENT OF Gβγ *. *J Biol Chem* **271**, 21309–21315 (1996).

90. Schander, A. *et al.* A Flexible 202-Channel Epidural ECoG Array With PEDOT: PSS Coated Electrodes for Chronic Recording of the Visual Cortex. *Ieee Sens J* **19**, 820–825 (2019).

91. Kedzior, K. K., Koch, M. & Basar-Eroglu, C. Auditory-evoked EEG oscillations associated with prepulse inhibition (PPI) of auditory startle reflex in healthy humans. *Brain Res* **1163**, 111–118 (2007).

92. Roach, B. J., D'Souza, D. C., Ford, J. M. & Mathalon, D. H. Test-retest reliability of time-frequency measures of auditory steady-state responses in patients with schizophrenia and healthy controls. *Neuroimage Clin* **23**, 101878 (2019).

93. Watt, A. J., Rossum, M. C. W. van, MacLeod, K. M., Nelson, S. B. & Turrigiano, G. G. Activity Coregulates Quantal AMPA and NMDA Currents at Neocortical Synapses. *Neuron* **26**, 659–670 (2000).

94. Metzner, C., Zurowski, B. & Steuber, V. The Role of Parvalbumin-positive Interneurons in Auditory Steady-State Response Deficits in Schizophrenia. *Sci Rep-uk* **9**, 18525 (2019).

95. Belforte, J. E. *et al.* Postnatal NMDA receptor ablation in corticolimbic interneurons confers schizophrenia-like phenotypes. *Nat Neurosci* **13**, 76–83 (2009).

96. Chang, C.-P. *et al.* Type VI adenylyl cyclase negatively regulates GluN2B-mediated LTD and spatial reversal learning. *Sci Rep-uk* **6**, 22529 (2016).

97. Wong, S. T. *et al.* Calcium-Stimulated Adenylyl Cyclase Activity Is Critical for Hippocampus-Dependent Long-Term Memory and Late Phase LTP. *Neuron* **23**, 787–798 (1999).

98. Bender, C. L. *et al.* Emotional Stress Induces Structural Plasticity in Bergmann Glial Cells via an AC5-CPEB3-GluA1 Pathway. *J Neurosci Official J Soc Neurosci* **40**, 3374–3384 (2020).

99. Neil, S. M., Lakey, T. & Tomlinson, S. Calmodulin regulation of adenylate cyclase activity. *Cell Calcium* **6**, 213–226 (1985).

100. Ferguson, G. D. & Storm, D. R. Why Calcium-Stimulated Adenylyl Cyclases? *Physiology* **19**, 271–276 (2004).

101. Livingstone, M. S., Sziber, P. P. & Quinn, W. G. Loss of calcium/calmodulin responsiveness in adenylate cyclase of rutabaga, a Drosophila learning mutant. *Cell* **37**, 205–215 (1984).

102. Cohen, S. M. *et al.* Excitation-Transcription Coupling in Parvalbumin-Positive Interneurons Employs a Novel CaM Kinase-Dependent Pathway Distinct from Excitatory Neurons. *Neuron* **90**, 292–307 (2016).

103. Sík, A., Hájos, N., Gulácsi, A., Mody, I. & Freund, T. F. The absence of a major Ca2+ signaling pathway in GABAergic neurons of the hippocampus. *Proc National Acad Sci* **95**, 3245–3250 (1998).

104. Lee, H.-K. *et al.* Phosphorylation of the AMPA Receptor GluR1 Subunit Is Required for Synaptic Plasticity and Retention of Spatial Memory. *Cell* **112**, 631–643 (2003).

105. Gainey, M. A., Hurvitz-Wolff, J. R., Lambo, M. E. & Turrigiano, G. G. Synaptic Scaling Requires the GluR2 Subunit of the AMPA Receptor. *J Neurosci* **29**, 6479–6489 (2009).

106. Wierenga, C. J., Ibata, K. & Turrigiano, G. G. Postsynaptic Expression of Homeostatic Plasticity at Neocortical Synapses. *J Neurosci* **25**, 2895–2905 (2005).

107. Maccaferri, G. & McBain, C. J. Passive propagation of LTD to stratum oriens-alveus inhibitory neurons modulates the temporoammonic input to the hippocampal CA1 region. *Neuron* **15**, 137–145 (1995).

108. Kim, T. *et al.* Cortically projecting basal forebrain parvalbumin neurons regulate cortical gamma band oscillations. *Proc National Acad Sci* **112**, 3535–3540 (2015).

109. Brenner, C. A. *et al.* Steady State Responses: Electrophysiological Assessment of Sensory Function in Schizophrenia. *Schizophrenia Bull* **35**, 1065–1077 (2009).

110. Shahriari, Y. *et al.* Impaired auditory evoked potentials and oscillations in frontal and auditory cortex of a schizophrenia mouse model. *World J Biological Psychiatry* **17**, 1–10 (2016).

111. Wang, H.-X. & Gao, W.-J. Cell type-specific development of NMDA receptors in the interneurons of rat prefrontal cortex. *Neuropsychopharmacol Official Publ Am Coll Neuropsychopharmacol* **34**, 2028–40 (2009).

112. LEWIS, D. A., CRUZ, D., EGGAN, S. & ERICKSON, S. Postnatal Development of Prefrontal Inhibitory Circuits and the Pathophysiology of Cognitive Dysfunction in Schizophrenia. *Ann Ny Acad Sci* **1021**, 64–76 (2004).

113. Monyer, H., Burnashev, N., Laurie, D. J., Sakmann, B. & Seeburg, P. H. Developmental and regional expression in the rat brain and functional properties of four NMDA receptors. *Neuron* **12**, 529–540 (1994).

114. Sheng, M., Cummings, J., Roldan, L. A., Jan, Y. N. & Jan, L. Y. Changing subunit composition of heteromeric NMDA receptors during development of rat cortex. *Nature* **368**, 144–147 (1994).

115. Matta, J. A. *et al.* Developmental origin dictates interneuron AMPA and NMDA receptor subunit composition and plasticity. *Nat Neurosci* **16**, 1032–1041 (2013).

116. Alvarez, R. J., Pafundo, D. E., Zold, C. L. & Belforte, J. E. Interneuron NMDA receptor ablation induces hippocampus-prefrontal cortex functional hypoconnectivity after adolescence in a mouse model of schizophrenia. *J Neurosci* **40**, JN-RM-1897-19 (2020).

117. Kahn, R. S. *et al.* Schizophrenia. *Nat Rev Dis Primers* **1**, 15067 (2015).

118. Owen, M. J., Sawa, A. & Mortensen, P. B. Schizophrenia. *Lancet* **388**, 86–97 (2016).

119. Takahashi, T. & Suzuki, M. Brain morphologic changes in early stages of psychosis: Implications for clinical application and early intervention. *Psychiat Clin Neuros* **72**, 556–571 (2018).

120. Mohn, A. R., Gainetdinov, R. R., Caron, M. G. & Koller, B. H. Mice with Reduced NMDA Receptor Expression Display Behaviors Related to Schizophrenia. *Cell* **98**, 427–436 (1999).

121. Isaac, J. T. R., Crair, M. C., Nicoll, R. A. & Malenka, R. C. Silent Synapses during Development of Thalamocortical Inputs. *Neuron* **18**, 269–280 (1997).

122. Lu, H.-C., Gonzalez, E. & Crair, M. C. Barrel Cortex Critical Period Plasticity Is Independent of Changes in NMDA Receptor Subunit Composition. *Neuron* **32**, 619–634 (2001).

123. Feldman, D. E., Nicoll, R. A., Malenka, R. C. & Isaac, J. T. R. Long-Term Depression at Thalamocortical Synapses in Developing Rat Somatosensory Cortex. *Neuron* **21**, 347–357 (1998).

124. Chetkovich, D. M., Gray, R., Johnston, D. & Sweatt, J. D. N-methyl-D-aspartate receptor activation increases cAMP levels and voltage-gated Ca2+ channel activity in area CA1 of hippocampus. *Proc National Acad Sci* **88**, 6467–6471 (1991).

125. Tang, W. J., Krupinski, J. & Gilman, A. G. Expression and characterization of calmodulin-activated (type I) adenylylcyclase. *J Biol Chem* **266**, 8595–8603 (1991).

126. Cali, J. J., Zwaagstra, J. C., Mons, N., Cooper, D. M. & Krupinski, J. Type VIII adenylyl cyclase. A Ca2+/calmodulin-stimulated enzyme expressed in discrete regions of rat brain. *J Biol Chem* **269**, 12190–12195 (1994).

127. Chern, Y. Regulation of adenylyl cyclase in the central nervous system. *Cell Signal* **12**, 195–204 (2000).

128. Wang, H. *et al.* Type 8 Adenylyl Cyclase Is Targeted to Excitatory Synapses and Required for Mossy Fiber Long-Term Potentiation. *J Neurosci* **23**, 9710–9718 (2003).

129. Conti, A. C. *et al.* Distinct regional and subcellular localization of adenylyl cyclases type 1 and 8 in mouse brain. *Neuroscience* **146**, 713–729 (2007).

130. Jacobowitz, O., Chen, J., Premont, R. T. & Iyengar, R. Stimulation of specific types of Gs-stimulated adenylyl cyclases by phorbol ester treatment. *J Biol Chem* **268**, 3829–3832 (1993).

131. Cardin, J. A. *et al.* Driving fast-spiking cells induces gamma rhythm and controls sensory responses. *Nature* **459**, 663–667 (2009).

132. Sohal, V. S., Zhang, F., Yizhar, O. & Deisseroth, K. Parvalbumin neurons and gamma rhythms enhance cortical circuit performance. *Nature* **459**, 698–702 (2009).

133. Cheng, C.-H. *et al.* Sensory gating, inhibition control and gamma oscillations in the human somatosensory cortex. *Sci Rep-uk* **6**, 20437 (2016).

134. Wood, K. C., Blackwell, J. M. & Geffen, M. Cortical inhibitory interneurons control sensory processing. *Curr Opin Neurobiol* **46**, 200–207 (2017).